NTT Technical Review

8
2013

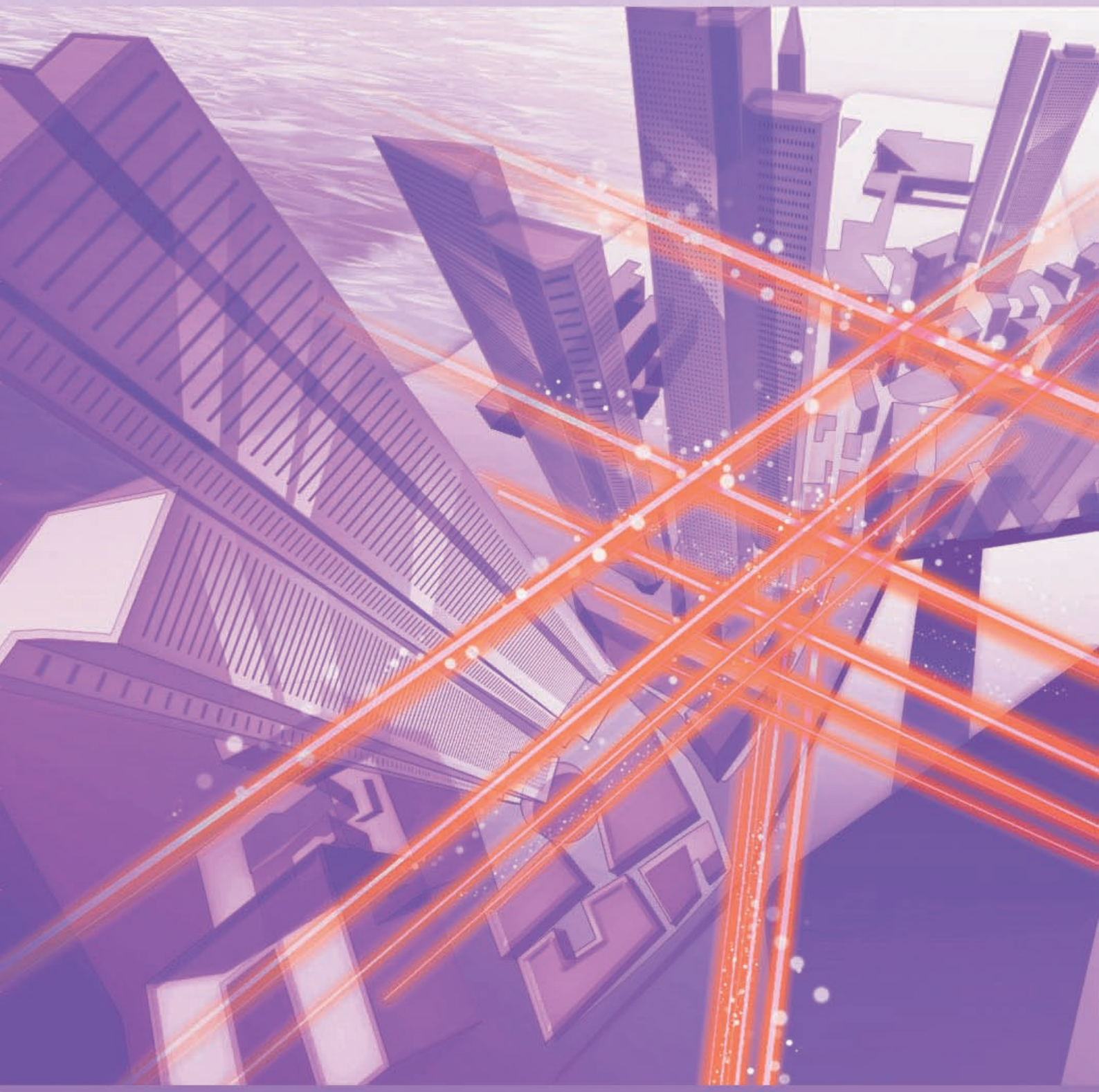

August 2013 Vol. 11 No. 8

NTT Technical Review

August 2013 Vol. 11 No. 8

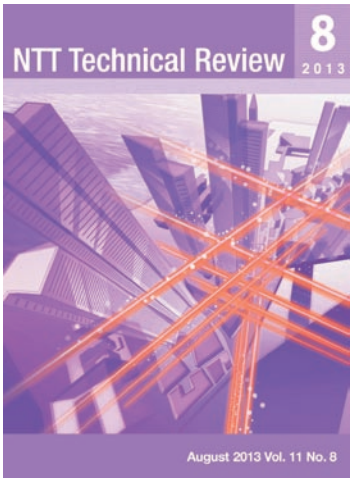

Applying Startup Experience with Silicon Valley Spirit to Make the NTT Group Universally Known

Srini Koushik
Chief Executive Officer
NTT Innovation Institute, Inc.

Overview

NTT I^3 (NTT Innovation Institute, Inc.) is an innovative enterprise with global aspirations that seeks to leverage its Silicon Valley location and core strengths in original cloud and security technologies. We asked newly appointed Chief Executive Officer (CEO) Srini Koushik to tell us more about NTT I^3's core strengths, and as someone who has had a long career in the IT industry, to talk about NTT Group's current standing in the world and NTT I^3's outlook for the future.

Off to a good start: NTT I^3 aims to become a multifaceted NTT Group hub

—Mr. Koushik, what are your feelings now that the opening reception has been completed?

Well, I feel quite excited that the reception went very well and that it succeeded in getting others to know NTT I^3 and its people. I was very happy to see that participants included dignitaries not only from Silicon Valley companies like Cisco and Salesforce. com but also from renowned global companies.

I remember one particular compliment from a Washington, D.C. reporter who said that our ceremony was the best of all receptions held by Japanese companies that he had seen.

In the light of all this encouragement, I would like to merge NTT's long history and solid traditions with Silicon Valley's startup culture to make the NTT Group name well-known throughout North America.

I plan, in particular, to focus our energies on three key strategies.

The first is to form close partnerships with leading companies and universities. Our second strategy is to invite talented people from NTT Group companies that have bases in North America to stimulate research activities. My aim here is to create a microcosm of the NTT Group and its strengths within NTT I^3 and to promulgate an image of NTT I^3 as a group hub. Finally, our third strategy is to pursue appropriate activities as a global market leader. We will work, in particular, on promoting research and developing services and products that can be used by our customers in the United States where NTT I^3 is located. Of course, our objective is not just the United States—we plan a global rollout that will include emerging countries.

Let me elaborate on our first strategy of partnering with major companies and universities.

We have already tied up with Georgia Institute of Technology (Georgia Tech) and Stanford University, and we are now looking for other universities to form connections with.

Forming tie-ups with academic organizations is extremely important. Such partnerships can be a source of new ideas and creativity, but they can also serve another important purpose: university students who participate in research activities at NTT I^3 may

see for themselves how attractive research and development (R&D) work at our institute can be. This would be one way for us to secure top-notch, talented people for the future.

In addition, we already have good partnerships with prominent corporations like Cisco, Salesforce.com, and Oracle, and we will continue to build upon those partnerships.

In terms of our second strategy, let me say that the success of NTT I^3 is dependent on the success of the NTT Group, so I will promote the participation of personnel from NTT Group operating companies. In fact, we have already obtained the participation of COO (Chief Operating Officer) Eiji Kuwana from NTT laboratories and other talented individuals, and from here on, I would like to bring in more talent from such group companies as Dimension Data, NTT DATA, and NTT Communications (NTT Com).

Finally, with respect to our third strategy, we already have three projects underway geared to putting NTT on a path to becoming a driver in the global market. One is research and development in the security field, another is the development of software defined networking in the cloud computing field, and the third one is the development of frameworks for migrating applications to the cloud.

So we're off to a good start. I think that NTT Group, the parent company, has done all they need to do to help us achieve a smooth launch. Looking forward, we can see that there is great interest in cloud services in the American market, and we are working to introduce our services and penetrate this market. Products like Infrastructure as a Service (IaaS) and Software as a Service (SaaS) are also used quite extensively in the United States. So, as I just mentioned, I think that the next step in cloud services is the migration of business applications to the cloud, which is a good business opportunity for us.

To become a global leader with this vision in mind, we have to show enterprises that we can provide a cloud environment that is secure and available 24 hours a day.

NTT is one of three companies that can expand such business in a global manner. The job of NTT I^3 is to provide support from the R&D side so that the NTT Group can roll out these services in the global market in a smooth and steady manner.

R&D hub where people have a strong desire to work above and beyond remuneration

—Can you give us some more specifics on capabilities, talented staff, and anything else that you are focusing on to provide this support?

Well, to begin with, we already have a strong foundation of technical engineers and designers, but it's important that we continue to welcome highly capable people to NTT I^3. Over the next few months, we will be solidifying our direction and projects even further, and we will need engineers and architects with a variety of capabilities and individuals with project-management skills as well.

We need project managers who understand business requirements and who know how to provide our products to our customers on a regular, stable basis.

Architects, meanwhile, must get the technologies from the various NTT operating companies to work together to enable the solutions we want to offer.

To this end, I think having a hub like NTT I^3 in North America and particularly in Silicon Valley is very beneficial. To develop compelling products and build attractive solutions, we need strong technology partnerships in addition to our joint development efforts within the NTT Group.

—By the way, how do you plan to apply your past CEO experience to your present position?

As a result of accumulating more than 28 years of experience in the technology industry, including about 16 years in technology companies and more than 10 years in the financial services and insurance industry, I have been able to be involved in the information technology (IT) industry in a variety of ways, including gaining experience in infrastructure and applications and as a service provider and user.

I feel that my business experience at technology

companies like IBM and HP, which are nearly as big as NTT, will prove useful not only in understanding technology but also in working with a big, complex company and managing NTT I^3. I also believe that my experience in the financial services and insurance industry will help me in understanding what consumers want. It is probably a common characteristic of technology companies that they want to sell the technologies that they develop, but it is important that they obtain a good understanding of what consumers want to buy. In this regard, I think that penetrating the buyer's mind is one ability that I can bring to NTT I^3.

My vision of success at NTT I^3 is that the industry accepts our innovative ideas, and that these ideas add value and drive growth for NTT's operating companies in North America. Another goal is to create an outstanding work environment so that anyone who comes to work at NTT I^3 does so because they truly enjoy working here above and beyond their paycheck. I will spare no effort in achieving such a workplace, and one year from now, I believe I will have new dreams as we move forward.

Transforming one's weakness into strength in the spirit of judo: flexibility over stiffness

—Why did you select NTT I^3 when there are other organizations like it in the IT industry? How do you think NTT is viewed in the world market?

Well, I wanted to work for a technology-related company but not for a company that pursues technology for technology's sake. Of course, NTT I^3 is also involved in technology research, but I believe that its goal is to change society through technology. This is what I find to be important!

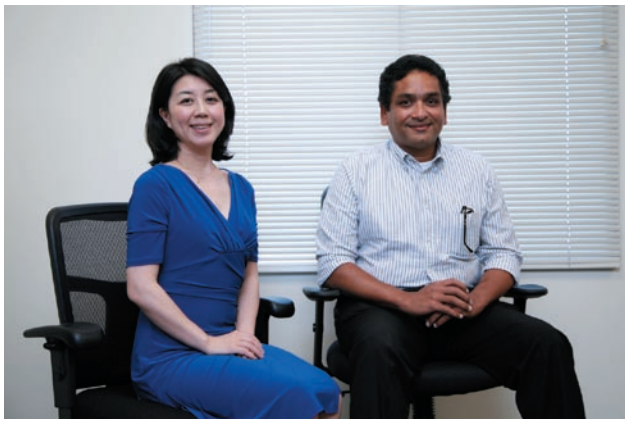

Despite NTT's long history of success, NTT I^3 is a new participant in the R&D field in the United States market, but given my history of solving IT problems through innovative products and services, this presents me with a great challenge that I am eager to undertake.

So how is the NTT Group positioned in the world market right now? I would say that NTT Com is recognized first and foremost as a network carrier, that NTT DATA, while having gained a certain amount of recognition, is still viewed as one of the smaller service providers, and that Dimension Data is a company that is just now starting to make an impact.

I think that these company attributes can also be viewed as strengths. For example, ordinary companies are sometimes reluctant to partner with huge providers because they fear that they will not be able to receive suitable and effective services tailored to their needs. So I think that NTT DATA can offer great flexibility precisely because of its small-scale stature. This is a great business opportunity for NTT.

By the way, two of my hobbies are skydiving and hang gliding. If there is something that is new and exciting that I might be afraid to do, I make sure to try it so that I am no longer afraid of it.

I also have a black belt in judo, and I think there is something in common here between judo and NTT I^3. No matter how small one's body may be, it's possible to transform one's weak point into a strength to use against your opponent.

In the cloud market, I think that NTT is in a very good position. NTT Com is viewed as a company that provides one of the most advanced carrier-enabled clouds. The advantage of a carrier-enabled cloud is that it can truly spread the workload across the globe

in a much easier way.

Dimension Data, meanwhile, is viewed as a company that can provide powerful functions for private clouds and that has very strong capabilities in implementing managed services on top of private clouds in the infrastructure space.

And NTT DATA and NTT Centerstance have very good capabilities in implementing SaaS and integrating it with legacy applications.

In this way, the NTT Group has laid out the framework to promote business support through a full lineup of services, from cloud services, managed services, and advisory services to application services too.

So what we have to do at NTT I^3 is to help our customers understand that we can tie all these group-company strengths together.

Furthermore, we can provide security in a comprehensive manner for a full range of services from applications to infrastructures and clouds. We are one of only a few companies—maybe two or three in the world—that can do so.

—How do you plan to work with R&D in Japan?

Needless to say, NTT has top-class R&D even from a global perspective. The R&D team is producing extraordinary intellectual property, and they have been helping us to understand what they have. Looking to the future, I want to do three things with NTT R&D.

The first is to commercialize NTT R&D results for the American market and to expand them into a tangible business. The second is to do further research in specific fields. And the third is to maintain a close relationship with NTT R&D, to know what NTT researchers are working on at any given time, and to help the NTT operating companies in North America to understand the content of that R&D work.

It's OK to fail! Acting like a startup to make NTT a global name

—Mr. Koushik, could you leave us with a message for all your colleagues at NTT I^3?

First of all, I would like to tell all my colleagues that I am very excited to be here and very proud to be a part of NTT I^3. I would like them to know that I am here to support them and to be a part of NTT I^3 as a key startup in the United States. This is the stance that I believe is important in getting the NTT name widely known throughout the United States market and in being a part of NTT growth. I also want every one at NTT I^3 to know how great a company NTT is, and how we can leverage that to "put a dent in the universe," as Steve Jobs was fond of saying.

You can hear many stories about people launching new companies and rising to the top, but those people often fail many times before succeeding. Generating new ideas and being innovative is the essence of NTT I^3. If only three of our ideas out of ten are successful, there is no need for us to lose sleep over the seven failures. What we need to do is focus our efforts on the three successful ideas.

I have attempted a number of startups in the past, and some of them worked and some of them didn't. Failure is never easy, but it is also the time when you learn the most. In other words, it is OK to fail, but repeating the same mistake is not so good!

There is some similarity between Japanese and Indian culture in that there is a tendency to look upon failure as a bad thing. In the United States, however, failure is OK—you learn from failures and you get better, and that is part of being a startup.

This kind of mind frame is essential at the startup stage, and I would ask our Japanese researchers to adopt this attitude as well.

Interviewee profile

■ Career highlights

Srini Koushik joined IBM in 1994 and became head of e-business development in 2000. He joined Nationwide Insurance in 2001 and became its CTO (chief technology officer) in 2009. In 2011, he joined HP and took up the post of chief development officer spearheading the development of global applications. He founded Right Brain Systems, a consulting company, in 2012, serving as president and CEO. He took up his present position at NTT Innovation Institute, Inc. in May 2013.

Graphene Research at NTT

Hiroki Hibino

Abstract

Graphene, a two-dimensional sheet of carbon atoms, was experimentally discovered in 2004. Since then, graphene research has progressed exponentially from basic science to applications. NTT aims to make a large impact on the information society through the materials science of graphene and is therefore promoting a wide range of graphene research projects from theory to devices. In this Feature Article, the current status of graphene research underway at NTT laboratories is presented.

1. Introduction

Historically, the development of new materials has revolutionized our way of life, and we have learned that an infinite variety of materials can be formed from different combinations of atoms and molecules. Research on materials science increases our knowledge of how to create and develop new materials and therefore has great potential for improving our lives and society. NTT laboratories have already created various new materials that have had a significant impact on the information society and are continuing to search for materials that will contribute to solving social issues in the future.

These Feature Articles focus on graphene, which is currently attracting a great deal of attention both at a fundamental level and in technological domains. NTT laboratories are approaching graphene multilaterally from various aspects: theory, synthesis, physical properties, and devices. In this article, I first explain why graphene is such a promising material and then present an overview of graphene research at NTT.

2. Graphene

2.1 Basic structure

Graphene is a two-dimensional crystal consisting of carbon atoms arranged in a honeycomb lattice (**Fig. 1**). A three-dimensional stack of graphene sheets is graphite, which is a familiar material in daily life. Graphene is also the basic element of fullerenes and carbon nanotubes, which are well-known carbon nanostructures. However, its experimental history is relatively new. Researchers from the University of Manchester first discovered graphene in 2004 when they managed to isolate it from thin graphite flakes that had been mechanically exfoliated from bulk graphite. It has been researched intensively ever since, owing to its novelty in science and the expectations of its having a wide range of applications. The Nobel Prize in Physics was awarded to the discoverers in 2010.

The scientific novelty of graphene is symbolized by its extraordinary electronic structure. Since the equation that describes the states of conduction electrons in graphene is the same as the relativistic quantum mechanical equation (Dirac equation) with mass equal to zero, conduction electrons in graphene are called massless Dirac particles. These electrons constitute a new class of two-dimensional electron system, which is truly different from the two-dimensional electron gas in semiconductors such as silicon (Si) and gallium arsenide (GaAs). For example, the energy of electrons is normally proportional to the square of the momentum, but the energy of conduction electrons in graphene is proportional to the momentum. This property is the same as that of light and is compatible with massless particles.

2.2 Properties and synthesis

Graphene has excellent mechanical, electrical, and optical properties. Its typical properties are summarized in **Table 1**. Graphene is mechanically very strong and flexible. The breaking strength of graphene is more than 100 times greater than that of steel. The crystal structure does not break even after being stretched up to 20%. From an electrical aspect,

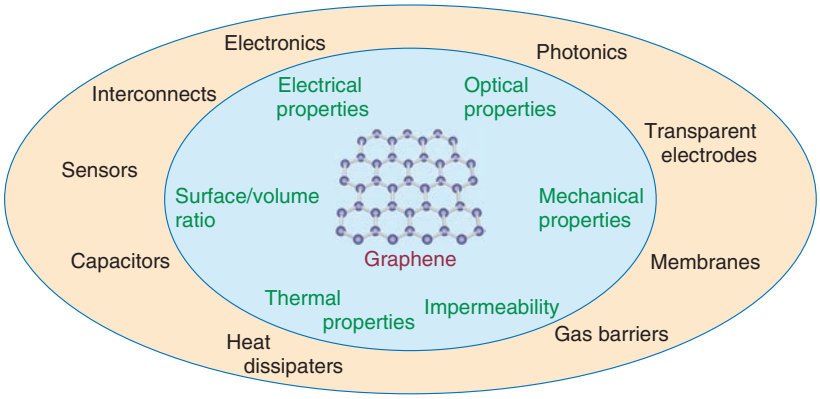

Fig. 1. Structure of graphene and its potential applications.

Table 1. Properties of graphene.

Property	Value	Comparison with other materials	References
Breaking strength	42 Nm^{-1}	More than 100 times greater than steel	[1], [2]
Elastic limit	~20%		[3]
Carrier mobility at room temperature	200,000 $cm^2V^{-1}s^{-1}$	More than 100 times higher than Si	[4]
Thermal conductivity	~5000 $Wm^{-1}K^{-1}$	More than 10 times higher than Cu	[2], [5]
Maximum current density	$>10^8$ Acm^{-1}	~100 times larger than Cu	[6]
Optical absorption coefficient	2.3%	~50 times higher than GaAs	[7], [8]

the carrier mobility of graphene at room temperature is more than 100 times higher than that of silicon. Furthermore, graphene is an ultra-wide-band optical material that interacts strongly with light of a wide range of wavelengths. Graphene absorbs 2.3% of light in the visible to infrared region. This absorption coefficient is one to three orders of magnitude higher than those of conventional semiconductor materials.

These properties of graphene suggest that various applications are possible. For example, several-layer-thick graphene films are transparent, electrically conductive, and flexible. Therefore, flexible transparent electrode applications, including touch screens and solar cells, have been extensively studied. High carrier mobility makes graphene promising as a channel material of high-speed electronics. However, since it is difficult to turn off an electrical current in graphene, progress has mainly been achieved in research on applications involving analog high-frequency devices. Graphene is also promising for photonics devices such as modulators and photodetectors. In general, the range of potential applications is very wide and includes sensors, interconnects, capacitors, heat dissipaters, gas barriers, and membranes.

High-quality graphene can be obtained by mechanically exfoliating graphene from graphite. This method is therefore ideal for basic research, but in terms of productivity and the small size of graphene sheets that can be obtained, it is not suitable for industrial applications. Therefore, in recent years, techniques for growing graphene on a substrate have been actively studied. Two growth methods are attracting intense interest: thermal decomposition of silicon carbide (SiC), in order to grow graphene on it, and chemical vapor deposition (CVD) to grow graphene on metal catalyst substrates. The quality of the graphene grown using these methods is improving rapidly. If single-crystal graphene substrates could be obtained routinely, they would dramatically advance graphene research and increase the number of potential applications.

3. Graphene research at NTT

NTT has a comprehensive research scope ranging from basic theory to applied research, and we are

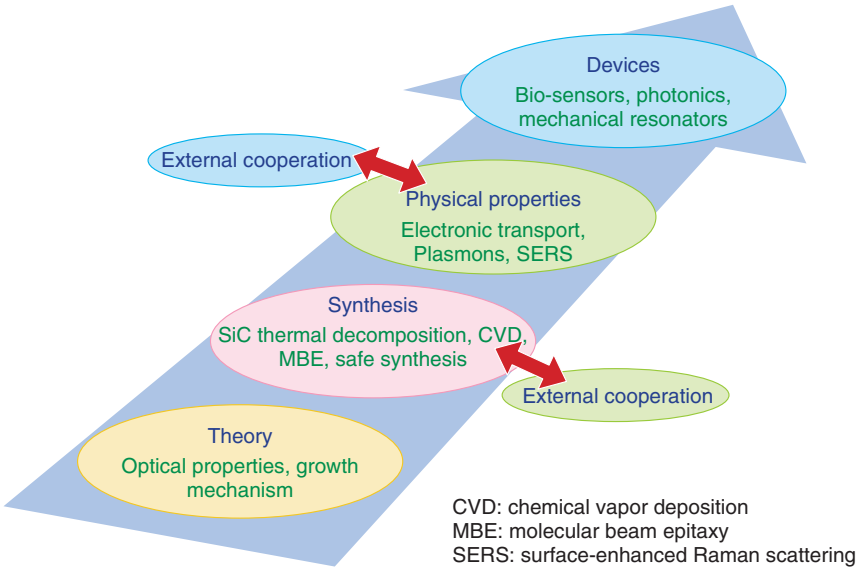

Fig. 2. Areas of research on graphene at NTT.

studying graphene across this entire spectrum. Further, to accelerate the research in order to elucidate graphene's fundamental properties and its synthesis, we are actively collaborating with research institutes outside NTT. Typical research topics in four research stages: theory, synthesis, physical properties, and devices are shown in **Fig. 2**.

3.1 Theory

The Feature Article in this issue entitled "Basic Principles of Raman Spectroscopy for Graphene" [9] covers the theory of the optical properties of graphene. Another important research subject is the theory of graphene growth. On the basis of our understanding of the stable structures of carbon atoms on SiC determined from first principles calculations[*1], we are trying to clarify the mechanism of graphene growth by thermal decomposition of SiC.

3.2 Synthesis

NTT possesses a low-energy electron microscope (LEEM)[*2] that is suitable for in-situ observation of the graphene growth process and for microscopic evaluation of the number of graphene layers. We used LEEM to investigate the growth process of graphene on SiC, and from the insights gained, we succeeded in growing highly uniform monolayer and bilayer graphene. These graphene substrates enabled us to evaluate the electronic transport properties at each thickness, as introduced in the Feature Article entitled "Exploring Relativistic Physics and Band Gap Detection in Epitaxial Graphene" [10].

NTT laboratories are working on growing not only graphene but also monolayer boron nitride (BN), a two-dimensional crystal consisting of boron and nitrogen, using CVD. In particular, we are promoting external cooperation with the aim of establishing a technique for growing single-crystal graphene and BN by using single-crystal metal thin films on a sapphire substrate. In addition to the results obtained in CVD and thermal decomposition of SiC, we have achieved many promising results in graphene and BN synthesis, as exemplified by a safe synthesis method that uses a solid material deposited on a metal substrate as a source, which is presented in the Feature Article entitled "A Novel and Simple Method of Growing Atomically Thin Hexagonal Boron Nitride" [11], and by the direct growth of graphene by molecular beam epitaxy (MBE)[*3].

*1 First-principles calculations: Method to calculate electronic states on the basis of quantum mechanics using only basic physical quantities.

*2 Low-energy electron microscope: A type of electron microscope that uses electron beams with an accelerating voltage as small as a few volts and that is therefore sensitive to differences in the surface structure of a material.

*3 Molecular beam epitaxy: A method of supplying material onto a substrate like a beam in a vacuum, resulting in growth of a material following the atomic arrangement of the substrate.

3.3 Physical properties

The Feature Articles entitled "Exploring Relativistic Physics and Detection of a Band Gap in Epitaxial Graphene" [10], "Plasmon Transport in Graphene" [12], and "Surface-enhanced Raman Scattering of Graphene on SiC" [13] report that NTT laboratories have obtained many notable results on the optical and electronic properties of graphene. Further, because the electronic transport properties of graphene grown on SiC are influenced by the substrate, we are also attempting to control the interface structure to improve the transport properties. In addition, we are working to clarify the fundamental physics of graphene by promoting collaboration with external research institutions that apply unique characterization methods such as high-sensitivity measurements of polarization rotation of terahertz waves and magneto-optical absorption measurements under an ultra-high magnetic field.

3.4 Devices

The Feature Article entitled "Biosensing on a Graphene Oxide Surface" [14] explains how graphene oxide produced by chemical oxidation and exfoliation of graphite can be used for protein detection. NTT laboratories are also investigating the vibration characteristics of mechanical resonators fabricated from graphene grown on SiC by electrochemically etching the substrate, and exploring the light transmission characteristics of optical waveguides integrated with graphene.

4. Future prospects

There is no doubt that graphene has enormous potential as a future material, but we face many challenges in achieving industrial applications. The synthesis method is a prime example. The CVD method is suitable for large-scale and low-cost synthesis of graphene, but electronics/photonics applications require that graphene on metal substrates be transferred onto other insulating substrates. Damage-free transfer technology is also a difficult challenge. Further, the ideal graphene does not have a band gap, which impedes the development of logic devices. In these Feature Articles, we will describe the electrical detection of a band gap in bilayer graphene on SiC. Various attempts to create a band gap in graphene have been made from materials science and device science approaches. On the other hand, the discovery of graphene has aroused increasing interest in two-dimensional crystals other than graphene, such as insulating BN and semiconducting molybdenum disulfide (MoS_2). It is expected that hybrid structures of two-dimensional materials with various properties will bring new functions. Although research on two-dimensional crystals containing graphene is very competitive, we are confident that NTT laboratories, with NTT's comprehensive research organization and research network outside NTT, will be at the center of graphene research and will attain new levels of understanding that will contribute to our society.

References

[1] C. Lee, X. Wei, J. W. Kysar, and J. Hone, "Measurement of the Elastic Properties and Intrinsic Strength of Monolayer Graphene," Science, Vol. 321, No. 5887, pp. 385–388, 2008.

[2] Scientific Background on the Nobel Prize in Physics 2010, Royal Swedish Academy of Sciences, Oct. 2010. http://www.nobelprize.org/nobel_prizes/physics/laureates/2010/advanced-physicsprize2010.pdf

[3] K. S. Kim, Y. Zhao, H. Jang, S. Y. Lee, J. M. Kim, K. S. Kim, J.-H. Ahn, P. Kim, J.-Y. Choi, and B. H. Hong, "Large-scale pattern growth of graphene films for stretchable transparent electrodes," Nature, Vol. 457, pp. 706–710, 2009.

[4] J.-H. Chen, C. Jang, S. Xiao, M. Ishigami, and M. S. Fuhrer, "Intrinsic and extrinsic performance limits of graphene devices on SiO_2," Nature Nanotechnol., Vol. 3, pp. 206–209, 2008.

[5] S. Ghosh, W. Bao, D. L. Nika, S. Subrina, E. P. Pokatilov, C. N. Lau, and A. A. Balandin, "Dimensional crossover of thermal transport in few-layer graphene," Nature Mater., Vol. 9, pp. 555–558, 2010.

[6] R. Murali, Y. Yang, K. Brenner, T. Beck, and J. D. Meindl, "Breakdown current density of graphene nanoribbons,"Appl. Phys. Lett.,Vol. 94, No. 24, pp. 243114, 2009.

[7] R. R. Nair, P. Blake, A. N. Grigorenko, K. S. Novoselov, T. J. Booth, T. Stauber, N. M. R. Peres, and A. K. Geim, "Fine Structure Constant Defines Visual Transparency of Graphene," Science, Vol. 320, No. 5881, pp. 1308, 2008.

[8] Q. Bao and K. P. Loh, "Graphene Photonics, Plasmonics, and Broadband Optoelectronic Devices," ACS Nano, Vol. 6, No. 5, pp. 3677–3694, 2012.

[9] K. Sasaki, "Basic Principles of Raman Spectroscopy for Graphene," NTT Technical Review, Vol. 11, No. 8, 2013. https://www.ntt-review.jp/archive/ntttechnical.php?contents=ntr201308fa2.html

[10] K. Takase and S. Tanabe, "Exploring Relativistic Physics and Band Gap Detection in Epitaxial Graphene," NTT Technical Review, Vol. 11, No. 8, 2013. https://www.ntt-review.jp/archive/ntttechnical.php?contents=ntr201308fa4.html

[11] S. Suzuki, "A Novel and Simple Method of Growing Atomically Thin Hexagonal Boron Nitride," NTT Technical Review, Vol. 11, No. 8, 2013. https://www.ntt-review.jp/archive/ntttechnical.php?contents=ntr201308fa3.html

[12] N. Kumada, "Plasmon Transport in Graphene," NTT Technical Review, Vol. 11, No. 8, 2013. https://www.ntt-review.jp/archive/ntttechnical.php?contents=ntr201308fa5.html

[13] Y. Sekine, H. Hibino, K.Oguri, T. Akazaki, H. Kageshima, M. Nagase, K. Sasaki, and H. Yamaguchi, "Surface-enhanced Raman Scattering of Graphene on SiC," NTT Technical Review, Vol. 11, No. 8, 2013. https://www.ntt-review.jp/archive/ntttechnical.php?contents=ntr201308fa6.html

[14] K. Furukawa and Y. Ueno, "Biosensing on a Graphene Oxide Surface," NTT Technical Review, Vol. 11, No. 8, 2013.

https://www.ntt-review.jp/archive/ntttechnical.php?contents=ntr201308fa7.html

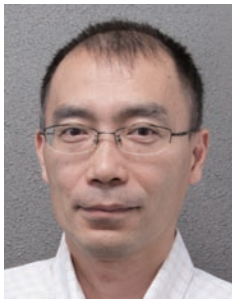

Hiroki Hibino

Executive Manager of the Materials Science Laboratory and Group Leader of the Low-dimensional Nanomaterials Research Group at NTT Basic Research Laboratories.

He received the B.S. and M.S. degrees in physics from the University of Tokyo in 1987 and 1989, respectively, and the Ph.D. degree in pure and applied physics from Waseda University, Tokyo, in 2006. In 1989, he joined NTT Basic Research Laboratories, where he has been studying surface dynamical processes using microscopic techniques. His research interests include step structures on vicinal surfaces, surface mass transport, step instability during epitaxial growth, self-assembled nanostructure formation, and epitaxial graphene growth. He spent one year as a visiting research professor at Arizona State University during 2000–2001. He also has experience as a visiting professor at Tokyo Institute of Technology (2007–), Kyushu University (2009–2010), and the University of Tokyo (2011–).

Basic Principles of Raman Spectroscopy for Graphene

Ken-ichi Sasaki

Abstract

Graphene is a planar honeycomb network composed of carbon atoms. Even though graphene has a very simple structure, it has received considerable attention from researchers in various fields. This article explains the basic principles of Raman spectroscopy for use with graphene in order to provide insight into the unique properties of graphene.

1. Overview of Raman spectroscopy

When laser light is applied to a sample, it is scattered with a finite probability. If we plot the intensity of scattered light as a function of its energy, we may find that several peaks (or bands) appear in the result, as shown in **Fig. 1**. The spectrum of scattered light as a function of the energy shift is known as the Raman spectrum, which is the main data obtained from Raman spectroscopy. Normally, the intensity is at a maximum when the energy of scattered light is equal to that of incident light. However, this is not the only peak. There are other peaks for which the energy shift is nonzero. Since the energy is conserved, the energy difference corresponds to the energy that is absorbed into the sample. When the peak originates from the interaction between light and a lattice vibration (called a phonon), the energy shift corresponds to the energy of a Raman active phonon.

If we know that the energy of a Raman active phonon in sample A is 500 cm^{-1} and that in sample B is 530 cm^{-1}, we can identify the sample by using Raman spectroscopy. This describes the basic use of Raman spectroscopy as a characterization tool. We know that for graphene there are two principal Raman bands: one peak appears at ~1580 cm^{-1}, which is called the G band, and the other peak is seen at ~2700 cm^{-1}, which is called the 2D band (or G' band). If a sample does not show a G or 2D band, we do not consider it to be graphene.

Raman spectroscopy is useful not only for characterizing a sample, but also for obtaining information about a sample. This is partly because there are several parameters that we can change in Raman spectroscopy measurements. For example, the energy of incident laser light (E_L) can be changed. For graphene,

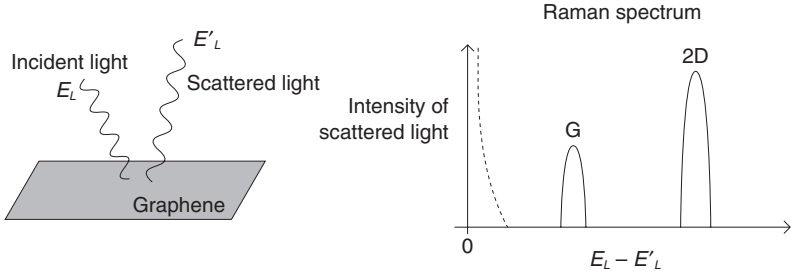

Fig. 1. Schematic illustration of Raman spectroscopy.

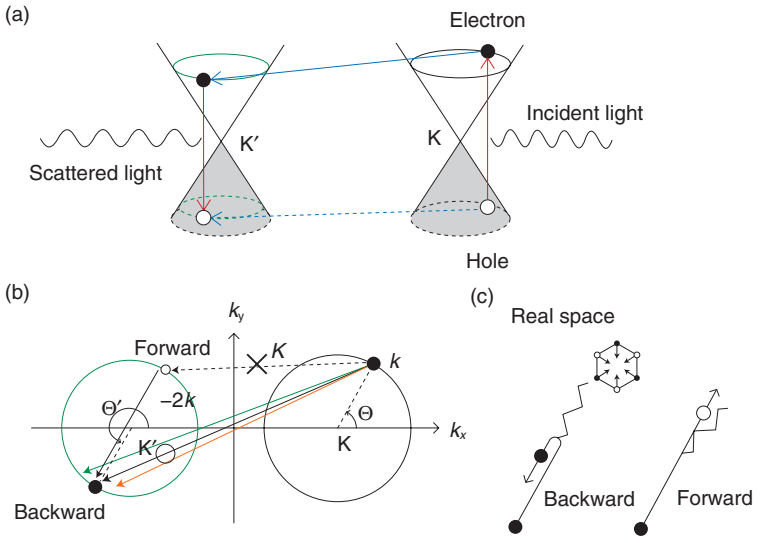

Fig. 2. (a) Schematic of a Raman process in the Dirac cones of graphene. (b) Top view of (a). (c) The A_{1g} phonon is emitted from an electron through backward scattering.

the G band energy is known to be insensitive to the change in E_L, whereas the 2D band energy increases linearly as E_L increases. What is the physics behind the dispersive (nondispersive) behavior of the 2D (G) band? This is the central issue that we would like to explore in this review article.

2. Phonon wave vector

Phonons in graphene form the energy band structures, and a phonon's energy is a function of the wave vector $\boldsymbol{q}$ as $\hbar\omega(\boldsymbol{q})$. If we assume that a phonon's energy does not depend on the E_L value used in the experiment (which is true for most experimental conditions), the nondispersive behavior of the G band suggests that the identical phonon with a fixed $\boldsymbol{q}$ value is created while E_L is changed. In fact, the wave vector of the G phonon is $\boldsymbol{q} = \boldsymbol{0}$ (the Γ point), and the nondispersive behavior of the G band is reasonably understood because $\hbar\omega(\boldsymbol{0})$ is independent of E_L. Meanwhile, many studies have revealed that the 2D band consists of two A_{1g} zone-boundary phonons. The wave vector of each phonon is near the K point; namely, it is written as $\boldsymbol{K} + \boldsymbol{q}$, where $\boldsymbol{q}$ represents a small derivation from $\boldsymbol{K}$ (the wave vector of the K point). A reasonable solution to explain the dispersive behavior of the 2D band is to think that the wave vector $\boldsymbol{q}$ is changed by changing E_L.

Let us explain the reason for the E_L dependence of $\boldsymbol{q}$. A process for the 2D band that is induced in the electronic band structures called Dirac cones by laser light is shown in **Fig. 2(a)**. Because the wave vector of light (typically ~1/600 nm) is much smaller than the wave vector of electrons and holes, optical transitions are possible only when an electron is transferred between the valence and conduction bands without a change in its wave vector. Thus, a vertical electron-hole pair is created by light, and it is annihilated by the emission of scattered light. An immediate consequence of such a direct transition in the Dirac cones is that E_L is related to the wave vector of a photo-excited electron (and hole) $\boldsymbol{k}$ as $E_L = 2\hbar v_F k$, where v_F is the electron's velocity and $k = |\boldsymbol{k}|$. Thus, increasing E_L is equivalent to increasing the radius of the circle defined with respect to the K point shown in **Fig. 2(b).**

When a photo-excited electron emits an A_{1g} phonon, the valley changes from K to K' due to momentum conservation. Let the wave vector of the scattered electron be $\boldsymbol{k'}$, which is measured from the K' point[*1]. Similarly, the photo-excited hole changes its valley from the K point to the K' point when it emits an A_{1g} phonon. In general, the hole is not scattered into the position just below the electron because the electron

*1 Strictly speaking, the radius of the circle near the K' point, i.e., $|\boldsymbol{k'}|$, shown in Fig. 1(b) must be a little smaller than that near the K point k = $|\boldsymbol{k}|$, because of energy conservation with respect to the phonon's energy. We consider the case in which $E_L = 2\hbar v_F k$ is much larger than the phonon energy (~0.15 eV); the difference between the radii is not essential in this discussion.

and hole are independently scattered by different A_{1g} phonons. Only when the wave vectors of the scattered hole and electron are identical (as shown in Fig. 2(a)) can the hole and electron be annihilated by scattered light emission, which can be observed as the 2D band in the Raman spectrum.

3. Dominance of backward scattering

If there is no preferred direction of $\boldsymbol{k}'$ for a given $\boldsymbol{k}$, the $\boldsymbol{q}$ ($\equiv \boldsymbol{k}' - \boldsymbol{k}$) value cannot be specified. This is easy to recognize by projecting the process shown in Fig. 2(a) onto the two dimensional $\boldsymbol{k}$-space shown in Fig. 2(b), in which the magnitude $q = |\boldsymbol{q}|$ is small for the forward scattering ($\boldsymbol{q} \approx \boldsymbol{0}$), denoted by the dashed arrow in Fig. 2(b), while it can be large for the backward scattering ($\boldsymbol{q} \approx -2\boldsymbol{k}$).

Interestingly, there is a strong probability that the electron will undergo backward scattering when it emits an A_{1g} phonon, as shown in **Fig. 2(c)**. Namely, although the forward scattering may be allowed by momentum conservation, it never takes place because the corresponding electron-phonon matrix element is suppressed. In fact, the calculated matrix element squared is proportional to $1 - \cos(\Theta' - \Theta)$, where Θ (Θ') is the angle between $\boldsymbol{k}$ ($\boldsymbol{k}'$) and the k_x-axis. The matrix element squared vanishes for the forward scattering ($\Theta' = \Theta$), while it takes the maximum for the backward scattering ($\Theta' = \Theta + \pi$). Thus, the phonons whose wave vector satisfies $q = |\boldsymbol{q}| \approx 2k$ contribute significantly to the 2D band. As a result, increasing the E_L is equivalent to increasing linearly the magnitude of the wave vector of the phonon, $q(E_L) \approx E_L/\hbar v_F$.[*2]

4. Phonon dispersion and self-energy

The next problem is the $\boldsymbol{q}$ dependence of $\hbar\omega(\boldsymbol{q})$. Normally, the dispersion relation of phonons is calculated by using a classical model in which carbon atoms are connected by springs with some force constants. If we assume that the force constants are nonzero only for nearest-neighbor carbon atoms, it can be shown that the $\boldsymbol{q}$ dependence is negligible: $\hbar\omega(\boldsymbol{q}) = constant$, for which we fail to explain the dispersive behavior of the 2D band. Thus, many studies have been done concerning the parameters including the force constants beyond the nearest-neighbor that can reproduce the experimental results. However, even if a classical model gives $\hbar\omega(\boldsymbol{q}) = constant$, quantum mechanics can modify the $\boldsymbol{q}$ dependence of $\hbar\omega(\boldsymbol{q})$ through the self-energy.

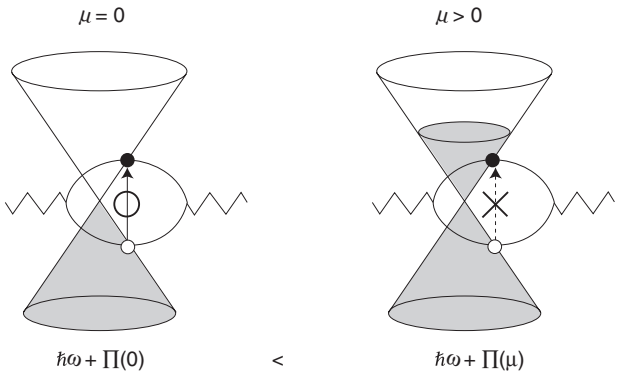

Fig. 3. The doping dependence of the presence/absence of intermediate states that contribute to the self-energy.

The concept of self-energy is also essential in explaining the experimental result in which the energy of the G band increases as the Fermi energy μ increases (by doping). Suppose that a phonon with wave vector $\boldsymbol{q}$ hits an electron with wave vector $\boldsymbol{k}$ through electron-phonon interaction. The electron is transferred from the valence to the conduction bands, and the wave vector becomes $\boldsymbol{k} + \boldsymbol{q}$ due to momentum conservation. Since $\boldsymbol{q} = \boldsymbol{0}$ for the G band, the electron undergoes a vertical transition (**Fig. 3**). There are different vertical transitions depending on the value of $\boldsymbol{k}$. These vertical electron-hole pairs are the intermediate (virtual) states of the phonon, so they return to the original phonon after a while. The important point here is that the presence/absence of the virtual states gives an observable consequence. Namely, the presence/absence of virtual states decreases/increases the phonon energy. As can be seen in Fig. 3, when μ is close to the Dirac point (i.e., $\mu \approx 0$), all possible virtual states exist. As a result, the phonon energy takes its minimum value because the correction to the energy, which is a negative quantity as $\Pi(\mu) \propto -\int_{\mu}^{\infty} dk/(2\hbar v_F)$, is maximal in this case. By contrast, when the graphene is doped, some of the virtual states are forbidden by the exclusion principle, and the energy of the phonon increases. In fact, it can be shown that the self-energy $\Pi(\mu)$ is proportional to the density of states at μ, so $\Pi(\mu)$ increases linearly with $|\mu|$.

*2 The origin of the anisotropy of the electron-phonon matrix element is the bonding or antibonding character (or pseudospin) in graphene, which is beyond the scope of this article. (See reference [1] for details on this point.)

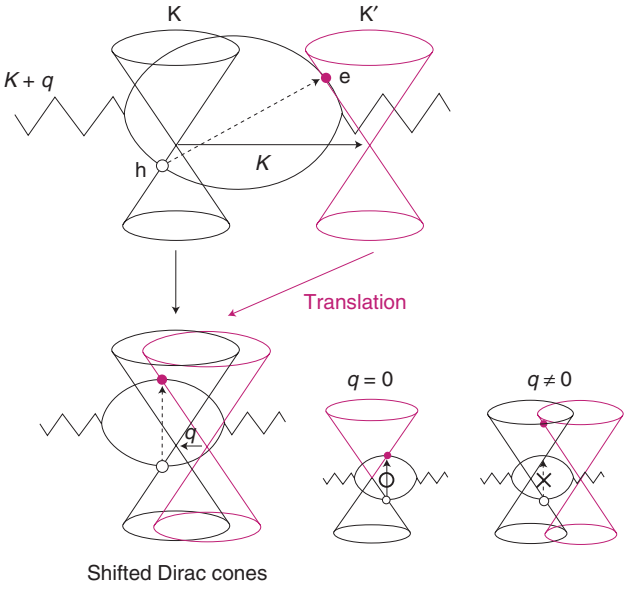

Fig. 4. The concept of shifted Dirac cones, which enables us to capture the virtual electron-hole pairs that contribute to the self-energy of an inter-valley phonon as direct electron-hole pairs.

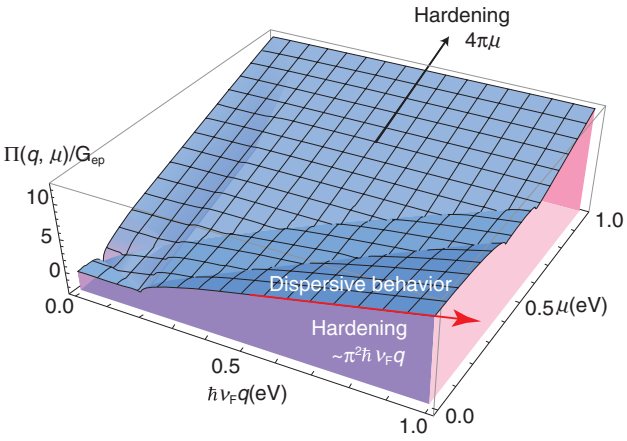

Fig. 5. Self-energy as a function of q and μ. The self-energy is scaled by the electron phonon coupling, G_{ep}.

The dispersive behavior of the 2D band can be understood in terms of self-energy in a similar manner to the doping dependence of the G band. Suppose that the A_{1g} phonon with wave vector $\boldsymbol{K} + \boldsymbol{q}$ hits an electron near the K point with $\boldsymbol{k}$, the electron is transferred from the valence to the conduction band, and the wave vector becomes $\boldsymbol{k} + (\boldsymbol{K} + \boldsymbol{q})$, due to momentum conservation. To understand the self-energy of the phonon, we need to discuss an electron-hole pair that crosses two Dirac cones. However, the fact that the electron is very far from the hole makes it very difficult to consider the presence or absence of a virtual state. Therefore, let us displace this Dirac cone from the K' point toward the K point by $-\boldsymbol{K} - \boldsymbol{q}$. Then the wave vector of the electron becomes $\boldsymbol{k}$ so that the electron is located just above the position where the hole is created. The vertical electron-hole pairs in shifted Dirac cones will be the virtual states of the A_{1g} phonon.

Let us assume that for clarity the Fermi energy is fixed at the Dirac point in **Fig. 4**. For the A_{1g} phonon with $\boldsymbol{q} \approx \boldsymbol{0}$, we can expect from the discussion of the G band that the energy will reach its minimum due to the self-energy. For the A_{1g} phonon with $\boldsymbol{q} \neq \boldsymbol{0}$, some of the low-energy virtual states are excluded, so the energy increases from $\boldsymbol{q} \approx \boldsymbol{0}$. This is very similar to the situation in which doping prevents the low-energy virtual states from contributing to the self-energy of the G band. The number of excluded virtual states increases almost linearly with the increasing q. In fact, a direct calculation shows that the self-energy is proportional to q, as $G_{ep} \times \pi^2 \hbar v_F q$, where G_{ep} is the electron-phonon coupling.

Since q is proportional to E_L, the phonon energy exhibits a linear dependence on E_L as $\hbar\omega\,(E_L) \propto \pi^2 G_{ep}\, E_L$, which is consistent with the measured dispersive behavior of the 2D band. The self-energy also depends on μ. More detailed information on the self-energy is shown in **Fig. 5**. Note that when $\mu \approx 0$, the self-energy follows $G_{ep} \times \pi^2 \hbar v_F q$.

5. Summary and discussion

We have explored the origin of the dispersive behavior for the 2D band, which is the most prominent peak in the Raman spectrum of graphene, by employing two fundamental concepts. One is the self-energy of phonons. The other is the dominance of backward scattering for the A_{1g} phonon, which is a property of electron-phonon interaction.

Some comments on the latter concept are in order. Strictly speaking, the electron-phonon matrix element squared being proportional to $1 - \cos(\Theta' - \Theta)$ does not necessarily mean that only the phonons that satisfy $q = 2k$ contribute to the 2D band, because the probability is nonzero not only for the exact backward scattering ($\Theta' = \Theta + \pi$) but also for the approximate backward scattering ($\Theta' \approx \Theta + \pi$). If we take the distribution of the approximate backward scatterings into account, it can be shown that the average q value

is a little smaller than $2k$. In fact, the average q value is given by introducing a numerical factor (1.3) as $q \approx E_L/1.3\hbar v_F$. This prediction can be verified by examining the μ dependence of the width of the 2D band [2]. A reduction factor seems to be necessary to explain the recent experimental data [3]. Meanwhile, a calculation of the S-matrix, which takes off-resonance processes into account, for the 2D band suggests that the contribution of the phonon with $q = 2k$ is strongly enhanced [4]. Thus, determining the exact q value is an unresolved problem.

The concept of migration of Dirac cones used in understanding the virtual states for the self-energy of an A_{1g} phonon may be important when graphene is subjected to strain. A uniform strain causes a shift of the Dirac cones, and the phonon's q value would be changed by applying strain to a graphene sample.

References

[1] K. Sasaki, Y. Tokura, and T. Sogawa, "The Origin of Raman D Band: Bonding and Antibonding Orbitals in Graphene," Crystals, Vol. 3, No. 1, pp. 120–140, 2013.

[2] K. Sasaki, K. Kato, Y. Tokura, S. Suzuki, and T. Sogawa, "Decay and frequency shift of both intervalley and intravalley phonons in graphene: Dirac-cone migration," Phys. Rev. B, Vol. 86, No. 20, 201403, 2012.

[3] C.-F. Chen, C.-H. Park, B. W. Boudouris, J. Horng, B. Geng, C. Girit, A. Zettl, M. F. Crommie, R. A. Segalman, S. G. Louie, and F. Wang, "Controlling inelastic light scattering quantum pathways in graphene," Nature, Vol. 471, pp. 617–620, 2011.

[4] D. M. Basko, "Theory of resonant multiphonon Raman scattering in graphene," Phys. Rev. B, Vol. 78, No. 12, 125418, 2008.

Ken-ichi Sasaki

Research Specialist, Quantum Optical Physics Research Group, Optical Science Laboratory, NTT Basic Research Laboratories.

He received the M.S. and Ph.D. degrees in science from Tohoku University, Miyagi, in 1999 and 2003, respectively. He joined NTT Basic Research Laboratories in 2010 and has been studying theoretical aspect of graphene physics. He is a member of the Physical Society of Japan and the American Physical Society.

A Novel and Simple Method of Growing Atomically Thin Hexagonal Boron Nitride

Satoru Suzuki

Abstract

Hexagonal boron nitride (h-BN), a structural analogue of graphene, is an insulating material with a large band gap. The combination of graphene and h-BN is expected to lead to a wide variety of applications. Thus, the demand for large-area and high-quality growth of h-BN is increasing. This article describes a novel and very simple method for growing a large-area and atomically thin h-BN film. In this method, an amorphous solid source is converted to crystalline h-BN through diffusion of boron and nitrogen atoms in metal foil followed by precipitation at the surface.

1. Overview of hexagonal boron nitride

Planar materials of atomic layer thicknesses, for example, graphene, are attracting much attention for their potential use as building blocks of future nanoelectronics. Hexagonal boron nitride (h-BN) is such a layered material that has a honeycomb atomic network similar to graphene. h-BN is an insulator with a large band gap of about 6 eV [1], which is in strong contrast to graphene, which has no band gap. Various applications can be expected by combining graphene and h-BN, whose structures are similar, but whose physical properties are largely different. For example, the mobility of a graphene device is known to be largely improved when h-BN is used as a substrate compared to a conventional SiO_2 substrate [2]–[5]. The reason for this is generally considered to be because h-BN has a much smaller quantity of charged impurities, which scatter carriers in graphene and reduce the mobility. Moreover, the combination of graphene and h-BN would overcome the greatest disadvantage of graphene: the poor switching property (low on/off ratio) in a FET (field-effect transistor), which originates intrinsically in the gapless electronic structure. A band gap opening is expected when graphene is transferred onto h-BN because of the stacking-induced symmetry breaking [6]–[10]. Furthermore, h-BN can also be applied as a gate insulator or a tunnel barrier in electronic devices [11], [12].

The exfoliation method has generally been used to obtain h-BN films [2], [3], [5]. In this method, a single crystal is cleaved by using adhesive tape, and a piece of the crystal is transferred onto a substrate by rubbing the tape on the substrate. (Initially, graphene was obtained exclusively using this method.) However, the typical size of the h-BN film obtained by exfoliation is only 10 μm, and the lack of scalability has prevented more common use of h-BN. Thus, the demand for large-area high-quality h-BN growth is increasing. Recently, many attempts have been made to grow large-area h-BN film by using thermal chemical vapor deposition (CVD) [4], [13]–[19]. However, the CVD method often uses a toxic and explosive gas as a feedstock.

We are researching a CVD method with the objective of obtaining high-quality and controlled growth of the number of h-BN layers [19]. We have also been developing a new method of growing h-BN that would replace the CVD technique [20]. Here, we report a novel and very simple method of growing an atomically thin h-BN film, in which an amorphous material is converted to crystalline h-BN.

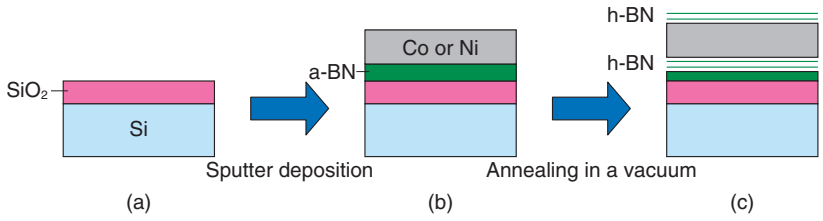

Fig. 1. Schematic of the growth method for h-BN film. (a) Initial substrate. (b) Sequential sputter deposition of a-BN and Co or Ni films on the substrate. (c) Annealing in vacuum results in the formation of h-BN films on both topmost and bottom surfaces of the metal film. Here, we focus on the h-BN film formed on the topmost surface.

2. Growth of h-BN using a solid source

Our method of growing a h-BN film is schematically shown in **Fig. 1**. A thermally stable SiO_2/Si wafer is used as a substrate (Fig. 1(a)). An amorphous boron nitride (a-BN) film 30 nm thick is deposited on the substrate by radio frequency (rf) magnetron sputtering using a sintered BN target. Sequentially, a polycrystalline Ni or Co film 300 nm thick is deposited by rf magnetron sputtering (Fig. 1(b)). The sample was inserted in a quartz tube furnace and heated at 930˚C for 10 to 30 min in a high vacuum. An atomically thin h-BN film is formed on the surface of the sample by the heating process (Fig. 1(c)). With this method, we can in principle obtain a h-BN film as large as the substrate that can be set in the furnace and sputtering machine. Another major advantage is that this method is much simpler and safer because no toxic or explosive gases are required.

The grown h-BN film can be transferred onto any kind of substrate by etching the metal film in an acid. An optical microscope image of a h-BN film transferred to a SiO_2/Si substrate is shown in **Fig. 2**. The h-BN film is scarcely visible because of the high transparency in the visible light. Similarly, graphene can also be transferred to a substrate. Therefore, we can fabricate various graphene/h-BN stacking structures by using the transfer technique.

h-BN has a band gap in the ultraviolet (UV) region and reflects a part of photons whose energy is larger than the band gap. UV reflectance spectra obtained from Ni and Co samples after heating are shown in **Fig. 3**. The peaks observed at about 6.3 eV are characteristic in h-BN, and thus, the appearance of the peaks is indicative of the formation of h-BN (The other part of each spectrum is mainly due to reflection by a Ni or Co film underneath the h-BN film.).

A cross-sectional transmission electron microscope image of a Co sample is shown in **Fig. 4**. The observed layered structure is also specific to h-BN. The figure indicates that the h-BN film consists of about four

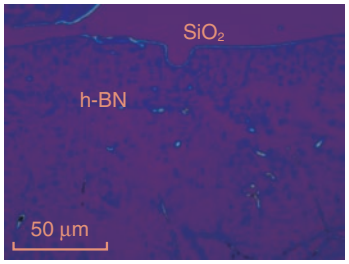

Fig. 2. Optical microscope image of a h-BN film transferred to a SiO_2/Si substrate.

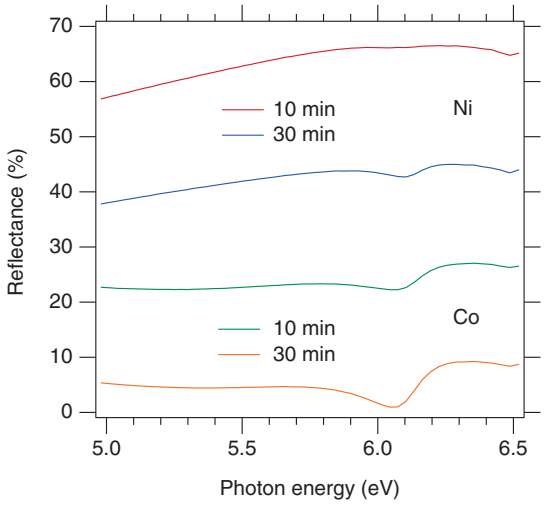

Fig. 3. UV reflectance spectra of h-BN films grown on Ni and Co.

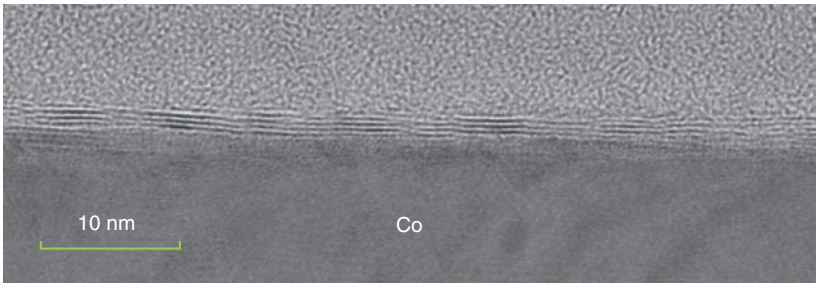

Fig. 4. Cross-sectional TEM image of a h-BN film grown on Co.

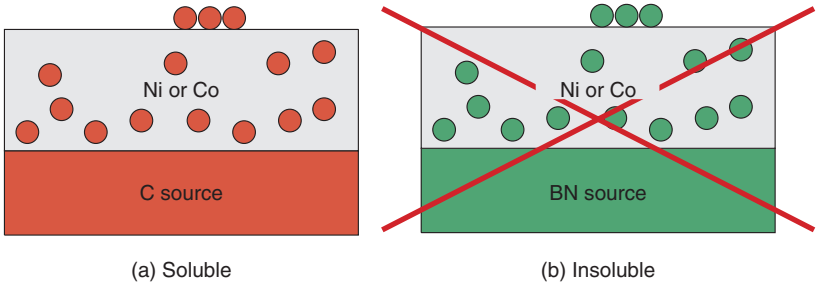

Fig. 5. Carbon is soluble, but BN is insoluble.

atomic layers. This growth method makes it possible to obtain such an atomically thin film.

3. Growth mechanism

Incidentally, why is a h-BN film formed in this method shown in Fig. 1? The B and N source material, a-BN, is initially embedded in the thick metal film. To begin with, how can B and N atoms reach the metal surface? It is known that a graphite film is formed on the surface by heating when the a-BN film in Fig. 1(b) is replaced with an amorphous carbon (a-C) film. This phenomenon is explained as follows. A considerable amount (~1 at.%) of carbon is soluble in Ni or Co at high temperatures near 1000˚C, as schematically shown in **Fig. 5(a)**. Thus, some of the carbon atoms are dissolved in the metal during the heating in the furnace. The carbon atoms dissolved at the interface move to the inside of the metal by diffusion. After a certain period, the dissolved carbon atoms are uniformly distributed in the metal. Here, heating is stopped and the temperature decreases. Accordingly, carbon solubility in the metal also decreases. Then, the excess carbon atoms, which can no longer be dissolved in the metal, precipitate on the surface and form a graphite film. One may expect that this scenario can be applied to the h-BN case. Unfortunately, however, this scenario cannot explain the h-BN formation. This is because BN or N solubility in Ni or Co is virtually zero even at high temperature. (B alone is known to be slightly soluble at high temperature.) Again, how can N atoms move in the metal and reach the surface? The detailed mechanism is not clear at present, but some experimental results have been obtained that provide some insight into the issue. A scanning electron microscope (SEM) image of a Ni sample after heating is shown in **Fig. 6(a)**. Although the entire surface is covered by a h-BN film, it is thin enough for electrons to penetrate, and the observed contrast is due to the morphology of the Ni film. The figure shows that a polycrystalline Ni film is formed after heating, in which the typical grain size is micrometer scale. B(KLL) and N(KLL) Auger electron* mapping images showing the amount of B and N at the surface are shown in **Figs. 6(b)** and

* Auger electron: An electron emitted from an excited atom having a core-hole. It has a kinetic energy specific to the atom. In this study, a K shell electron in a B or N atom is excited by a high energy electron from an electron gun, and one of the L shell electrons is emitted when the atom is relaxed.

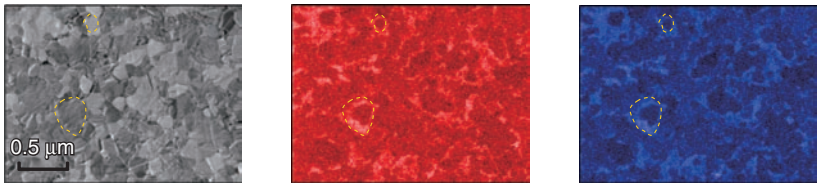

(a) SEM (b) B (c) N

Fig. 6. (a) SEM image of a Ni sample. (b) B (KLL) and (c) N (KLL) Auger mapping images from the same region as (a).

(c), respectively. The two images are largely correlated due to the formation of h-BN. The position-dependent intensity variation shows a thickness variation of the h-BN film. The thick (white) part often forms a closed curve along the fringe of a Ni grain. These results suggest that N atoms reach the surface by the grain boundary diffusion.

4. Future prospects

Currently, we are trying to make this method of h-BN growth further simpler. In this study, the a-BN and metal films were deposited by the sputtering method. Recently, however, we succeeded in growing an atomically thin h-BN film using a spin-coated solid source and commercially obtained metal foil [23]. Thus, an evaporation machine is no longer necessary for growing h-BN. We are also studying the mechanism of h-BN formation. Recent experiments suggest that the diffusion of N atoms is much slower than B and that the h-BN formation is restricted by the provision of N atoms at the surface [23]. We will also try to fabricate stacking structures of h-BN and graphene with the aim of achieving high performance and high functionality graphene devices.

References

[1] K. Watanabe, T. Taniguchi, and H. Kanda, "Direct-bandgap properties and evidence for ultraviolet lasing of hexagonal boron nitride single crystal," Nature Mater., Vol. 3, No. 6, pp. 404–409, 2004.

[2] C. R. Dean, A. F. Young, I. Meric, C. Lee, L. Wang, S. Sorgenfrei, K. Watanabe, T. Taniguchi, P. Kim, K. L. Shepard, and J. Hone, "Boron nitride substrates for high-quality graphene electronics," Nature Nanotechnol., Vol. 5, No. 10, pp. 722–726, 2010.

[3] W. Gannett, W. Regan, K. Watanabe, T. Taniguchi, M. F. Crommie, and A. Zettl, "Boron nitride substrates for high mobility chemical vapor deposited graphene," Appl. Phys. Lett., Vol. 98, No. 24, 242105, 2011.

[4] K. Lee, H. Shin, J. Lee, I. Lee, G. Kim, J. Choi, and S. Kim, "Large-Scale Synthesis of High-Quality Hexagonal Boron Nitride Nanosheets for Large-Area Graphene Electronics," Nano Lett., Vol. 12, No. 2, pp. 714–718, 2012.

[5] N. Petrone, C. R. Dean, I. Meric, A. M. van der Zande, P. Y. Huang, L. Wang, D. Muller, K. L. Shepard, and J. Hone, "Chemical Vapor Deposition-Derived Graphene with Electrical Performance of Exfoliated Graphene," Nano Lett., Vol. 12, No. 6, pp. 2751–2756, 2012.

[6] G. Giovannetti, P. A. Khomyakov, G. Brocks, P. K. Kelly, and J. van den Brink, "Substrate-induced band gap in graphene on hexagonal boron nitride: Ab initio density functional calculations," Phys. Rev. B, Vol. 76, No. 7, 073103, 2007.

[7] J. Slawinska, I. Zasada, P. Kosinski, and Z. Klusek, "Reversible modifications of linear dispersion: Graphene between boron nitride monolayers," Phys. Rev. B, Vol. 82, No. 8, 085431, 2010.

[8] A. Ramasubramaniam, "Tunable Band Gaps in Bilayer Graphene–BN Heterostructures," Nano Lett., Vol. 11, No. 3, pp. 1070–1075, 2011.

[9] N. Kharche, and S. K. Nayak, "Quasiparticle Band Gap Engineering of Graphene and Graphone on Hexagonal Boron Nitride Substrate," Nano Lett., Vol. 11, No. 12, pp. 5274–5278, 2011.

[10] R. Quhe, J. Zheng, G. Luo, Q. Liu, R. Qin, J. Zhou, D. Yu, S. Nagase, W. Mei, Z. Gao, and J. Lu, "Tunable and sizable band gap of single-layer graphene sandwiched between hexagonal boron nitride," NPG Asia Mater., Vol. 4, e16, 2012.

[11] L. Britnell, R. V. Gorbachev, R. Jalil, B. D. Belle, F. Schedin, A. Mishchenko, T. Georgiou, M. I. Katsnelson, L. Eaves, S. V. Morozov, N. M. R. Peres, J. Leist, A. K. Geim, K. S. Novoselov, and L. A. Ponomarenko, "Field-Effect Tunneling Transistor Based on Vertical Graphene Heterostructures," Science, Vol. 335, pp. 947–950, 2012.

[12] G. Lee, Y. Yu, C. Lee, C. Dean, K. L. Shepard, P. Kim, and J. Hone, "Electron tunneling through atomically flat and ultrathin hexagonal boron nitride," Appl. Phys. Lett., Vol. 99, No. 24, 243114, 2011.

[13] L. Song, L. Ci, H. Lu, P. B. Sorokin, C. Jin, J. Ni, A. G. Kvashinin, D. G. Kvashnin, J. Lou, B. I. Yakobson, and P. M. Ajayan, "Large Scale Growth and Characterization of Atomic Hexagonal Boron Nitride Layers," Nano Lett., Vol. 10, No. 8, pp. 3209–3215, 2010.

[14] Y. Shi, C. Hamsen, X. Jia, K. Kim, A. Reina, M. Hofmann, A. L. Hsu, K. Zhang, H. Li, Z. Juang, M. S. Dresselhaus, L. Li, and K. Kong, "Synthesis of Few-Layer Hexagonal Boron Nitride Thin Film by Chemical Vapor Deposition," Nano Lett., Vol. 10, No. 10, pp. 4134–4139, 2010.

[15] P. Sutter, J. Lahiri, P. Albrecht, and E. Sutter, "Chemical Vapor Deposition and Etching of High-Quality Monolayer Hexagonal Boron Nitride Films," ACS Nano, Vol. 5, No. 9, pp. 7303–7309, 2011.

[16] K. Kim, A. Hsu, X. Jia, S. Kim, Y. Shi, M. Hofmann, D. Nezich, J. F. Rodriguez-Nieva, M. Dresselhaus, T. Palacios, and J. Kong, "Synthesis of Monolayer Hexagonal Boron Nitride on Cu Foil Using Chemical Vapor Deposition," Nano Lett., Vol. 12, No. 1, pp. 161–166, 2012.

[17] A. Ismach, H. Chou, D. A. Ferrer, Y. Wu, S. McDonnell, H. C. Floresca, A. Covacevich, C. Pope, R. Piner, M. J. Kim, R. M. Wallace, L. Colombo, and R. S. Ruoff, "Toward the Controlled Synthesis of Hexagonal Boron Nitride Films," ACS Nano, Vol. 6, No. 7, pp. 6378–6385, 2012.

[18] S. Suzuki and H. Hibino, "Chemical Vapor Deposition of Hexagonal Boron Nitride," e-J. Surf. Sci. Nanotechnol., Vol. 10, pp. 133–138,

2012.
[19] C. M. Orofeo, S. Suzuki, H. Kageshima, and H. Hibino, "Growth and low-energy electron microscopy characterization of monolayer hexagonal boron nitride on epitaxial cobalt," Nano Res. Vol. 6, No. 5, pp. 335–347, 2013.
[20] S. Suzuki, R. M. Pallares, and H. Hibino, "Growth of atomically thin hexagonal boron nitride films by diffusion through a metal film and precipitation," J. Phys. D, Vol. 45, No. 38, 385304, 2012.
[21] M. Zheng, K. Takei, B. Hsia, H. Fang, X. Zhang, N. Ferralis, H. Ko, Y. Chueh, Y. Zhang, R. Maboudian, and A. Javey, "Metal-catalyzed crystallization of amorphous carbon to graphene," Appl. Phys. Lett., Vol. 96, No. 6, 063110, 2010.
[22] K. L. Saenger, J. C. Tsang, A. A. Bol, J. O. Chu, A. Grill, and C. Lavoie, "In situ x-ray diffraction study of graphitic carbon formed during heating and cooling of amorphous-C/Ni bilayers," Appl. Phys. Lett., Vol. 96, No. 15, 153105, 2010.
[23] S. Suzuki, R. Molto Pallares, C. M. Orofeo, and H. Hibino, "Boron nitride growth on metal foil using solid sources," J. Vac. Sci. Technol. B, Vol. 31, No. 4, 041804, 2013.

Satoru Suzuki
Senior Research Scientist, NTT Basic Research Laboratories.
He received the B.S., M.S., and Ph.D. degrees from Tohoku University, Miyagi, in 1990, 1992, and 1999, respectively. He joined NTT in 1992. Since 1994, he has studied synthesis and physical properties of carbon-based nanomaterials. He has also studied the correlation between the electronic structure and electrochemical properties of transition-metal-based electrode materials of rechargeable lithium ion batteries. Currently, he is studying the synthesis and properties of graphene and hexagonal boron nitride. He is a member of the Japan Society of Applied Physics, the Physical Society of Japan, and the Surface Science Society of Japan.

Exploring Relativistic Physics and Band Gap Detection in Epitaxial Graphene

Keiko Takase and Shinichi Tanabe

Abstract

Graphene is a relatively new type of material whose charge carriers exhibit unique relativistic quantum behavior. Recent progress in graphene research has revealed that high-quality and large-scale epitaxial graphene can be obtained through thermal decomposition of SiC. This article describes electrical transport measurements of carrier-density-tunable epitaxial graphene devices that shed new light on graphene. For epitaxial monolayer graphene, we first report on the unusual quantum Hall effect derived from the relativistic nature of the charge carriers and further elucidate its associated physical features. For epitaxial bilayer graphene, we present a signature of a band-gap opening that can be induced by the field effect.

1. Introduction

Graphene is a two-dimensional honeycomb lattice of carbon atoms. It was first mentioned by Dr. P. R. Wallace in the 1940s as a fascinating but imaginary concept. He found that charge carriers in graphene were governed by the relativistic quantum theory instead of by the usual quantum mechanics or classical mechanics that normally describes the motions of carriers in a solid. However, it was presumed that graphene did not exist in the real world because researchers thought that it went against the Mermin–Wagner theorem stating that a macroscopic crystalline order does not exist in two-dimensional systems at finite temperatures. This consensus on graphene was broken in 2004 and 2005 with the report stating that a monolayer of graphite, i.e., graphene, exfoliated from bulk graphite on SiO_2/Si, shows transport features of massless Dirac fermions, which are derived from the relativistic theory. Shortly after these reports were published, the stability of graphene was found to be compatible with the Mermin–Wagner theorem due to its corrugation structures, and the remarkable discovery of graphene sparked research in a variety of fields. This is because graphene is more than just a new material; it opens up possibilities for table-top experiments demonstrating relativistic physics, which have conventionally been investigated using large accelerators. This breakthrough was so remarkable that it resulted in the 2010 Nobel Prize in Physics being awarded to the researchers only five to six years after their discovery. However, studies on graphene still have a long way to go. It is likely that such studies will be extended to even more diverse fields and will also face various problems. One important issue that should be addressed is the need to develop a means of growing high-quality and large-area graphene that is suitable for industrial applications.

In this article, we present our recent research on the transport properties of monolayer and bilayer graphene grown on SiC, which we hereafter refer to as epitaxial monolayer graphene and epitaxial bilayer graphene, respectively. We first show that devices fabricated from epitaxial monolayer graphene have a high level of quality that is comparable to those fabricated using the standard exfoliation technique. This is demonstrated by the observation of a robust half-integer quantum Hall effect, which is a hallmark of the relativistic nature of charge carriers [1]. Then we show that transport measurements of epitaxial monolayer graphene can also be used as a form of energy

spectroscopy of graphene [2]. Unlike monolayer graphene, bilayer graphene is predicted to have a band gap, which has previously been investigated by optical measurements. We report here that transport measurements of epitaxial bilayer graphene can detect the signature of the band gap [3].

2. Experimental methods

We obtained epitaxial monolayer graphene and epitaxial bilayer graphene through thermal decomposition of SiC(0001). By choosing the appropriate growth conditions, we can preferentially grow either a monolayer or bilayer of graphene on a wafer scale in a controlled manner. We fabricated top-gated Hall bar devices using these graphene layers as the channel. Schematics of the top and cross-sectional views of the devices used in this study are shown in **Figs. 1(a)** and **(b)**. A gate electrode was formed above the graphene channel, separated by a dielectric layer. Applying a gate voltage between the graphene channel and the gate electrode allows us to tune the carrier density over a wide range across the charge neutrality point. Transport measurements were performed at temperatures ranging between ~1.5 and 300 K. Magnetic fields of up to 10 T were applied perpendicular to the graphene sheet for Hall measurements (Fig. 1(a)). These experimental conditions are sufficient to study the physics discussed in this article.

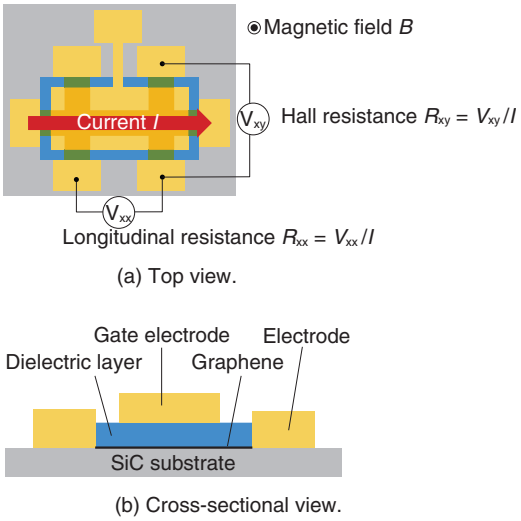

Fig. 1. Schematic of device structure.

3. Monolayer graphene: half-integer quantum Hall effect

Here, we describe the results of transport measurements of an epitaxial-monolayer graphene device, obtained at a temperature of 1.5 K and in fields from 0 to 10 T. The Hall resistance (red line) and longitudinal resistance (black line) as a function of magnetic field, obtained with gate voltage V_g fixed at zero are shown in **Fig. 2(a)**. At low fields, the Hall resistance increases proportionally with the field, while at high fields a region referred to as a plateau appears, which is characterized by a constant Hall resistance accompanied by zero longitudinal resistance. This is a phenomenon universally observed in two-dimensional electron or hole systems induced at high-quality semiconductor interfaces, and is a consequence of the discrete energy levels referred to as Landau levels that form at high fields. If we consider for simplicity spin-split Landau levels, then charge carriers filled in one Landau level contribute to Hall conductance by e^2/h. Accordingly, the Hall resistance is quantized to h/ie^2 with i being an integer, the phenomenon known as the integer quantum Hall effect (QHE). For the QHE in monolayer graphene, the Hall resistance is predicted to take the values $h/\{4(N+1/2)e^2\}$ (N: integer) at the plateaus. Because graphene has a fourfold degeneracy due to spin and valley degrees of freedom, the integer in the denominator changes by $4N$. Interestingly, a unique feature arises at the first ($N = 0$) plateau. The resistance becomes $h/\{4\times(0+1/2)e^2\}=h/(2e^2)$, and thus, a half-integer shift seems to occur. This shift is a consequence of the relativistic energy spectrum, because at high fields graphene has a zero-energy state arising from the coexistence of electrons and holes, which are equally responsible for the fourfold degeneracy.

In Fig. 2(a), plateaus labeled by the resistance values of $\pm h/(2e^2)$ and $h/(6e^2)$ are observed, and at the same time, longitudinal resistance becomes zero at the $\pm h/(2e^2)$ plateaus. We can thus say that the $\nu = 2$ quantum Hall effect (ν: the filling factor, i.e., the number of Landau levels filled with electrons or holes) is well developed. Furthermore, we can also confirm that graphene has bipolar charged carriers by observing the dependence of Hall resistance on V_g (**Fig. 2(b)**), which changes from positive to negative at $V_g = -22$ V because of changes in the positive and negative signs of the carriers. These observations in which we verified the bipolar half-integer quantum Hall effect led to the conclusion that our device fabricated from epitaxial monolayer graphene is as high in quality as those fabricated from graphene exfoliated

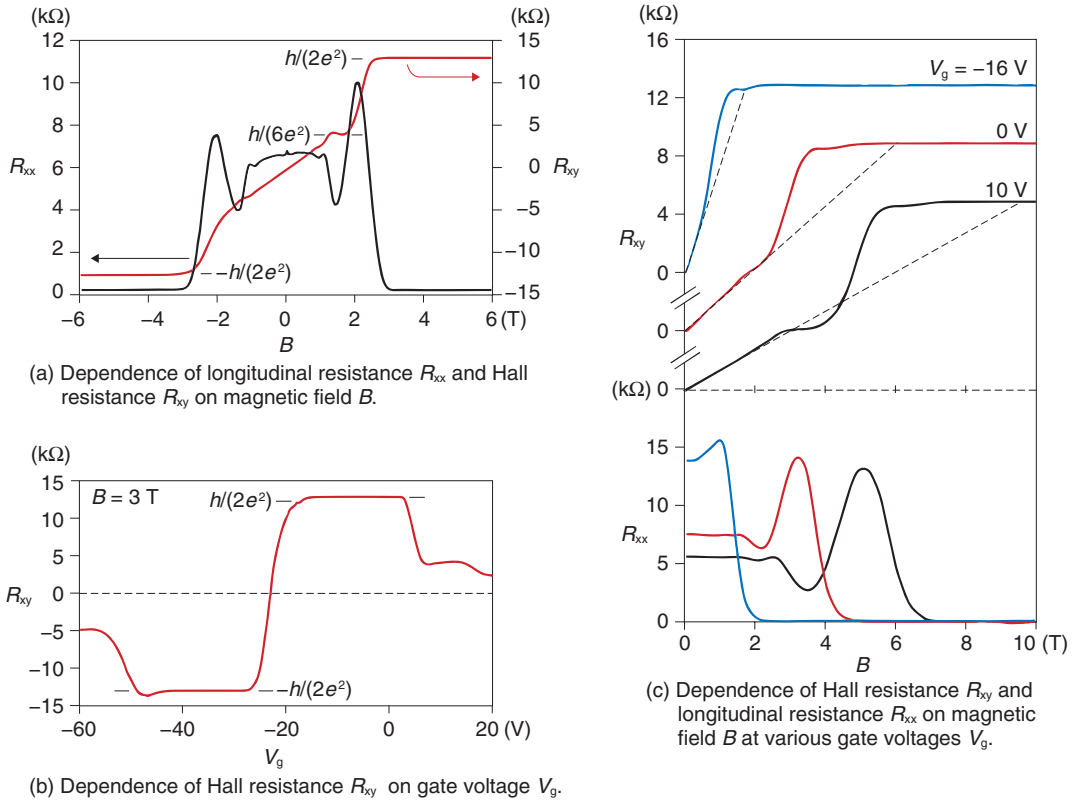

(a) Dependence of longitudinal resistance R_{xx} and Hall resistance R_{xy} on magnetic field B.

(b) Dependence of Hall resistance R_{xy} on gate voltage V_g.

(c) Dependence of Hall resistance R_{xy} and longitudinal resistance R_{xx} on magnetic field B at various gate voltages V_g.

Fig. 2. Half-integer quantum Hall effect in epitaxial monolayer graphene.

from bulk graphite [1]. Moreover, in our devices, the carrier density can be modulated over a wide range using the gate electrode. Then the type of carrier can be varied between electrons and holes across the Dirac point, where electrons and holes ideally vanish. Such a device using epitaxial monolayer graphene has not been demonstrated previously. This gives us a definite advantage in exploring an area of physics that has not been revealed for epitaxial monolayer graphene.

4. Monolayer graphene: spectroscopy through transport measurements

Next, we show an example to illustrate the advantage of the wide tunability offered by our epitaxial-monolayer graphene devices. The results were measured for another sample and show the field-dependence of Hall and longitudinal resistances obtained for different gate voltages; these results are shown in **Fig. 2(c)**. As the graph clearly shows, the $\nu = 2$ QH regime starts from lower fields for lower carrier densities, and it persists up to the highest field for all the carrier densities shown. This feature has not been observed for graphene on SiO_2/Si, and is thus a feature specific to epitaxial monolayer graphene, referred to as *the anomalously wide $\nu = 2$ QH state*. The mechanism for this anomalous behavior has remained elusive but was recently revealed by our study, as reported below.

A mapping of longitudinal resistance R_{xx} plotted as a function of gate voltage and magnetic field is shown in **Fig. 3(a)**. The trajectories of R_{xx} peaks displayed in Fig. 2(c) are represented in Fig. 3(a) as parabolic curves centered at $V_g = -37$ V. R_{xx} mapping obtained for a conventional exfoliated graphene device shows linear trajectories of the R_{xx} peaks, as presented in **Fig. 3(b)**. A comparison of Figs. 3(a) and (b) demonstrates that the $\nu = 2$ QH regime is significantly wider in epitaxial monolayer graphene than in exfoliated graphene. This anomalous wideness is intuitively attributed firstly to the parabolic trajectories of the R_{xx} peaks and secondly to the width of the R_{xx} peak at $\nu = 0$, which is nearly unchanged with increasing fields.

To clarify the underlying mechanism of the

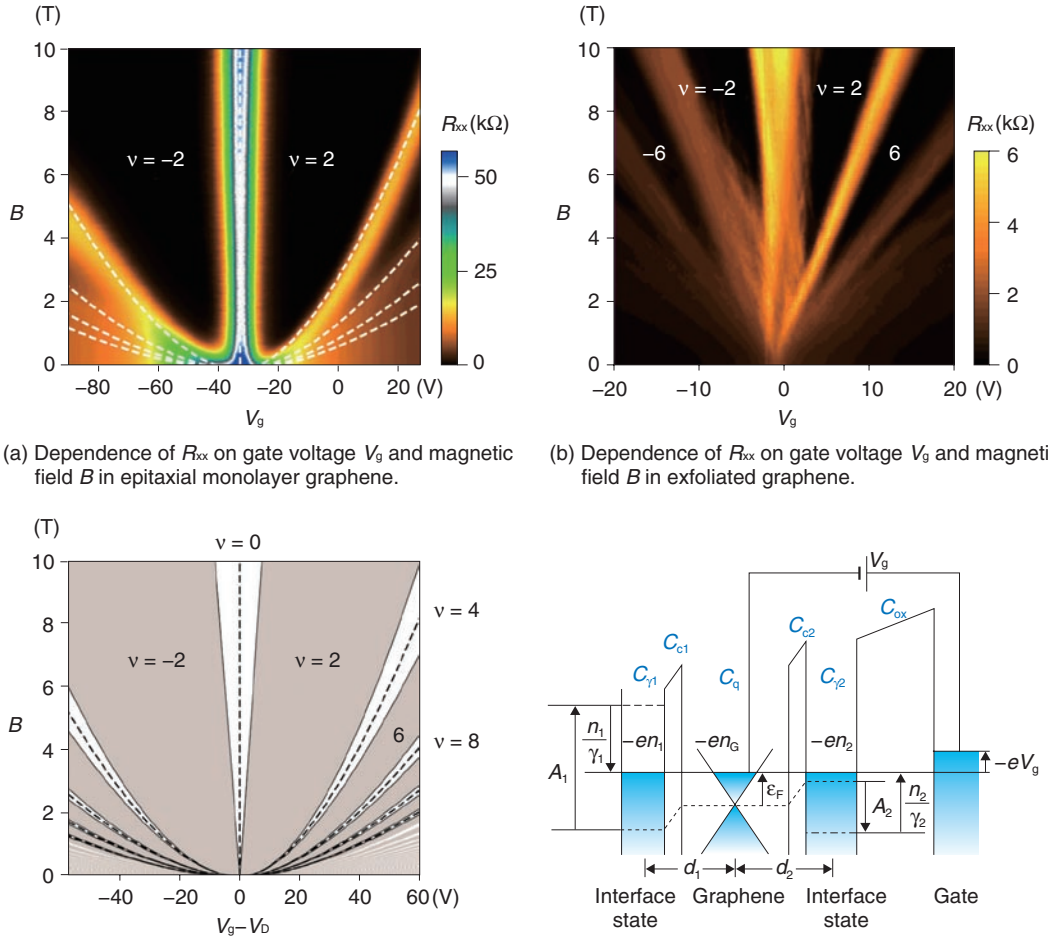

(a) Dependence of R_{xx} on gate voltage V_g and magnetic field B in epitaxial monolayer graphene.

(b) Dependence of R_{xx} on gate voltage V_g and magnetic field B in exfoliated graphene.

(c) Simulation to reproduce experimental results in (a).

(d) Model used for simulation in (c).

Fig. 3. Experimental data and simulation results on the *anomalously wide* ν = 2 *quantum Hall state*.

anomalously wide ν = 2 QH regime, we first examined the V_g dependence of the carrier density deduced from Hall resistance at low fields. The V_g dependence would be linear in ideal two-dimensional systems; however, it is parabolic in our epitaxial-monolayer graphene devices. In addition, around the Dirac point, the change in carrier density induced by a change in V_g is much smaller than that expected from the device geometry. This may indicate that some additional charge reservoir other than graphene exists in the devices. Likely candidates are interface states such as dangling-bond states at the interface with the SiC substrate or those in the gate insulator; the former is known to inevitably occur in devices fabricated from epitaxial monolayer graphene grown under standard conditions. We then developed a model describing the interplay between graphene quantum capacitance and interface-state capacitances (**Fig. 3(d)**). By applying this model to the V_g dependence of the carrier density deduced at low fields, we can deduce the interface state densities and reproduce the trajectories of the R_{xx} peaks in the gate-voltage vs. field plane (Fig. 3(a), white dashed lines). Furthermore, when we take into account the fourfold degeneracy of graphene Landau levels, we can calculate the borderlines separating integer and noninteger ν, which are in good agreement with our experiment. Therefore, our study demonstrates that the origin of the anomalously wide ν = 2 QH state is the interplay between graphene quantum capacitance and interface-state capacitances [2]. More importantly, when the interface state densities are much larger than the density of states in graphene, the Fermi energy of graphene becomes proportional to the gate voltage. Consequently, the R_{xx} peaks plotted vs. V_g and field closely resemble the relativistic LL (Landau level) diagram plotted vs.

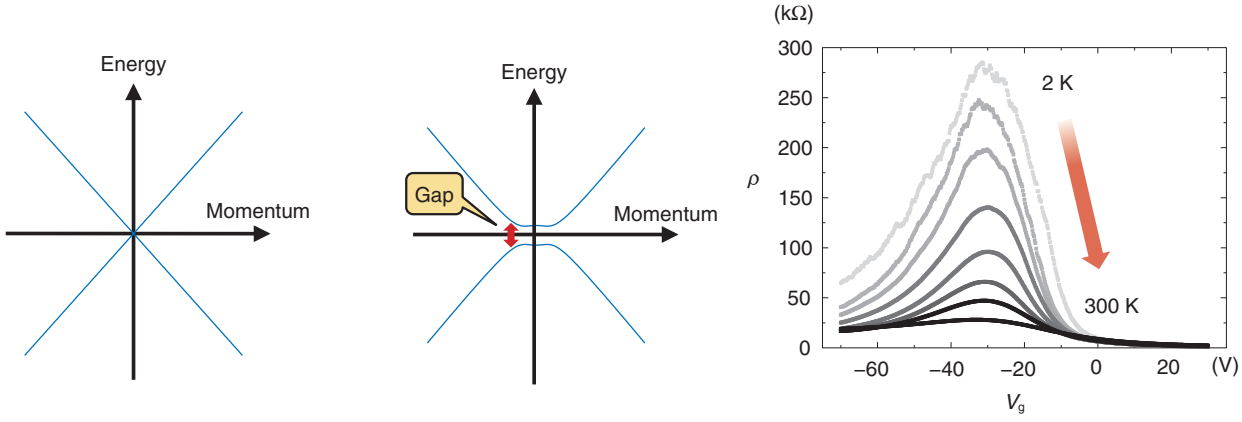

(a) Band structure of monolayer graphene.

(b) Band structure of bilayer graphene under electric field perpendicular to the plane.

(c) Dependence of resistivity ρ on gate voltage V_g in epitaxial bilayer graphene.

Fig. 4. Band structures of monolayer and bilayer graphene together with transport properties of epitaxial bilayer graphene.

energy and field. This indicates that transport measurements serve as a kind of spectroscopy, which allows us to deduce the energy width of the disorder-broadened LLs, which has been an important issue in graphene research.

5. Bilayer graphene: electrical detection of band gap opening

We next present a signature of a band gap opening in epitaxial bilayer graphene. In order to explain our experimental results, we briefly describe the band structures of monolayer graphene and bilayer graphene.

The energy band structure of monolayer graphene is shown in **Fig. 4(a)**. The conduction and valence bands touch each other at the Dirac point, which means that monolayer graphene does not have a band gap. This becomes a drawback of monolayer graphene when it is used as a channel in logic devices because a large on/off ratio cannot be expected. Although graphene that is patterned into nanoribbons, which are strips of graphene in nanometer-scale width, is predicted to have a band gap, making such nanoribbons with uniform widths and controlled edge structures is still a formidable experimental challenge.

However, opening a band gap was more easily achieved in bilayer graphene, where a band gap appears between the valence and conduction bands when there is a potential difference between the two graphene layers, as shown in **Fig. 4(b)**. The potential difference can be easily induced by applying an electric field perpendicular to the two graphene planes in a gated structure, as shown in Fig. 1. Thus, opening a band gap is more feasible in bilayer graphene than in monolayer graphene.

Our experimental results on the gate-voltage dependences of resistivity of a top-gated Hall bar device using epitaxial bilayer graphene are shown in **Fig. 4(c)**. The data at 2 K indicate that when the gate voltage is reduced from 0 to −30 V, the resistivity increases and reaches a maximum at −30 V. The resistivity decreases as the gate voltage is further reduced from −30 to −70 V. In a Hall effect measurement, the polarity of the Hall voltage indicates that from 0 to −30 V the carriers are electrons, and their density decreases as the gate voltage approaches −30 V. The polarity of the Hall voltage is reversed when the gate voltage is reduced from −30 to −70 V, which indicates that carriers are holes in this gate voltage range. Also, the hole density increases as the gate voltage approaches −70 V. These results indicate that the increase in resistivity is due to the decrease in carrier density.

It is also clear from Fig. 4(c) that the value of the maximum resistivity decreases with increasing temperature. The strong temperature dependence of the maximum resistivity indicates that epitaxial bilayer graphene exhibits insulating behavior. This is compatible with the theoretical prediction that a band gap can be opened by the applied field effect, since the observed features can be understood by the scenario where the carriers are thermally excited from the

Fermi level situated in the gap to the conduction or valence bands. Therefore, we can conclude that we have observed a signature of the band gap opening in epitaxial bilayer graphene. Such a band gap can be tuned by the field effect and scalability of the graphene growth to an arbitrary size, which makes epitaxial bilayer graphene a very promising material for use as channels in integrated transistors.

6. Summary and future prospects

We have reported our recent experimental results on charge transport in monolayer and bilayer graphene grown on SiC. We demonstrated that epitaxial monolayer graphene shows significant relativistic charge transport and that our field-effect gated device is useful for further study of unique graphene physics. We found that for epitaxial bilayer graphene, a band gap could be opened because of the applied field effect, which will enable future applications as channels of electronic devices.

References

[1] S. Tanabe, Y. Sekine, H. Kageshima, M. Nagase, and H. Hibino, "Half-Integer Quantum Hall Effect in Gate-Controlled Epitaxial Graphene Devices," Appl. Phys. Exp., Vol. 3, No. 7, 075102, 2010.
[2] K. Takase, S. Tanabe, S. Sasaki, H. Hibino, and K. Muraki, "Impact of graphene quantum capacitance on transport spectroscopy," Phys. Rev. B, Vol. 86, 165435, 2012.
[3] S. Tanabe, Y. Sekine, H. Kageshima, M. Nagase, and H. Hibino, "Observation of Band Gap in Epitaxial Bilayer Graphene Field Effect Transistors," Jpn. J. Appl. Phys., Vol. 50, No. 4, 04DN04, 2011.

Keiko Takase
Researcher, Quantum Solid State Physics Research Group, Physical Science Laboratory, NTT Basic Research Laboratories.
She received the B.Sc., M.Sc., and Ph.D. degrees in physics from the University of Tokyo in 2004, 2006, and 2009, respectively. Since joining NTT Basic Research Laboratories in 2009, she has been engaged in research on the bilayer quantum Hall state in GaAs and the quantum Hall effect in graphene. She is a member of the Physical Society of Japan and the Surface Science Society of Japan.

Shinichi Tanabe
Researcher, Low-Dimensional Research Group, Materials Science Laboratory, NTT Basic Research Laboratories.
He received the B.E. and M.E. degrees in materials engineering from Osaka University in 2007 and 2009, and the Ph.D. degree in physics from the University of Tsukuba in 2013. Since joining NTT Basic Research Laboratories in 2009, he has been engaged in research on the transport properties of SiC graphene. He is a member of the Japan Society of Applied Physics.

Plasmon Transport in Graphene

Norio Kumada

Abstract

This article describes time-resolved measurements of plasmon transport in graphene. It is demonstrated that the plasmon velocity can be varied over two orders of magnitude by changing the magnetic field, carrier density, and the gate screening effect.

1. Introduction

Optical interconnections have the advantages of low-loss and high-speed data transmission over electrical interconnections, and consequently, optical fibers have replaced the metal cables formerly used for short-distance connections between racks and boards in supercomputers as well as for long-distance transmission over the Internet. Furthermore, many research efforts have recently been directed at controlling optical signals and replacing some electronic devices with optical ones, with the aim of further reducing the power consumption. However, the integration of optical devices into electronic chips has been hampered by the diffraction limit of light, which is typically 1000 nm.

One possible way to solve this problem is to confine optical signals to nanoscale regions in the form of plasmons. This field of research is called plasmonics, and it is being actively studied, mainly using surface plasmons on metal surfaces. However, there are fundamental limitations to using metals in plasmonics. Namely, the properties of surface plasmons are fixed by the material and the geometry. Furthermore, the loss during the propagation of plasmons is large.

NTT Basic Research Laboratories has been investigating plasmons in graphene, where tunable properties and low-loss transport of plasmons are expected. There are two kinds of plasmons in graphene (**Fig. 1**). One is called a sheet plasmon, which propagates in the two-dimensional plane. The other is called an edge magnetoplasmon (EMP), which appears only in high magnetic fields. EMPs propagate along the sample edge.

2. Methods of plasmon measurement

In this work, we carried out time-resolved measurement of plasmon transport in graphene. The device structure and the experimental setup are shown in **Fig. 2**. The graphene used was obtained by thermal decomposition of a silicon carbide (SiC) substrate. The devices are about 1 × 1 mm^2 and have four

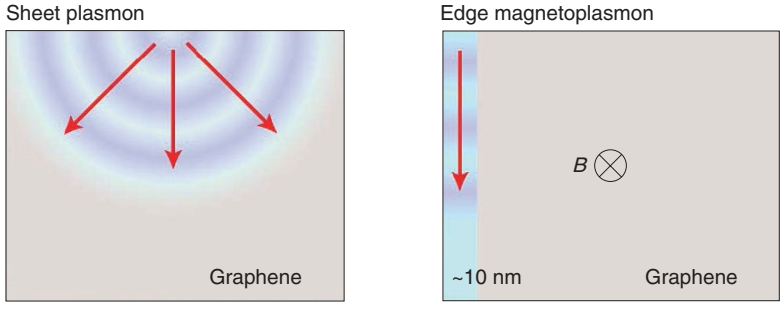

Fig. 1. Plasmons in graphene.

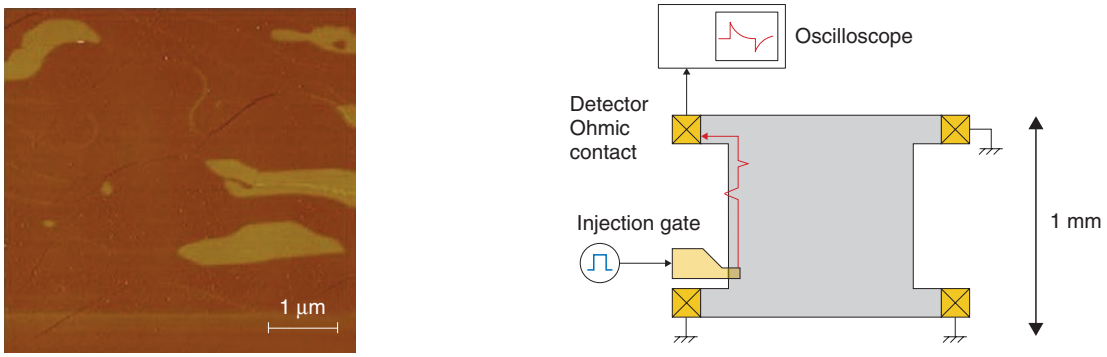

(a) Image of graphene on SiC

(b) Diagram of experimental setup.

Fig. 2. Graphene on SiC and the experimental technique.

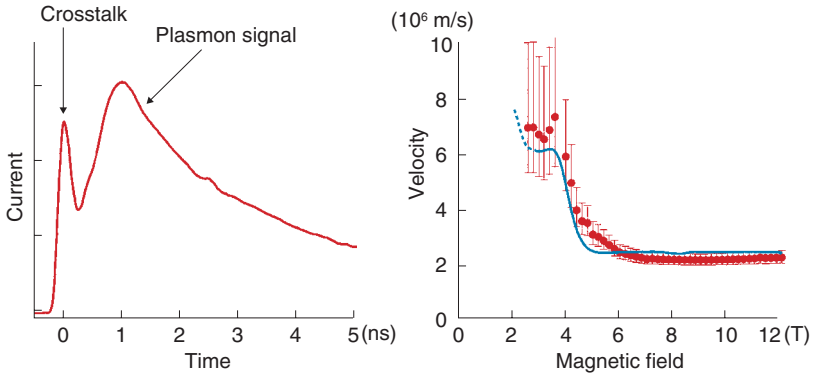

(a) Typical current trace

(b) Plasmon velocity as a function of magnetic field

Fig. 3. Plasmon velocity in the ungated sample.

Ohmic contacts. The surfaces of the devices were covered with 100-nm-thick hydrogen silsesquioxane (HSQ) and 40-nm-thick silicon dioxide (SiO_2) insulating layers. We used two samples, one with and the other without a large top gate.

For the time-resolved transport measurement, a pulsed plasmon is generated in graphene by applying a voltage step to the injection gate deposited across the sample edge. The plasmons propagate in graphene and are detected as a time-dependent current through the detector Ohmic contact using a sampling oscilloscope. The plasmon velocity can be determined by measuring the time of flight of plasmons at a time resolution of 100 ps. Although all data shown here were taken at 1.5 K in order to investigate the physics of plasmon transport in detail, we confirmed that the plasmon signal does not change much even at much higher levels, for example, up to several ten K.

3. Effects of magnetic field on plasmon transport

A typical current trace is shown in **Fig. 3(a)**. The origin of the time corresponds to the time when plasmons are injected. The sharp peak is due to crosstalk between injection and detection high-frequency lines. Since the crosstalk propagates with the speed of light, it appears with virtually zero time delay. The broader peak that appears with a time delay of about 1 ns is the plasmon signal. The time delay of the plasmon signal from the crosstalk roughly corresponds to the time of flight of plasmons. The plasmon velocity is obtained from the time of flight and the path length.

The plasmon velocity in the ungated sample as a

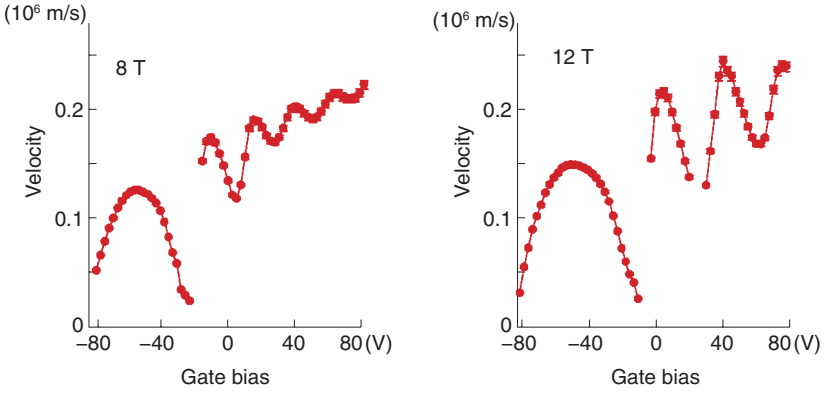

Fig. 4. Plasmon velocity in the gated sample.

function of the magnetic field is shown in **Fig. 3(b)**. The velocity is about 6000 km/s at 3 T and decreases to 2000 km/s as the magnetic field increases. This behavior can be well reproduced theoretically for EMPs (blue trace). For the magnetic field lower than 2 T, the plasmons are too fast and the velocity cannot be determined accurately. This indicates that the plasmon velocity around zero magnetic field is above the maximum measurable value of 6000 km/s.

4. Effects of carrier density and the gate screening effect on plasmon transport

The plasmon velocity in the gated sample as a function of the gate bias at magnetic fields of 8 and 12 T is shown in **Fig. 4**. The velocity is about 100 km/s, which is one order of magnitude smaller than that in the ungated sample. The smaller velocity is due to the gate screening effect. When there is a metal gate close to the graphene, the electric field in plasmons is partially screened, which reduces the velocity. As the gate bias and thus the electron density decrease, the velocity decreases to several ten km/s with oscillations. This behavior can also be qualitatively explained by EMP theory.

In summary, the velocity of plasmons in graphene can be tuned over a wide range from several ten to thousand km/s by changing the magnetic field, carrier density, and the gate screening effect. The tunability of the velocity indicates the tunability of the refractive index and the impedance. By controlling these parameters, it would be possible to develop plasmonic devices with functionalities such as plasmon switching, guiding, and routing.

This work was a collaboration between NTT Basic Research Laboratories and Tokyo Institute of Technology.

5. Future work

NTT Basic Research Laboratories has succeeded in controlling the plasmon velocity in graphene over two orders of magnitude. We will try to exploit this result in order to control the plasmon transport. Furthermore, we will estimate the loss of the plasmon signal during the propagation, which is expected to be much smaller than that in metallic systems.

References

[1] S. Tanabe, Y. Sekine, H. Kageshima, M. Nagase, and H. Hibino, "Half-integer Quantum Hall Effect in Gate-controlled Epitaxial Graphene Device," Applied Physics Express, Vol. 3, p. 075102, 2010.
[2] N. Kumada, S. Tanabe, H. Hibino, H. Kamata, M. Hashisaka, K. Muraki, and T. Fujisawa, "Plasmon transport in graphene investigated by time-resolved electrical measurements," Nature Communications, Vol. 4, p. 1363, 2013.

Norio Kumada
Senior Research Scientist (Distinguished researcher), Quantum Solid-State Physics Research Group, Physical Science Laboratory, NTT Basic Research Laboratories.
He received the B.S., M.S., and Ph.D. degrees in physics from Tohoku University, Miyagi, in 1998, 2000, and 2003, respectively. He joined Basic Research Laboratories in 2003. Since then, he has been engaged in the study of highly correlated electronic states realized in semiconductor heterostructures. He received the Young Scientist Award of the Physical Society of Japan in 2008 and the Young Scientists' Prize from the Minister of Education, Culture, Sports, Science and Technology in 2012. He is a member of the Physical Society of Japan.

Surface-enhanced Raman Scattering of Graphene on SiC

Yoshiaki Sekine, Hiroki Hibino, Katsuya Oguri, Tatsushi Akazaki, Hiroyuki Kageshima, Masao Nagase, Ken-ichi Sasaki, and Hiroshi Yamaguchi

Abstract

Raman scattering spectroscopy is a well-known optical tool for identifying the properties of graphene such as the number of layers, carrier concentration, and strain. Interaction between incident light and a metallic nanoparticle such as gold or silver enhances the intensity of light, which can be used in Raman scattering spectroscopy. This article describes our investigation of graphene properties by using surface-enhanced Raman scattering.

1. Introduction

Graphene can be grown on a silicon carbide (SiC) substrate by sublimating silicon (Si) in a high-temperature furnace. The use of high-quality and large-area graphene on SiC has enabled a high-frequency transistor and a metrological resistance standard based on the quantum Hall effect[*1] to be demonstrated. The interaction between graphene and SiC modifies the graphene carrier concentration and strain, which are basic properties for electronic devices. An electron in strained graphene behaves as if it is in a magnetic field. Strain, along with carrier concentration, is therefore a prominent property of electronic devices. Raman scattering is a non-destructive method for examining these properties. However, the Raman spectrum of SiC is superimposed on the salient spectrum of graphene, which makes it difficult to analyze the graphene's properties. Here, we explain how surface-enhanced Raman scattering (SERS) enhances only the graphene spectrum and thereby makes it possible to quantitatively analyze the Raman spectrum of graphene on SiC.

2. Raman scattering and Raman peaks of graphene

In Raman scattering, the energy of light scattered from a substance is slightly different from that of the incident light. A schematic view of Raman scattering is shown in **Fig. 1**. The process involves (i) the excitation of electrons from a ground state, (ii) the scattering of the excited electrons with energy relaxation driven by a lattice vibration, and (iii) the transition of the scattered electrons to the ground state and the emission of scattered light. The energy difference between the incident and scattered light is called a Raman shift, which is expressed in an energy unit of cm^{-1}. The energy of the lattice vibration in a material is derived from the Raman shift. Furthermore, electron states can be examined because both an electron and a lattice vibration are related to Raman scattering. The ratio of Raman scattered light to total scattered light is extremely small, and most of the scattered light is Rayleigh scattered light whose energy is the same as that of the incident light. Nonetheless, Raman scattering spectroscopy is a powerful tool for identifying material properties such as the lattice vibration and electron state.

Here, we explain the origin of the salient Raman peaks of graphene on SiC. G (~1600 cm^{-1}) and D

*1 Quantum Hall effect: In a two-dimensional electron system with a high magnetic field, the Hall resistance exhibits a quantized value, i.e., a specified fraction of an integer of a universal value of h/e^2 = 25.8128056 kΩ. The quantized Hall resistance is applied to a metrological resistance standard.

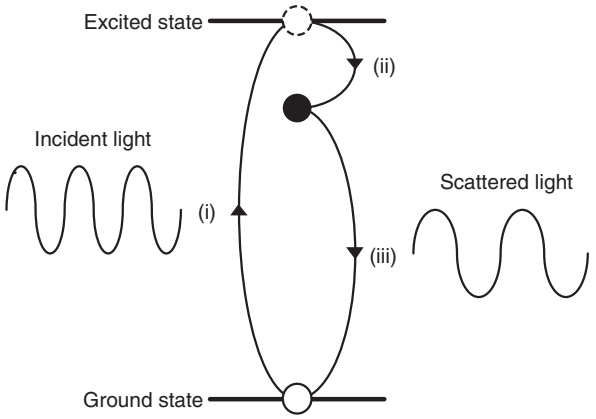

Fig. 1. Depiction of Raman scattering.

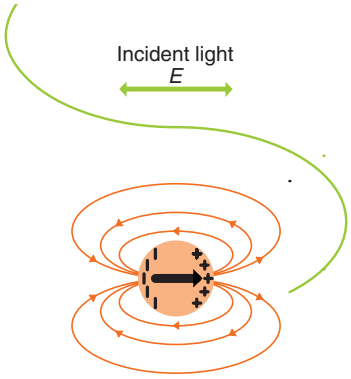

Fig. 2. Localized surface plasmon resonance.

(~1350 cm^{-1}) peaks are observed in carbon materials. The D peak originates from defects and bindings to other materials (including carbon). The D′ peak (~1630 cm^{-1}) is also due to defects and bindings and is smaller than the G and D peaks. The 2D peak (~2710 cm^{-1}) with a Raman shift nearly twice that of the D peak is observed in graphene without defects and bindings. The 2D intensity decreases as the density of defects and bindings increases.

3. Enhancement of light intensity due to localized surface plasmon resonance

The interaction between incident light and a metallic nanoparticle such as gold or silver enhances the light intensity in a small region near the nanoparticle, which is illustrated in **Fig. 2**. Incident light induces polarization in a metallic nanoparticle. The polarization generates an electric field outside the metallic nanoparticle, which can be derived by solving the electric-field equation with the boundary condition of the nanoparticle's spherical surface. The generated electric field is equivalent to the electric field induced by an electric dipole[*2] in the center of the nanoparticle. The difference between the air and metal dielectric constants, which depends on the wavelength, results in a remarkable phenomenon: in a resonance with an appropriate wavelength, i.e., localized surface plasmon[*3] resonance (LSPR), the electric dipole induces a strong electric field compared with the electric field of the incident light. The LSPR for gold and silver occurs in the visible light range (380–800 nm), and many applications exploiting LSPR have been developed because of its ability to greatly enhance the light intensity. Nanometer-scale metallic nanoparticles exhibit LSPR, and the intensity of the enhanced light decreases rapidly as the distance from the nanoparticles increases. The light enhancement only occurs in a region equivalent to the size of the metallic nanoparticle.

4. Sample fabrication and transmission electron microscopy image

Silver (Ag) nanoparticles were deposited on graphene by Ag evaporation in a high-vacuum chamber[*4]. The deposited Ag stays in the form of particles rather than forming a layer because of the inertness of graphene. These particles can move and they combine to form aggregate particles about 10 nm in size. A transmission electron microscopy[*5] (TEM) image of hemispherical Ag nanoparticles on graphene is shown in **Fig. 3(a)**. The magnified image in **Fig. 3(b)** shows that there is no damage to the graphene even

*2 Electric dipole: Positive and negative electric charges +Q and –Q are next to each other; these separated charges are referred to as an electric dipole.

*3 Plasmon: A state where charged particles such as electrons and ions move freely is called a plasma state. Collective oscillation of charged particles is known as plasma oscillation, and a quantum of plasma oscillation is referred to as a plasmon.

*4 Vacuum evaporation: A method for forming a layer on a solid surface with an evaporating or sublimating material in a vacuum. The evaporated or sublimated material attaches to a solid surface (substrate), and the deposited material generally takes the form of a thin film.

*5 Transmission electron microscopy: A microscopy technique in which a thin (less than 1 μm) specimen is irradiated with an electron beam and the contrast of the transmitted electron beam is examined.

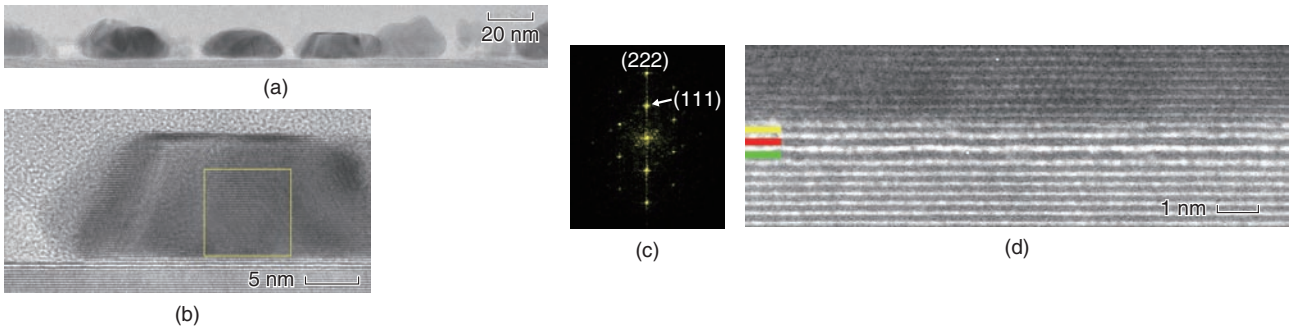

Fig. 3. (a) TEM image of Ag-deposited graphene. (b) Magnified TEM image of Ag-deposited graphene, (c) Fourier transform image of yellow square in (b), and (d) enlarged image at interface between graphene and Ag nanoparticles.

though Ag was directly deposited on it.

We first investigated the structure of crystallized Ag nanoparticles on graphene. In **Fig. 3(c)**, a Fourier transform*6 image of the yellow square in Fig. 3(b) is displayed with the corresponding reciprocal lattice vector of a point that represents the distance of a lattice plane. It is clearly seen that the (111) plane of Ag (face-centered cubic) attaches to the graphene, which is reasonable by considering the lattice constants of Ag and graphene. A magnified image at the interface between an Ag nanoparticle and graphene is shown in **Fig. 3(d)**, where yellow, red, and green lines indicate Ag, graphene, and a buffer layer (a non-conductive carbon layer between the graphene and SiC, where a carbon atom binds to the SiC). We measured the distance between an Ag nanoparticle and the graphene from the TEM image and averaged the distance measured at many points to obtain a distance of 3.14 ± 0.13 Å. By considering a theoretical calculation that the distance is 3.33 Å for physisorption and less than 2.3 Å for chemisorption [1], we conclude that Ag nanoparticles attach to graphene without chemical bonds, i.e., in a physisorbed state, which is consistent with there being no degradation of the graphene under the nanoparticles.

5. Surface-enhanced Raman scattering of graphene on SiC

Without the Ag deposition, the SiC peaks overwhelm the graphene feature of D and G peaks as shown in **Fig. 4(a)**. Enlarged plots of the D, G, and 2D peaks of graphene without Ag nanoparticles are shown in **Fig. 4(b)**. Although there is no SiC peak around the 2D peak of graphene, the SiC peak is superimposed on the graphene D and G peaks, which makes quantitative analysis difficult. With the Ag deposition, the spectrum of graphene with Ag nanoparticles (red) overwhelms that of the SiC substrate (gray). A comparison of the signals of graphene with Ag nanoparticles (red) and without them (green), shows that the enhanced signal of graphene with Ag nanoparticles exhibits clear graphene features of D, G, and 2D peaks. By comparing the 2D peak intensity of graphene with and without Ag nanoparticles, we obtain a nominal enhancement of 37.

The large enhancement paves the way to quantitatively analyzing the D and G peaks of graphene on SiC as shown in **Fig. 4(c)**. Sub-peaks at 1320 and 1400 cm^{-1} are observed in addition to the main D peak at 1360 cm^{-1}. Our SERS method reveals the sub-peak structure, which cannot be resolved in conventional Raman spectroscopy. The G peak also has a sub-peak structure at 1580 cm^{-1} below the most prominent peak at 1600 cm^{-1}. Furthermore, the D′ peak is observed at 1630 cm^{-1}. The peaks at 1580 and 1600 cm^{-1} are graphene peaks, not SiC peaks. We know this because those peaks are observed in micromechanically cleaved graphene*7 on a Si substrate [2]. As shown in the graph, three-curve fitting is applied to the spectrum around the G peak. The yellow curves represent the summation of the three fitting curves, and the yellowish-brown ones represent each fitting curve.

*6 Fourier transform: A mathematical transform to investigate a periodic structure. With the Fourier transform, the distance of a lattice plane can be obtained from a crystalline image.

*7 Micromechanically cleaved graphene: Graphene (monolayer) can be cleaved from graphite (comprising many layers of graphene) with adhesive tape. Though micromechanically cleaved graphene can be obtained using only adhesive tape, it is difficult to obtain large-area and homogeneously layered graphene.

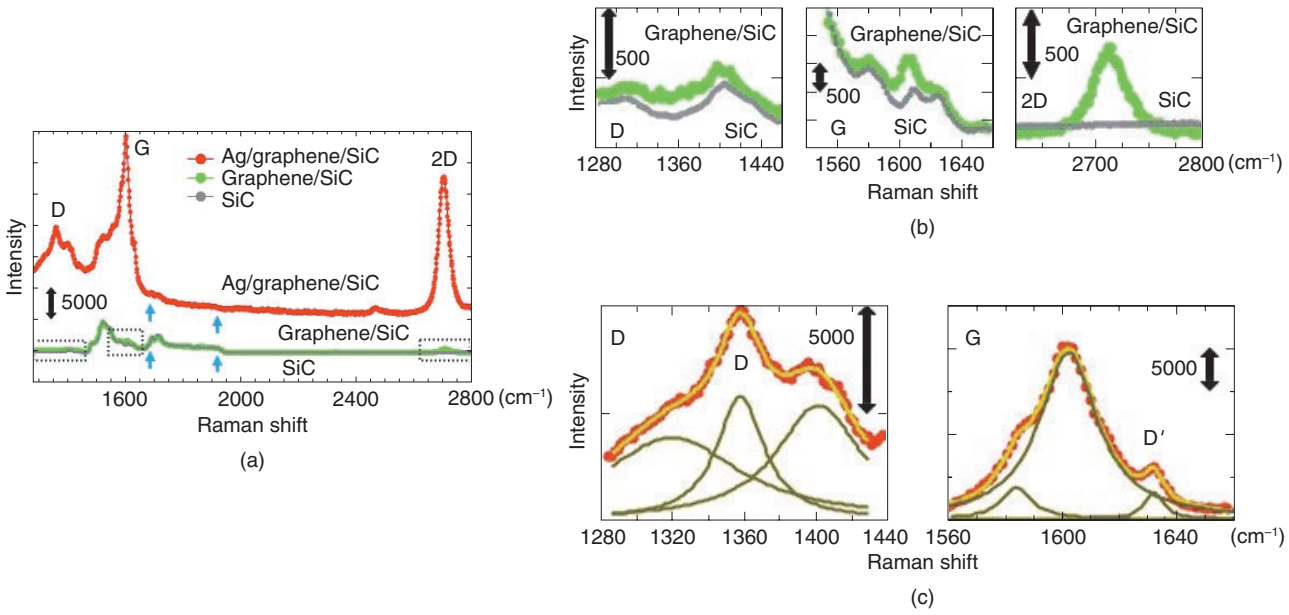

Fig. 4. Raman scattering of graphene on SiC: (a) Raman spectra of Ag-deposited graphene, graphene, and SiC, (b) magnified graphs of D, G, and 2D peaks of graphene, and (c) enlarged plots of D and G peaks of Ag-deposited graphene.

The D and D′ peaks, which are caused by disorder, are observed in graphene with Ag nanoparticles. We attribute them to defects or the buffer layer that was originally present in our sample because no damage is found in the TEM images. Quantitative analysis of the D, D′, and G peaks makes it possible to assess disorder in graphene. The peak intensity ratio of D to G and that of D′ to G are obtained from the fitting, and they are an order smaller than those of nanocrystalline graphene [3]. Our SERS technique is a powerful method for analyzing the D and G peaks of graphene on SiC and resolving the sub-peak structures, which cannot be observed in conventional Raman spectroscopy.

6. Doping effect

The Ag deposition has a doping effect on graphene, which can be estimated by SERS. The carrier density of graphene is derived from the peak intensity ratio of 2D to G [4]. An electron density of 1.9×10^{13} cm^{-2} is obtained for graphene with Ag nanoparticles. Using an electrical measurement, we estimated a typical electron density of approximately 1×10^{12} cm^{-2} for graphene without Ag nanoparticles. Our results are consistent with a theoretical calculation that shows Ag-deposited graphene is electron-doped [1].

Care should be taken in estimating the SERS enhancement because the 2D peak intensity decreases as the carrier density increases [5]. By considering the doping effect due to the Ag deposition, the nominal enhancement of 37 is modified to the actual enhancement of approximately 100. The estimation of the correct enhancement is obtained by quantitatively analyzing the electron density of graphene.

7. Enhancing only the graphene signal

The enhancement of only the graphene signal is what makes the quantitative analysis possible. The graphene spectrum is enhanced, while the SiC spectrum is suppressed. The SiC spectrum with Ag nanoparticles becomes around half that without Ag nanoparticles, which is clearly seen in the two peaks at 1700 cm^{-1} and the shoulder at 1930 cm^{-1} as indicated by the blue arrows in Fig. 4(a). The light incident to SiC and the light scattered from it are blocked by the Ag nanoparticles. Furthermore, the small region of enhanced light due to LSPR has an impact on the observed phenomenon, as shown in **Fig. 5**. The region of enhanced light is on the order of the size of the Ag nanoparticles, i.e., 10 nm; therefore, the observed region is also 10 nm in depth. The spot size of the laser in our experiments was 1 μm, and the

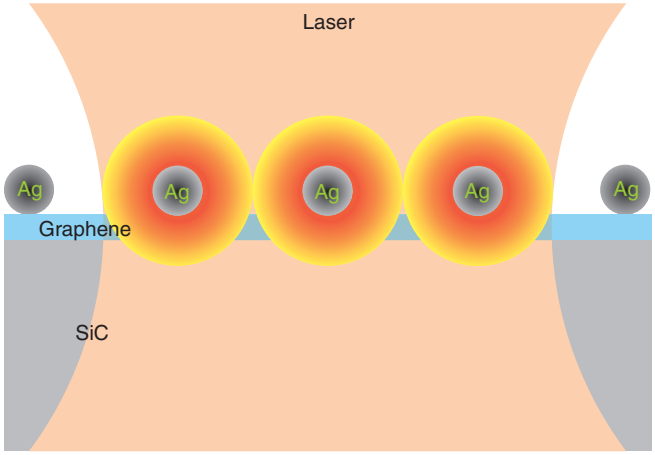

Fig. 5. Enhancement of graphene by localized surface plasmon resonance.

observed region without Ag nanoparticles was 1 μm in depth. Here, we consider the volume of graphene (monolayer) to the observed region. The volume with Ag nanoparticles is monolayer in 10 nm, and that without them is monolayer in 1 μm, respectively. The volume of monolayer graphene to the observed region with Ag nanoparticles was 100 times larger than that without them. Consequently, our SERS method makes it possible to enhance only the graphene signal efficiently.

8. Further study

In this article, we showed that the sub-peak structure of the D and G peaks of graphene on SiC with Ag nanoparticles can be revealed using SERS. Thanks to the efficient enhancement of only the graphene signal, the carrier concentration can be obtained by quantitatively analyzing the graphene peaks. We plan to use our SERS technique to estimate the strain due to the interaction between graphene and SiC. The buffer layer between graphene and SiC has an impact on the strain in graphene, and it is removed by high-temperature annealing in a hydrogen atmosphere. We will also investigate the difference between the strain in graphene with and without the buffer layer. Our SERS technique is therefore effective for quantitatively obtaining the basic properties of graphene on SiC.

References

[1] G. Giovannetti, P. A. Khomyakov, G. Brocks, V. M. Karpan, J. van den Brink, and P. J. Kelly, "Doping Graphene with Metal Contacts," Phys. Rev. Lett., Vol. 101, No. 2, 026803, 2008.
[2] J. Lee, K. S. Novoselov, and H. S. Shin, "Interaction between Metal and Graphene: Dependence on the Layer Number of Graphene," ACS Nano, Vol. 5, No. 1, pp. 608–612, 2011.
[3] E. H. Martins Ferreira, M. V. O. Moutinho, F. Stavale, M. M. Lucchese, R. B. Capaz, C. A. Achete, and A. Jorio, "Evolution of the Raman spectra from single-, few-, and many-layer graphene with increasing disorder," Phys. Rev. B, Vol. 82, No. 12, 125429, 2010.
[4] A. Das, S. Pisana, B. Chakraborty, S. Piscanec, S. K. Saha, U. V. Waghmare, K. S. Novoselov, H. R. Krishnamurthy, A. K. Geim, A. C. Ferrari, and A. K. Sood, "Monitoring dopants by Raman scattering in an electrochemically top-gated graphene transistor," Nat. Nanotechnol., Vol. 3, No. 4, pp. 210–215, 2008.
[5] C. Casiraghi, "Doping dependence of the Raman peaks intensity of graphene close to the Dirac point," Phys. Rev. B, Vol. 80, No. 23, 233407, 2009.

Yoshiaki Sekine
Researcher, Low-Dimensional Nanomaterials Research Group, Materials Science Laboratory, NTT Basic Research Laboratories.

He received the B.S. degree in engineering from Hokkaido University in 1994 and the M.S. and Ph.D. degrees in science from the University of Tokyo in 1996 and 1999, respectively. He joined NTT Basic Research Laboratories in 1999 and has been studying low-dimensional semiconductor physics. He is currently engaged in an experimental study of the optical and electrical properties of graphene. He is a member of the Physical Society of Japan (JPS) and the Japan Society of Applied Physics (JSAP).

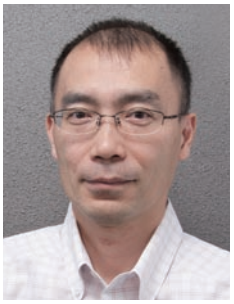

Hiroki Hibino
Executive Manager of the Materials Science Laboratory and Group Leader of the Low-Dimensional Nanomaterials Research Group at NTT Basic Research Laboratories.

He received the B.S. and M.S. degrees in physics from the University of Tokyo in 1987 and 1989, respectively and the Ph.D. degree in pure and applied physics from Waseda University, Tokyo, in 2006. In 1989, he joined NTT Basic Research Laboratories, where he has been studying surface dynamical processes using microscopic techniques. His research interests include step structures on vicinal surfaces, surface mass transport, step instability during epitaxial growth, self-assembled nanostructure formation, and epitaxial graphene growth. He spent one year as a visiting research professor at Arizona State University during 2000–2001. He also has experience as a visiting professor at Tokyo Institute of Technology (2007–), Kyushu University (2009–2010), and the University of Tokyo (2011–).

Katsuya Oguri
Senior Research Scientist, Quantum Optical Physics Research Group, Optical Science Laboratory, NTT Basic Research Laboratories.

He received the B.S., M.S., and Ph.D. degrees from the University of Tokyo in 1996, 1998, and 2006, respectively. He joined NTT Basic Research Laboratories in 1998. Since then, he has been engaged in the study of ultrafast x-ray spectroscopy with laser-produced-plasma x-rays and high-order harmonics. His current interest is ultrafast graphene dynamics investigated with ultrafast x-ray spectroscopy techniques. He is a member of JSAP and the Optical Society of America.

Tatsushi Akazaki
Professor, Department of Electrical Engineering and Information Science, Kochi National College of Technology.

He received the B.S. and M.S. degrees in physics from Kyushu University, Fukuoka, in 1984 and 1986, respectively, and the Ph.D. degree in electrical engineering from Osaka University in 1995. He joined NTT Basic Research Laboratories in 1986, where he engaged in research on the transport properties of semiconductor-coupled superconducting devices. In 2013, he moved to Kochi National College of Technology. He is a member of JPS and JSAP.

Hiroyuki Kageshima
Senior Research Scientist, Nano-devices Research Group, Physical Science Laboratory, NTT Basic Research Laboratories. Joint Graduate Program Visiting Professor in Department of Nanosystem Science, Graduate School of Nanobioscience, Yokohama City University. Visiting Lecturer in Graduate School of Science and Technology, Keio University.

He received the Ph.D. degree in science from the University of Tokyo in 1991. He joined NTT Basic Research Laboratories in 1991 and has been studying semiconductor physics theory. He is a member of JPS and JSAP.

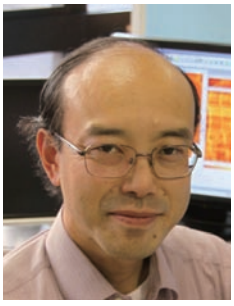

Masao Nagase
Professor, Material Science and Devices, Department of Electrical and Electronic Engineering, Faculty of Engineering, the University of Tokushima.

He received the B.E., M.S., and Dr.Eng. degrees in nanometrology for nanodevices from Waseda University, Tokyo, in 1982, 1984, and 1997, respectively. In 1984, he joined the LSI Laboratories of Nippon Telegraph and Telephone Public Corporation (now NTT), where he worked on R&D of fabrication processes for submicrometer VLSIs. In 1996, he moved to NTT Basic Research Laboratories, where he researched fabrication processes for mesoscopic devices such as single-electron, NEMS, and graphene devices in the Nanostructure Technology Research Group of the Physical Science Laboratory. He moved to the University of Tokushima in 2010. His current research field is nanocarbon engineering. He is a member of JSAP.

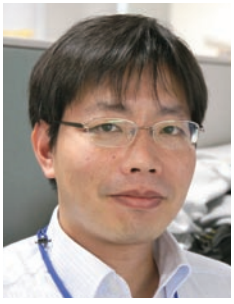

Ken-ichi Sasaki
Research Specialist, Quantum Optical Physics Research Group, Optical Science Laboratory, NTT Basic Research Laboratories.

He received the M.S. and Ph.D. degrees in science from Tohoku University, Miyagi, in 1999 and 2003, respectively. He joined NTT Basic Research Laboratories in 2010 and has been studying theoretical aspect of graphene physics. He is a member of JPS and the American Physical Society.

Hiroshi Yamaguchi
Senior Distinguished Researcher and Group Leader of the Hybrid Nanostructure Physics Research Group, Physical Science Laboratory, NTT Basic Research Laboratories.

He received the B.E. and M.S. degrees in physics and the Ph.D. degree in engineering from Osaka University in 1984, 1986, and 1993, respectively. He joined NTT Basic Research Laboratories in 1986. His current interests are micro/nanomechanical devices using semiconductor heterostructures. He has been a guest professor at Tohoku University since 2006. He is a fellow of the Institute of Physics and a member of JPS, JSAP, and IEEE.

Biosensing on a Graphene Oxide Surface

Kazuaki Furukawa and Yuko Ueno

Abstract

This article describes our recent research on a selective protein detection system built on a graphene oxide (GO) surface. Our original idea is to fix pieces of GO on a solid support. This enables direct observation of chemical reactions occurring on the GO surface and on-chip device fabrication. The basic principle can be applied to other proteins as well as other biological molecules simply by changing the molecules to be modified, which makes GO a versatile platform for integrated biosensing devices.

1. Introduction to graphene oxide

Graphene oxide (GO) has a sheet-like structure similar to graphene, but its preparation method and electronic properties are very different from those of graphene. Let us take a brief look at the similarities and differences between GO and graphene. The schematic chemical structure of graphene and GO are shown in **Fig. 1**. Graphene consists solely of benzene rings made of carbon (C) atoms with C=C double bonds (sp^2 bonds). In GO, many of the double bonds in graphene are scissored and linked to oxygen (O) to form C-O bonds, which yields C-C single bonds (sp^3 bonds). Mobile π electrons that dominate the conductivity in graphene are lost at the oxidized bonds. Thus, GO becomes an insulator. Many articles in this special issue describe research concerning the conductive nature of graphene, and this is a big difference between the two materials.

The preparation of GO is totally different from that of graphene. We can chemically synthesize GO by oxidizing graphite in strong acid conditions [1]. This yields a large quantity of GO in glassware. In contrast to graphene, GO is well dispersed in water. This is because of the many hydroxyl (-OH) groups existing on the GO surface. The synthesized GO has a sheet-like structure about 1 nm thick and with 1–100 μm edges, which was determined by atomic force microscopy (AFM) [2], [3]. GO is a very large material compared with molecule-scale materials. It is surprising that such large pieces of GO can float and are not precipitated in water. Note that GO does not dissolve in water: it forms a colloid solution. Thus, GO is precipitated when we centrifuge the solution.

2. Mechanism of biomolecule detection

GO is known to behave as a very efficient fluorescence quenching material [4]. When a fluorescent molecule such as a dye is located in the vicinity of the GO surface, the fluorescence from the dye is not observed. As the distance between the dye and the GO surface increases, the quenching efficiency drastically decreases, and the dye fluorescence becomes observable. This is an important feature of the biosensing architecture presented in this article. We fabricated the protein detection system on the surface of GO that is fixed on a solid support through chemical modification [5]. We first explain the fabrication method and the detection mechanism.

GO that is fixed on a solid support is readily prepared by spin-coating an aqueous dispersion of GO on a hydrophilic surface such as a silicon (Si) wafer with silicon dioxide (SiO_2) (SiO_2/Si) and quartz. The density of GO pieces can be controlled by the concentration of the dispersion and the spin-coating conditions. For the experiments described here, we used relatively large pieces of GO fixed on SiO_2/Si at low density in order to access a single piece of the GO.

The function for biological molecule detection can be built on the GO surface through chemical modification (**Fig. 2**). There are many sp^2 domains, which

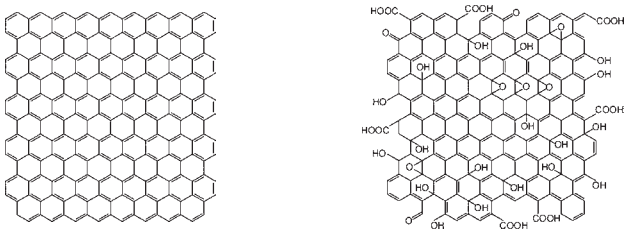

(a) Graphene (b) Graphene oxide

Fig. 1. Schematic chemical structure of graphene and GO.

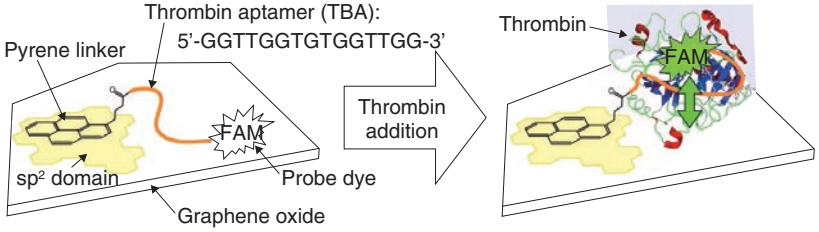

Fig. 2. Schematic illustrations of modified GO before and after thrombin addition. Note that the GO is fixed on a solid support.

remain as graphene-like structures, in GO. Pyrene, a molecule made of four benzene rings, is known to have a strong affinity to graphene surfaces. We thus prepared pyrene with a reactive site (a succinimide group) and adsorbed the pyrene molecule to the sp^2 domains in GO.

Deoxyribonucleic acid (DNA) was linked to the reactive site in the next step. DNA is a polymer composed of four bases that forms a double helix structure with its complementary DNA. The DNA we used here is called an aptamer, which is single-stranded DNA with a determined base sequence. The aptamer can bind with a specific protein molecule to form a complex structure. Biosensors that use aptamers are often referred to as aptasensors. We used a thrombin aptamer, which forms a complex with thrombin, a protein important in blood clotting. Thrombin is produced in our body after an injury. It facilitates clotting in order to prevent the loss of blood. It is not ordinarily present in the blood; if it were, it might induce an infarct in a blood vessel. An infarct is an area of tissue that undergoes necrosis as a result of an obstruction in the blood supply.

The base sequence of the thrombin aptamer is shown in Fig. 2. One of the aptamer termini has an NH_2 group that forms a chemical bond with a pyrene linker. The other is bonded to a dye used for the detection. The intended base sequences with modified termini can be easily synthesized by modern bioengineering. We can therefore order and purchase the designed DNA molecule.

The single-stranded DNA has a great affinity to the GO surface and is adsorbed on the surface in both atmospheric and solution conditions. Thus, the dye molecule is located in the vicinity of the GO surface, and its fluorescence is not observed because of the efficient quenching by GO. Since the biomolecule usually functions in solution conditions, let us consider the case where we add thrombin into a molecular system in water. As shown in Fig. 2 (right), the aptamer recognizes thrombin and forms a three-dimensional complex structure. This forces the dye at the terminus to be separated from the GO surface. Then the dye fluorescence that was quenched at the initial stage is recovered. Although the change in distance is very small, the recovery sensitively responds to the difference. By observing the recovered fluorescence, we can detect the protein, in this case thrombin.

3. Direct observations of protein detection on GO surface

We show the experimental results of thrombin detection in this section. The fluorescence microscope images of a GO aptasensor before and after thrombin addition are shown in **Fig. 3**. The image was dark before the addition; it fluoresces green after the addition. This is attributed to the fluorescence from the dye at the aptamer terminus. We demonstrate the protein detection using our GO aptasensor in this manner. Time lapse observations of the green fluorescence revealed that the fluorescence intensities become about four times more than the background fluorescence. As we can imagine from the fluorescence images, the increase is significant enough to detect the specific proteins.

A detection system similar to the one we constructed on GO has been reported by other research groups, but they demonstrated the detection using an aqueous dispersion of GO [6]. The means of biosensing using a GO aptasensor fixed on a solid support is NTT's original idea [5]. The fixation enables us to perform several interesting experiments that have not been possible with the dispersion system.

The images shown in Fig. 3 were taken by a confocal microscope that detects fluorescence only at the focused plain. Therefore, the green fluorescence in Fig. 3 originated from the complex formation between thrombin and the thrombin aptamer on the GO surface. However, it is impossible to determine how much thrombin adsorbs on the surface, and how densely, only from the fluorescence intensities. To estimate them, we observed the GO surface using AFM, which cannot be applied to GO in aqueous dispersion. By observing the same piece of GO using a confocal fluorescence microscope and AFM, we can make a reliable determination.

The AFM topographies before and after thrombin detection are shown in **Fig. 4**. The shape of the piece corresponds to that of the green fluorescence in Fig. 3, which is good proof that we are observing the same piece of GO. The average thickness of GO is 1.7 nm before and 3.6 nm after the thrombin detection. This obvious increase in thickness is due to the thrombin adsorption. The thrombin is about 5 nm in diameter in solution conditions. The increase in the thickness is smaller than the diameter, which suggests that the thrombin does not fully cover the GO surface. In addition, the AFM topographies were taken in dry atmospheric conditions, which may cause transformation and shrinkage of the thrombin. Another important feature in Fig. 4 is that no thrombin was observed on the hydrophilic SiO_2 surface. Although proteins like thrombin often adsorb on many kinds of surfaces, it is suppressed in our system. We would therefore not have been able to detect the selectivity of thrombin adsorption without the AFM observations.

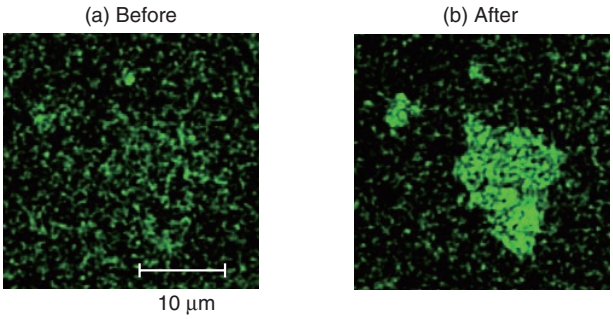

Fig. 3. Fluorescence images of single piece of GO before and after thrombin addition.

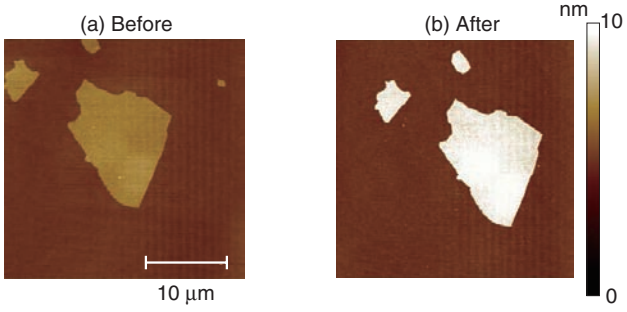

Fig. 4. AFM topographies of single piece of GO before and after the addition of thrombin. The piece of GO is the same as that in Fig. 3.

4. On-chip device application

The unique feature of our system is that the GO aptasensor is fixed on a solid support. This enables us to introduce the microchannel device on the GO aptasensor and to extend the technology to on-chip device applications. The prototype device, the GO aptasensor equipped with two microchannels, is shown in **Fig. 5** [7].

Practical sensor applications always require high sensitivity. We expect that higher sensitivity is achieved with this device by using substrates covered densely with GO, rather than the isolated GO as in

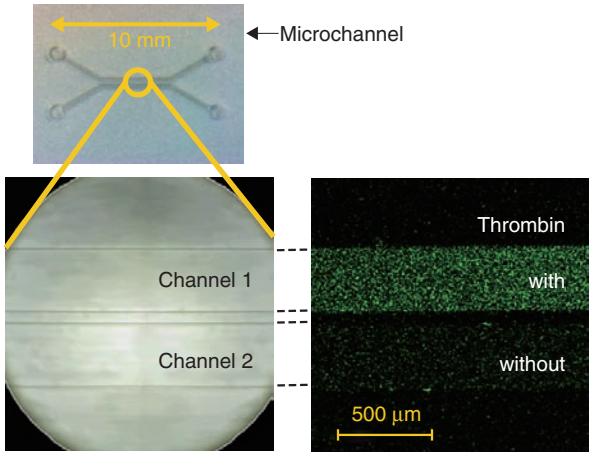

(a) Optical microscope (b) Fluorescence microscope

Fig. 5. Optical images of microchannel device (top), and GO aptasensor equipped with it (bottom left). Fluorescence microscope image when the top and bottom channels are respectively filled with thrombin solution and water (bottom right).

Fig. 3. We prepared such substrates by spin-coating fine pieces of GO onto them. The fine GO had edges less than 1 µm, which was obtained by irradiating the ultrasound beam to the aqueous dispersion of the original GO. The appropriate conditions will yield substrates with more than 70% surface coverage by GO. The substrate was modified with the aptamer and overlaid with the dual microchannel on the top.

The fluorescence microscope image of the microchannels filled with thrombin solution (channel 1) and water (channel 2) is shown in Fig. 5. It is clear that the whole area is green fluorescent in channel 1. This originates from the dye tethered on the GO surface fixed on a solid support. By contrast, the green fluorescence is at a background level in channel 2, which has no thrombin in the solution.

One of the advantages of the microchannel configurations is that we can examine the characteristics of the GO aptasensor easily and accurately. This is because we can compare the response of the aptasensor to several different samples at the same time, while maintaining the other identical experimental conditions. This is a powerful technique for optimizing the molecular structure in order to achieve higher sensitivity and for estimating the selectivity of proteins.

5. Future perspectives

In this article, we presented our protein detection system built on a GO surface and its use in detecting thrombin. We combined materials science research conducted in NTT Basic Research Laboratories and microfluidics technology developed in NTT Microsystem Integration Laboratories to develop an original idea that has many advantages and potential applications in various areas of research.

In future, the protein detection system can be applied to a variety of target molecules by choosing the corresponding aptamers. We have already demonstrated the detection of PSA (prostate specific antigen), a protein known as a cancer marker. The detection sensitivity can be increased by designing the molecular structure for GO surface modification. We have also demonstrated a significant increase in the thrombin detection sensitivity by adding a DNA spacer. The accumulation and combination of individual technologies is expected to lead to an integrated on-chip GO aptasensor that enables us to simultaneously detect a wide variety of biological molecules with a small quantity of samples solution.

References

[1] W. S. Hummers Jr. and R. E. Offeman, "Preparation of Graphitic Oxide," J. Am. Chem. Soc., Vol. 80, No. 6, p. 1339, 1958.
[2] K. Furukawa and H. Hibino, "Self-spreading of Supported Lipid Bilayer on SiO_2 Surface Bearing Graphene Oxide," Chem. Lett., Vol. 41, No. 10, pp. 1259–1261, 2012.
[3] Y. Ueno, E. Tamechika, K. Furukawa, S. Suzuki, and H. Hibino, "Near-Infrared Photoluminescence Spectral Imaging of Chemically Oxidized Graphene Flakes," e-J. Surf. Sci. Nanotech. Vol. 10. pp. 513–517, 2012.
[4] E. Treossi, M. Melucci, A. Liscio, M. Gazzano, P. Samorì, and V. Palermo, "High-Contrast Visualization of Graphene Oxide on Dye-Sensitized Glass, Quartz, and Silicon by Fluorescence Quenching," J. Am. Chem. Soc., Vol. 131, No. 43, pp. 15576–15577, 2009.
[5] K. Furukawa, Y. Ueno, E. Tamechika, and H. Hibino, "Protein Recognition on Single Graphene Oxide Surface Fixed on Solid Support," J. Mater. Chem. B, Vol. 1, No. 26, pp. 1119–1124, 2013.
[6] C.-H. Lu, H.-H. Yang, C.-L. Zhu, X. Chen, and G.-N. Chen, "A Graphene Platform for Sensing Biomolecules," Angew. Chem. Int. Ed., Vol. 48, No. 26, pp. 4785–4787, 2009.
[7] Y. Ueno, K. Furukawa, S. Inoue, K. Hayashi, H. Hibino, and E. Tamechika, "Label-Free Thrombin Detection in a Microchannel Using Aptamer Modified Graphene Oxide Surface," Proc. of the µTAS2012, Okinawa, Japan, Oct. 2012.

Kazuaki Furukawa
Senior Research Scientist, NTT Basic Research Laboratories.

He received the B.S. and M.S. degrees in physics and the Dr.Sci. degree from Waseda University, Tokyo, in 1986, 1988, and 2000, respectively. He joined NTT Basic Research Laboratories in 1988. He has been engaged in research on the chemical physics of soft materials such as functional polymers and lipid bilayers. His current interest is in graphene and graphene oxide, especially for their chemistry and biological applications. He is a member of the Japan Society of Applied Physics, the Physical Society of Japan, the Chemical Society of Japan (CSJ), and the Society of Polymer Science, Japan.

Yuko Ueno
Senior Research Scientist, NTT Microsystem Integration Laboratories.

She received the B.S., M.S., and Ph.D. degrees in chemistry from the University of Tokyo in 1995, 1997, and 2002, respectively. She joined NTT Integrated Information & Energy Systems Laboratories in 1997. She was a post-doctoral fellow at the University of California at Berkeley and at Lawrence Berkeley National Laboratory, Berkeley, CA, USA, from 2004 to 2005. She received the Encouragement Award (award for a young scientist) from the Japan Society for Analytical Chemistry (JSAC) in 2008. She is a member of JSAC, CSJ, and the Spectroscopical Society of Japan.

Monolithic Integration of Polarization-entangled Photon Pair Source Using Silicon Photonics Technology

Nobuyuki Matsuda, Hiroshi Fukuda, Tai Tsuchizawa, William John Munro, Kaoru Shimizu, Koji Yamada, Yasuhiro Tokura, and Hiroki Takesue

Abstract

Quantum entanglement is an essential resource for quantum information processing technologies, including quantum communication and quantum computation. In this article, we present the world's first-ever monolithically integrated polarization-entangled photon pair source on a silicon chip.

1. Introduction

Quantum entanglement, or in other words, nonlocal quantum correlation between two or more quantum-mechanical objects, is a quintessential feature of quantum mechanics. At the same time, quantum entanglement is a substantial resource for quantum information processing (QIP) technologies including quantum cryptography, quantum metrology, and quantum computation [1]–[4].

A number of physical systems are being investigated for their potential application in the development of QIP. Among them, photons are excellent media to generate, process, and distribute entanglements. This is because quantum states encoded in physical quantities of light are highly robust, thanks to an inherent weakness in the interactions between light and electromagnetic environments. The physical freedom of light includes polarizations, optical paths, frequencies, and time bins. Of these quantum states, polarization is particularly important, since polarization is a true two-level photonic system, which is easy to manipulate with conventional bulk optics such as wave plates. Thus, many QIP protocols have been proposed [3], [5] and experimentally demonstrated [4], [5] using polarization-encoded quantum states of light. In such experiments, sources of polarization-entangled photons have been inevitably playing a key role [6], [7].

Very recently, integrated optical circuits have been attracting much attention as the next platform of QIP using photons [8]. Such an approach promises to scale up the experiments by exploiting the miniature physical size and highly stable interferometers of integrated waveguides. To achieve such integrated photonic QIP systems, it is essential to develop integrated subsystems to generate, manipulate, and measure the quantum states on a chip. In particular, an integrated polarization-entanglement source, which generates polarization-entangled photons into a waveguide mode on a chip, is necessary in order for us to utilize the wealth of QIP protocols. However, no such demonstration of an integrated polarization-entanglement source has been reported to date; nevertheless, it is necessary for a practical integrated QIP system. In this article, we present the world's first ever polarization-entanglement source, which NTT achieved using silicon photonics technology [9] (**Fig. 1**). We have implemented the source as a simple and stable silicon-on-insulator photonic circuit so the

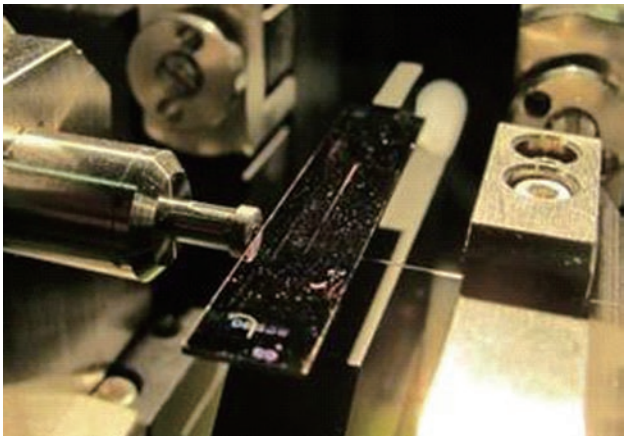

Fig. 1. Picture of the chip of monolithic polarization-entangled photon pair sources. By injecting pump pulses from the left hand side, we can obtain polarization-entangled photon pairs to be collected by the output optical fiber on the right hand side.

source could successfully generate a high degree of polarization entanglement.

2. Building blocks of polarization-entangled photon pair source

An entangled photon pair source requires two building blocks: a source to generate photon pairs having a time correlation, and a device to manipulate the polarization state of photons to ensure that photon pairs are entangled in the polarization degree of freedom. NTT has already realized both components by using on-chip silicon photonics technology.

A silicon-wire waveguide is a highly efficient source of time-correlated photon pairs (**Fig. 2(a)**) [10]–[15]. The silicon-wire waveguide is a single-mode waveguide whose core is made of single-crystalline silicon with a typical cross-sectional size of 400 nm (width) and 200 nm (height). Thanks to this extremely small core, the optical power density in the waveguide becomes very high, and as a result, we can observe a huge nonlinear optical effect. The nonlinear coefficient of our silicon-wire waveguide is five orders of magnitude larger than that of a silica optical fiber. This coefficient represents the optical-nonlinearity strength of a waveguide.

When we input a telecom-wavelength pump light whose frequency is ν_p into the silicon-wire waveguide, we can generate a photon pair with frequencies of ν_s and ν_i through spontaneous four-wave mixing (SFWM), which is one of the third-order nonlinear effects. The process occurs under the energy conservation of photons as follows

$$2\nu_p = \nu_s + \nu_i \quad (1)$$

This indicates that two pump photons are annihilated, and subsequently a signal-idler photon pair is created. Since the two photons are created simultaneously, we can generate time-correlated photon pairs. In addition, the use of the single-crystalline silicon core enables us to avoid background noise photons caused by spontaneous Raman scattering, which has been a serious problem for photon pair sources based on other types of nonlinear waveguides such as fused silica [1] whose core has an amorphous structure. A single-mode waveguide supports two propagating modes with orthogonal polarization states of light: transverse-electric (TE) and transverse-magnetic (TM) fields. In the silicon wire waveguide, TE-polarized photon pairs are efficiently generated by a TE-polarized pump field. This is because the waveguide has a field confinement of TE-polarized light into the core that is stronger than that of TM-polarized light [13].

The second building block is a silicon polarization rotator [16], which is used in polarization-diversity optical circuits for telecommunication applications [17]. The device has an off-axis double-core structure consisting of a 200-nm^2 silicon wire core and a second 840-nm^2 silicon-oxynitride (SiON) core on the silicon core (**Fig. 2(b)**). The structure exhibits two orthogonal eigenmodes, which have different effective refractive indices and eigen-axes tilted at 45° to the normal with respect to the silicon substrate. The birefringence in the eigenmodes provides an integrated wave plate, which causes the polarization plane to rotate by an amount that depends on the length of the rotator. We show the measured polarization rotation characteristics of a 30-μm-long polarization rotator in **Fig. 2(c)**. A TE-polarized input field was successfully converted to TM polarization with the rotator. The polarization rotation angle was estimated to be 86.7 ± 0.1° with a polarization extinction ratio as high as 30 dB. Thus, we obtained a polarization rotation angle of almost 90° with a high polarization extinction ratio. This high performance of the rotator enabled us to generate a high degree of polarization entanglement as we show later.

3. On-chip polarization-entanglement source

We combined the two building blocks fabricated on

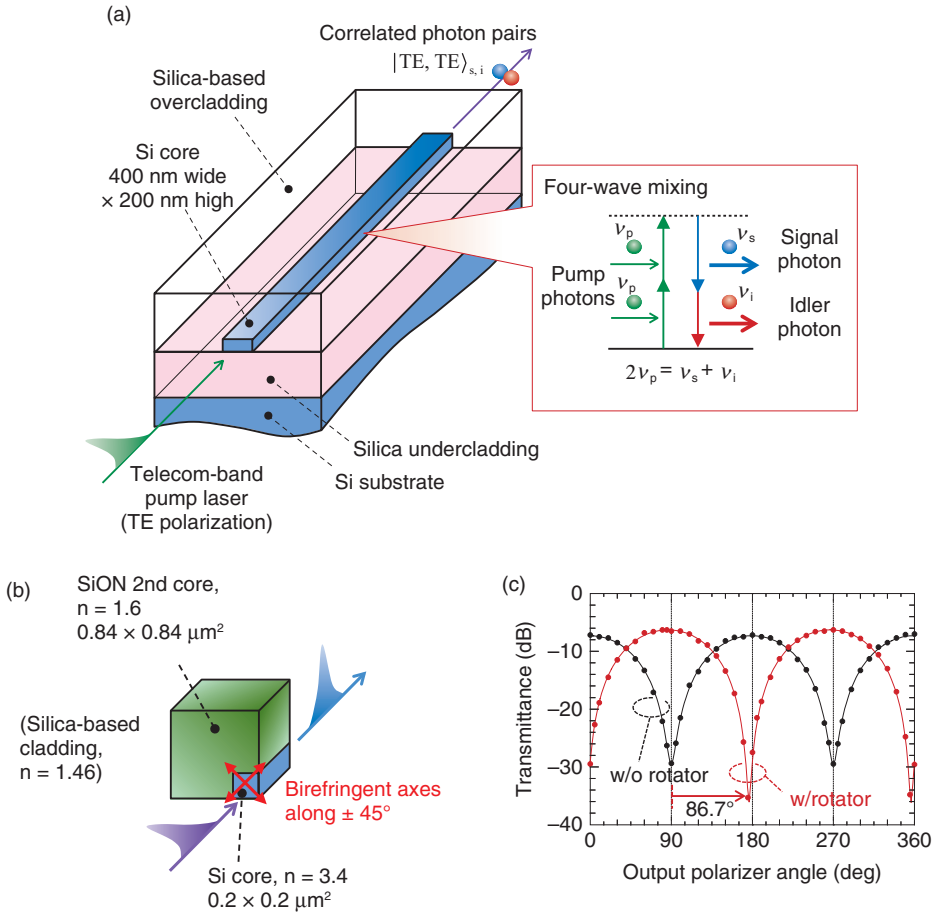

Fig. 2. Building blocks of polarization-entanglement source. (a) Silicon-wire waveguide source of correlated photon pairs. (b) Ultrasmall silicon polarization rotator. Claddings are not shown for clarity. (c) Characterization of polarization rotation angle at the silicon polarization rotator.

the same silicon photonics platform to implement the monolithic polarization entanglement source on a chip [9]. Our polarization-entanglement source (**Fig. 3**) consists of two silicon-wire waveguides connected by a silicon-wire polarization rotator. Both silicon wire waveguides are 1.5 mm long. The silicon wire waveguides and the silicon polarization rotator are connected by 10-μm-long tapered silicon wires. The over- and under-cladding of the silicon wire waveguides and the silicon polarization rotator were made of silica (not shown).

The operating principle of the device is as follows. We use a pump beam with + 45° linear polarization, which is a 1:1 combination of the TE and TM modes in the silicon wire waveguides. In the first silicon wire waveguide, the TE component of the pump creates a photon pair in the $|1\rangle_{TE,s}|1\rangle_{TE,i}$ state, which means that there is one TE-polarized photon in the signal frequency channel and one TE-polarized photon in the idler frequency channel. In the following, we rewrite the state as $|TE\rangle_s|TE\rangle_i$ for simplicity. Then, the silicon polarization rotator rotates this state to the $|TM\rangle_s|TM\rangle_i$ state as a result of 90° polarization rotation. Here, the subscripts denote the frequency modes of the signal and idler photons. At the same time, the silicon polarization rotator rotates the TM component of the pump field to provide it with TE polarization, and the second silicon wire waveguide creates other $|TE\rangle_s|TE\rangle_i$ photons. Since we cannot distinguish whether the pair was generated in the first or second silicon waveguides, we obtain the maximally polarization-entangled state:

$$|\psi\rangle = (|TE\rangle_s|TE\rangle_i + e^{-i\phi}|TM\rangle_s|TM\rangle_i)/\sqrt{2}, \quad (2)$$

at the output of the polarization-entanglement source.

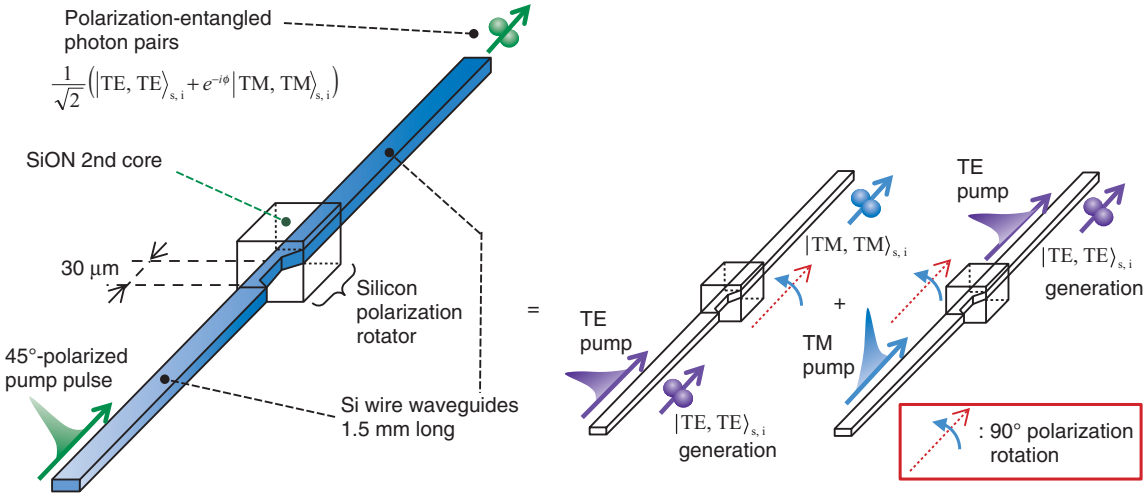

Fig. 3. Monolithically integrated polarization-entangled photon pairs. The source, fabricated on a silicon-on-insulator substrate, consists of a silicon 90° polarization rotator sandwiched by two nonlinear silicon wire waveguides. The device generates the polarization entanglement as a superposition of the two events shown on the right hand side.

Here, the relative phase difference ϕ is a fixed value and depends on the difference in length between the first and second silicon waveguides.

Generally, it is difficult to precisely control a birefringence of nonlinear waveguides with an ultrasmall core. The residual birefringence causes significant polarization-mode dispersion (PMD), which degrades the degree of polarization entanglement. To avoid this degradation, the conventional polarization-entanglement sources adopt off-chip PMD compensators such as birefringent crystal or polarization-maintaining fiber. In those cases, photons cannot be polarization-entangled inside the waveguide chip. In our case, since the polarization-entanglement source is designed to be symmetric about the polarization states with respect to the midpoint of the device, the polarization-mode dispersion of the pump pulses and photon pairs are completely cancelled out. Therefore, our polarization-entanglement source generates a polarization-entangled state inside the waveguide chip. This feature enables us to directly integrate the source with quantum-state controllers and detectors to construct a quantum information processor on a chip. Moreover, the device can automatically balance the amplitude of the two terms in Eq. (2) even in the presence of practical waveguide losses, leading to highly robust polarization entanglement (see Ref. [9] for details).

4. Experiment

We generated and analyzed polarization-entangled photon pairs using the setup shown in **Fig. 4**. We injected optical pump pulses whose polarization was set at + 45° linear polarization and a wavelength centered at 1551.1 nm into the polarization-entanglement source. The photons generated from the chip were introduced into the wavelength-division-multiplexing (WDM) filter, which suppressed the residual pump light and separated the signal and idler photons into different fiber channels. Each output port had a center wavelength of 1546.4 nm (signal) and 1556.0 nm (idler) with a channel bandwidth of 0.14 nm. Then, the photons passed through the polarization analyzers, each of which consisted of a half and a quarter wave plate, and a polarizer. Finally, the photons were received by InGaAs (indium/gallium/arsenide) single photon detectors. The detection signals from the two detectors were input into the time interval analyzer (TIA), with which we carry out time-correlation measurement of photon pairs.

We first reconstruct the density matrix of the generated polarization-entangled state to evaluate the degree of entanglement. The density matrix ρ of the state in Eq. (2) can be expressed as

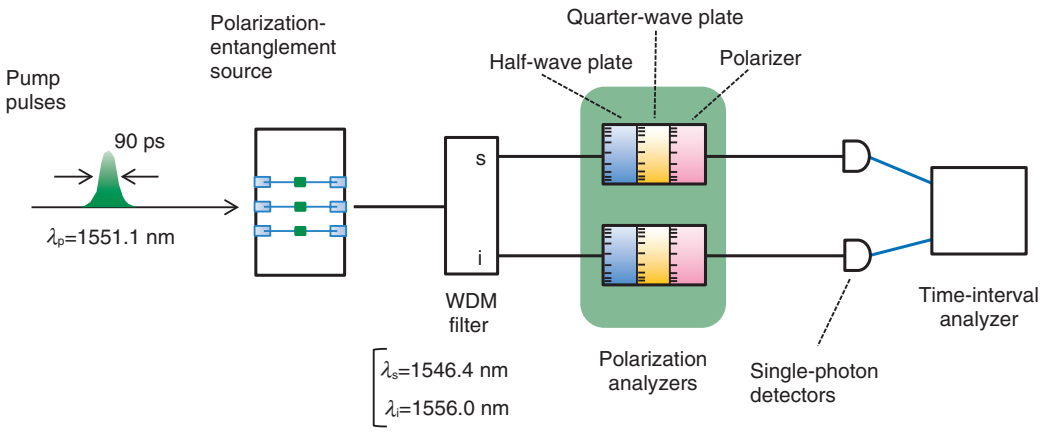

Fig. 4. Experimental setup.

$$\rho = \Sigma |\psi\rangle\langle\psi|$$
$$= \frac{1}{2}(|\mathrm{TE}\rangle_s|\mathrm{TE}\rangle_i + e^{-i\phi}|\mathrm{TM}\rangle_s|\mathrm{TM}\rangle_i)$$
$$(\langle\mathrm{TE}|_s\langle\mathrm{TE}|_i + e^{i\phi}\langle\mathrm{TM}|_s\langle\mathrm{TM}|_i), \quad (3)$$
$$= \frac{1}{2}\begin{pmatrix} 1 & 0 & 0 & e^{-i\phi} \\ 0 & 0 & 0 & 0 \\ 0 & 0 & 0 & 0 \\ e^{i\phi} & 0 & 0 & 1 \end{pmatrix}$$

when the state is purely in the maximally entangled state. Here, the summation takes over all the generated photon pairs. In this representation, we used $|\mathrm{TE}\rangle_s|\mathrm{TE}\rangle_i$, $|\mathrm{TE}\rangle_s|\mathrm{TM}\rangle_i$, $|\mathrm{TM}\rangle_s|\mathrm{TE}\rangle_i$, and $|\mathrm{TM}\rangle_s|\mathrm{TM}\rangle_i$ as a basis set. Each diagonal element represents the probability (population) of the system, and the off-diagonal elements represent the quantum coherence. If the generated system has no coherence, the density matrix becomes

$$\rho = \Sigma\ |\psi\rangle\langle\psi| = \frac{1}{2}\begin{pmatrix} 1 & 0 & 0 & 0 \\ 0 & 0 & 0 & 0 \\ 0 & 0 & 0 & 0 \\ 0 & 0 & 0 & 1 \end{pmatrix}. \quad (4)$$

Therefore, the density matrix that has the off-diagonal elements whose absolute values are as high as those of the diagonal elements shows the full coherence of the entanglement.

To experimentally obtain the density matrix of the two-photon polarization state, we first carried out the correlation measurement of the photon pairs under 16 different polarization combinations that were selected based on the angles of the four wave plates in the polarization projection units [18]. This is analogous to the measurement of the polarization state of classical light, in which projection measurements of four different polarization states are at least required to estimate Stokes vectors. In the present case with the two-photon state, we require $4^2 = 16$ projection measurement. Then, using a procedure called quantum state tomography, we can reconstruct the density matrix. The reconstructed density matrix is shown in **Fig. 5**. For simplicity, we have only displayed the absolute values of each matrix element. The result exhibits off-diagonal amplitudes as high as 0.5, which represent a high coherence of the system. Note that the results include any background (noise) counts.

Regarding the degree of entanglement, we evaluate the fully entangled fraction $F(\rho) = \max_{\Psi}\langle\Psi|\rho|\Psi\rangle$, where the maximum is taken over all maximally entangled states $|\Psi\rangle$. From the measured ρ values in accordance with the procedure described by Badziag et al. [19], we obtained an $F(\rho)$ value of (94 ± 2)%. This value is much higher than the classical limit of 0.5. Furthermore, the $F(\rho)$ value is much greater than $1/\sqrt{2} \sim 71\%$, implying that the generated state has strong nonlocal correlation. Hence, we successfully generated photon pairs with a high degree of polarization entanglement from the chip.

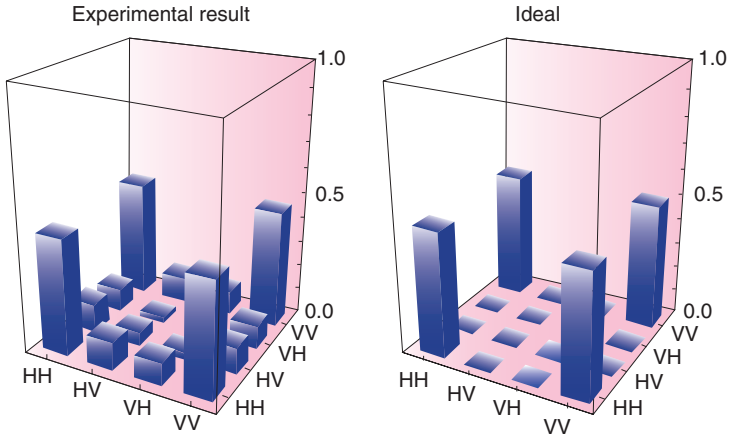

Fig. 5. Reconstructed density matrix. Here, the absolute values of each element are shown. H and V represent the TE and TM bases, respectively.

5. Conclusion

We have demonstrated the world's first ever source of polarization-entangled photon pairs on a chip. The device we constructed is capable of generating a high degree of polarization entanglement thanks to nanofabrication technology of silicon photonic devices. To achieve a photonic QIP system on a chip, it is necessary to integrate our source with subsequent quantum processors, which manipulate or project the polarization-encoded quantum state of photons. Such integration would also be possible, since our source is equipped with spot-size converters, which can be a versatile interface with other types of integrated waveguide platforms [20]. Our monolithic polarization-entangled photon pair source helps pave the way to the full-scale implementation of a photonic quantum information system on a chip.

References

[1] H. Takesue, "Generation of Polarization-entangled Photon Pairs in 1.5-μm Telecommunication Band," NTT Technical Review, Vol. 3, No. 12, 2005. https://www.ntt-review.jp/archive/ntttechnical.php?contents=ntr200512052.pdf

[2] K. Edamatsu, "Entangled Photons: Generation, Observation, and Characterization," Japan. J. of Appl. Phys., Vol. 46, pp. 7175–7187, 2007.

[3] M. A. Nielsen and I. L. Chuang, "Quantum Computation and Quantum Information," Cambridge University Press, Cambridge, 2000.

[4] H. Takesue, "Quantum Communication Using Entangled Photon Pairs—Toward Quantum Repeaters," NTT Technical Review, Vol. 9, No. 9, 2011. https://www.ntt-review.jp/archive/ntttechnical.php?contents=ntr201109fa10.html

[5] P. Kok, W. J. Munro, K. Nemoto, T. C. Ralph, J. P. Dowling, and G. J. Milburn, "Linear Optical Quantum Computing with Photonic Qubits," Rev. Mod. Phys., Vol. 79, No. 1, pp. 135–174, 2007.

[6] P. G. Kwiat, K. Mattle, H. Weinfurter, A. Zeilinger, A. V. Sergienko, and Y. Shih, "New High-Intensity Source of Polarization-Entangled Photon Pairs," Phys. Rev. Lett., Vol. 75, No. 24, pp. 4337–4341, 1995.

[7] P. G. Kwiat, E. Waks, A. G. White, I. Appelbaum, and P. H. Eberhard, "Ultrabright Source of Polarization-entangled Photons," Phys. Rev. A, Vol. 60, No. 2, pp. R773–R776, 1999.

[8] A. Politi, M. Cryan, J. G. Rarity, S. Yu, and J. L. O'Brien, "Silica-on-Silicon Waveguide Quantum Circuits," Science, Vol. 320, No. 5876, pp. 646–649, 2008.

[9] N. Matsuda, H. Le Jeannic, H. Fukuda, T. Tsuchizawa, W. J. Munro, K. Shimizu, K. Yamada, Y. Tokura, and H. Takesue, "A monolithically integrated polarization entangled photon pair source on a silicon chip," Sci. Rep., Vol. 2, 817, 2012.

[10] H. Takesue, Y. Tokura, H. Fukuda, T. Tsuchizawa, T. Watanabe, K. Yamada, and S. Itabashi, "Entanglement generation using silicon wire waveguide," Appl. Phys. Lett., Vol. 91, No. 20, 201108, 2007.

[11] H. Takesue, H. Fukuda, T. Tsuchizawa, T. Watanabe, K. Yamada, Y. Tokura, and S. Itabashi, "Generation of polarization entangled photon pairs using silicon wire waveguide," Opt. Express, Vol. 16, No. 8, pp. 5721–5727, 2008.

[12] K. Harada, H. Takesue, H. Fukuda, T. Tsuchizawa, T. Watanabe, K. Yamada, Y. Tokura, and S. Itabashi, "Generation of high-purity entangled photon pairs using silicon wire waveguide," Opt. Express, Vol. 16, No. 25, pp. 20368–20373, 2008.

[13] K. Harada, H. Takesue, H. Fukuda, T. Tsuchizawa, T. Watanabe, K. Yamada, Y. Tokura, and S. Itabashi, "Frequency and polarization characteristics of correlated photon-pair generation using a silicon wire waveguide," Selected Topics in Quantum Electronics, IEEE Journal of, Vol. 16, No. 1, pp. 325–331, 2010.

[14] K. Harada, H. Takesue, H. Fukuda, T. Tsuchizawa, T. Watanabe, K. Yamada, Y. Tokura, and S. Itabashi, "Indistinguishable photon pair generation using two independent silicon wire waveguides," New J. Phys., Vol. 13, 065005, 2011.

[15] H. Takesue, "Entangled photon pair generation using silicon wire waveguides," Selected Topics in Quantum Electronics, IEEE Journal of, Vol. 18, No. 6, pp. 1722–1732, 2012.

[16] H. Fukuda, K. Yamada, T. Tsuchizawa, T. Watanabe, H. Shinojima, and S. Itabashi, "Polarization rotator based on silicon wire waveguides," Opt. Express, Vol. 16, No. 4, pp. 2628–2635, 2008.

[17] H. Fukuda, K. Yamada, T. Tsuchizawa, T. Watanabe, H. Shinojima, and S. Itabashi, "Silicon photonic circuit with polarization diversity,"

Opt. Express, Vol. 16, No. 7, pp. 4872–4880, 2008.
[18] D. F. V. James, P. G. Kwiat, W. J. Munro, and A. G. White, "Measurement of qubits," Phys. Rev. A, Vol. 64, No. 5, 052312, 2001.
[19] P. Badziąg, M. Horodecki, P. Horodecki, and R. Horodecki, "Local environment can enhance fidelity of quantum teleportation," Phys. Rev. A, Vol. 62, No. 1, 012311, 2000.
[20] T. Tsuchizawa, K. Yamada, T. Watanabe, S. Park, H. Nishi, R. Kou, H. Shinojima, Y. Ishikawa, K. Wada, and S. Itabashi, "Monolithic Integration of Silicon-, Germanium-, and Silica-Based Optical Devices for Telecommunications Applications," IEEE J. Sel. Topics Quantum Electron., Vol. 17, No. 3, pp. 516–525, 2011.

Nobuyuki Matsuda
Research Scientist, Quantum Optical State Control Research Group, NTT Basic Research Laboratories and NTT Nanophotonics Center.
He received the B.E., M.E., and Ph.D. degrees in electronic engineering from Tohoku University, Miyagi, in 2005, 2006, and 2009, respectively. During 2009–2010, he was a visiting research scholar at the University of Bristol, UK. He joined NTT Basic Research Laboratories in 2010 and has since been engaged in research on integrated quantum photonics and single-photon nonlinear optics. He is a member of the Physical Society of Japan (JPS) and the Japan Society of Applied Physics (JSAP).

Hiroshi Fukuda
Senior Research Engineer, Photonic Integrated Interface Research Group, NTT Microsystem Integration Laboratories and NTT Nanophotonics Center.
He received the B.E. and M.E. degrees in nuclear engineering from Tohoku University, Miyagi, in 1993 and 1995, respectively. In 1995, he joined NTT Microsystem Integration Laboratories, where he has been engaged in research on microphotonics devices. He is a member of JSAP, the Institute of Electronics, and Information and Communication Engineers (IEICE).

Tai Tsuchizawa
Senior Research Engineer, Photonic Integrated Interface Research Group, NTT Microsystem Integration Laboratories and NTT Nanophotonics Center.
He received the B.S. and M.S. degrees in physics from Sophia University, Tokyo, and the Ph.D. degree from the University of Tokyo in 1984, 1986, and 1990, respectively. Since joining NTT in 1999, he has been engaged in studies on ECR plasma technology and its application to an etching process for microfabrication. His current research interest is fabrication technologies for silicon based optoelectronics devices. He is a member of JSAP.

William John Munro
Research Specialist, Quantum Optical State Control Research Group, NTT Basic Research Laboratories.
He received the BSc. degree in chemistry and physics, the MSc. degree in physics, and the D.Phil degree in quantum optics from the University of Waikato, New Zealand, in 1989, 1991, and 1994, respectively. In early 1995, he moved to the computer industry, where he worked on various projects. In July 1997 he accepted an Australian Research Council Fellowship in the Department of Physics at the University of Queensland, Australia. During this fellowship he investigated multiparticle tests of quantum mechanics and developed an interest in entanglement, methods to characterize it, and its practical use in QIP. In 2000, he became a senior researcher at the Australian Special Centre for Quantum Information Processing. In November 2000, he joined HP Labs. as a research scientist, and in early 2010 joined NTT Basic Research Laboratories as a research specialist.

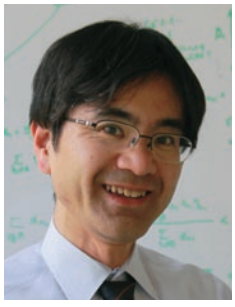

Kaoru Shimizu
Senior Research Scientist, Supervisor, Quantum Optical State Control Research Group Leader, NTT Basic Research Laboratories.
He received the B.E., M.E, and Ph.D. degrees in applied physics from Waseda University, Tokyo, in 1988, 1990, and 1995, respectively. He joined NTT Transmission System Laboratories in 1990 and studied lightwave technologies for surveillance of optical fiber networks. He moved to NTT Basic Research Laboratories in 1996 and studied quantum information processing including quantum communication and quantum cryptography. During 2003–2005, he worked at the human resource management section of NTT Science and Core Technology Laboratories and was mainly engaged in recruitment. Then he returned to NTT Basic Research Laboratories and studied quantum memory devices. He was a visiting professor at Nara Institute of Science and Technology in 2006 and 2009. He is a member of JPS.

Koji Yamada
Senior Research Engineer, Supervisor, Distinguished Technical Member, Photonic Integrated Interface Research Group, NTT Microsystem Integration Laboratories and NTT Nanophotonics Center.

He received the B.E., M.E., and Ph.D. degrees in nuclear engineering from Kyushu University, Fukuoka, in 1986, 1988, and 2003, respectively. He joined NTT in 1988. In NTT laboratories, he was engaged in studies on synchrotron light sources, and since 2000 he has been engaged in studies on silicon photonics platforms. From 2010, he also joined the Photonics Electronics Technology Research Association (PETRA) as a leader of photonic wiring and the waveguide research team of Photonics-Electronics Convergent System Technology research project (PECST). He is a member of JSAP, IEICE, the Atomic Energy Society of Japan, the Particle Accelerator Society of Japan, and IEEE.

Yasuhiro Tokura
Professor, the University of Tsukuba and Research Professor, NTT Basic Research Laboratories.

He received the B.E., M.E., and Ph.D. degrees in arts and science from the University of Tokyo in 1983, 1985, and 1998, respectively. He joined NTT Basic Research Laboratories in 1985 and studied semiconductor electronic transport in nano-structures. During 1998–1999, he stayed at Technical University of Delft in the Netherlands as a guest researcher to study transport in carbon nanotubes. He was an executive manager of the Optical Science Laboratory of NTT Basic Research Laboratories from 2005 to 2012. He became a Professor of the Graduate School of Pure and Applied Sciences at the University of Tsukuba in 2012. He is currently working on the physics of quantum transport and quantum information science in solid state systems. He is a member of JPS, JSAP, and the American Physical Society.

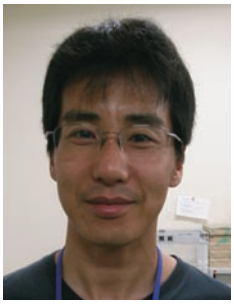

Hiroki Takesue
Senior Research Scientist, Supervisor, Distinguished Researcher, Quantum Optical State Control Research Group, NTT Basic Research Laboratories.

He received the B.E., M.E., and Ph.D. degrees in engineering science from Osaka University in 1994, 1996, and 2002, respectively. In 1996, he joined NTT, where he engaged in research on lightwave frequency synthesis, optical access networks using wavelength division multiplexing, and quantum optics. His current research interests include quantum optic experiments using nonlinear waveguides and quantum communication based on entanglement. He has received several awards, including the ITU-T Kaleidoscope Conference 2nd Best Paper Award in 2008 and the Commendation for Science and Technology by the Minister of Education, Culture, Sports, Science and Technology of Japan (The Young Scientist's Prize) in 2010. From 2004 to 2005, he was a visiting scholar at Stanford University, CA, USA. He is a member of JSAP and IEEE.

The ITU Workshop on eHealth and the Fourth Meeting of ITU-T FG-DR&NRR in Tokyo

Hideo Imanaka, Masahito Kawamori, and Noriyuki Araki

Abstract

The International Telecommunication Union (ITU) workshop on eHealth and the fourth meeting of the ITU-T (ITU-Telecommunication Standardization Sector) Focus Group on Disaster Relief Systems, Network Resilience and Recovery (FG-DR&NRR) were held in Shinjuku, Tokyo, February 4–8, 2013. These ITU events were held together in order to promote mutual understanding between working areas in healthcare and disaster response, and to increase NTT's presence in both fields. This article describes the main results of these events.

1. Introduction

The ITU workshop on eHealth was held in Tokyo, Japan, on Monday and Tuesday, February 4–5, 2013. This workshop was hosted by the Ministry of Internal Affairs and Communications (MIC), Japan, and was attended by 135 people from more than 20 countries. The workshop included an introduction to the needs and expectations of developing countries with regard to eHealth and the advanced technology that may have to be considered for standardization in the future.

Following this workshop, the fourth meeting of the ITU-T Focus Group on Disaster Relief Systems, Network Resilience and Recovery (FG-DR&NRR) was held at the same venue from Tuesday through Friday, February 5–8, 2013. This meeting was hosted by the National Institute of Information and Communications Technology (NICT), and attended by approximately 80 people from 15 countries. In addition to the usual discussions on standardization, this event included a visit to the disaster-affected area in Tohoku and the NICT Resilient ICT Research Center.

The schedules of the ITU events are shown in **Fig. 1**. Part of the workshop (in the afternoon on February 5) was organized as a session on eHealth in the event of a disaster to promote mutual understanding between people working in eHealth and in disaster response.

2. ITU eHealth workshop

2.1 Background

In developed countries including Japan, the aging society problem is causing a chronic shortage of doctors. Meanwhile, developing countries also have a chronic shortage of doctors but for a different reason, namely, the limited availability of medical services.

Tele-medicine and eHealth are being studied as solutions to these problems. In ITU-T SG16 (Study Group 16) and ITU-D (ITU-Telecommunication Development Sector) SG2, studies are being pursued with the aim of standardizing eHealth and making it widely available in developing countries. In November 2012, the ITU and World Health Organization (WHO) launched a partnership called the mHealth initiative, which aims to use mobile phones to deliver eHealth services to combat non-infectious illnesses [1]. Since 2012, an ITU-T focus group called FG-M2M has been studying the standardization of eHealth as a machine-to-machine (M2M) application.

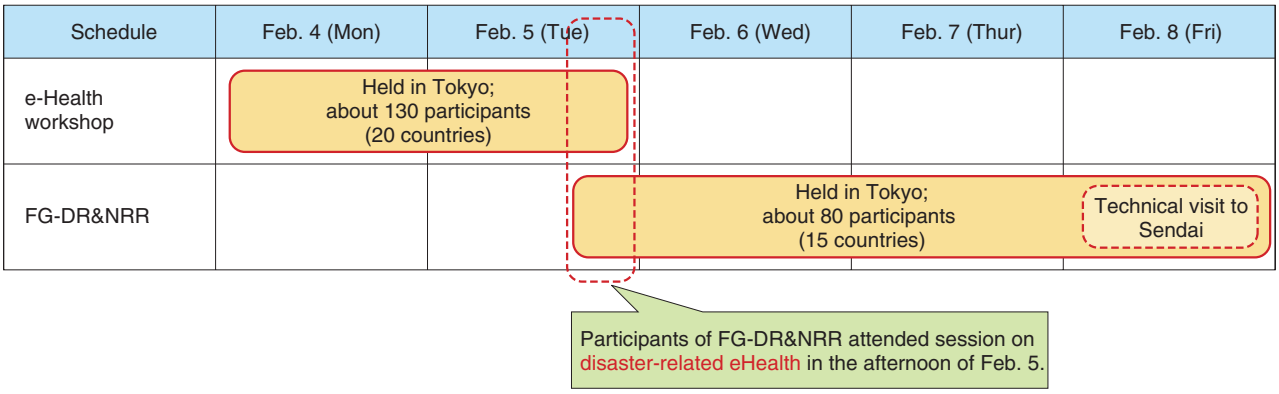

Fig. 1. Schedules of ITU events.

With the aim of ensuring that eHealth standardization proceeds smoothly in the future, ITU-D and ITU-T held a joint eHealth workshop [2] to provide a forum for dialogue and to exchange information between their members. In this way, we aim to clarify the special requirements of developing countries, and to specify the items for future standardization as part of efforts to implement eHealth using advanced technology.

2.2 Overview of the workshop

(1) Opening and keynote speeches

Opening speeches were made by Eiichi Tanaka, Vice-Minister for Policy Coordination of MIC, Japan (**Photo 1**), and by Sameer Sharma of the ITU Asia-Pacific regional office on behalf of the ITU Secretary-General. These were followed by keynote speeches from Tetsushi Sakamoto, the State Secretary for MIC, Japan, on the subject of Japan's eHealth policies, and Kiyoshi Kurokawa of the National Graduate Institute for Policy Studies, who gave a presentation entitled *Global Agenda in Post Fukushima*, in which he raised issues that should be addressed not just by Japan but by the whole world in the wake of the Great East Japan Earthquake. This speech stressed the importance of resilience based on the assumption of diverse risks. It also pointed out that as the world evolves from the Web 2.0 era into the Web 3.0 era, mobile devices such as tablet computers will come to play a more important role. Mark Landry of WHO Western Pacific regional office in the Philippines gave a speech on behalf of WHO in which he described some examples of eHealth policies across Asia, and the current status of cooperation between WHO and government in Asian countries.

Photo 1. Opening speech made by Eiichi Tanaka, Vice-Minister for Policy Coordination of MIC, Japan.

(2) Requirements from developing countries

Under the theme of implementing eHealth in a low-resource setting, representatives from India, Sudan, Uganda, Algeria, the United Arab Emirates, Bangladesh, Vietnam, and Myanmar gave presentations on the current situation of eHealth in their respective countries, the issues that need to be addressed, and the requirements in each case. The requirements of developing countries are characterized by delayed development of infrastructure not only for medical care but also for insurance, sanitation, and health management, and by a shortage of healthcare workers coupled with a poor educational environment. Instead of the advanced eHealth systems that are being considered in developed countries, these presentations introduced solutions such as Web-based sharing and education of medical information, using video

conferencing to facilitate collaboration between medical workers including doctors, and using mobile phones for medical consulting (mHealth), whereby eHealth is expected to provide a broad range of benefits.

(3) Items for standardization from developed countries

Representatives from Japan, South Korea, Singapore, and the United States introduced some advanced examples of eHealth initiatives and discussed the challenges of implementing eHealth. NTT DATA gave a presentation introducing use cases of personal health record (PHR) management and monitoring as examples of mHealth services in Japan, and stressed the importance of security and privacy protection. The representative from Singapore introduced a Smart TV (television) health management system based on ITU standards, and showed that interactive eHealth using TV sets and remote control devices may be suitable for an aging society since these devices can be easily used by elderly people. The US representative also introduced the importance of considering eHealth for people with disabilities; NICT introduced the possibility of a body area network (BAN) that people can wear in order to connect to healthcare equipment; and Fujitsu introduced the research of a heart simulator that aims to improve healthcare technology. These presentations highlighted the need for standardization of the data structures and protocols required for the transmission of PHR and other data, of the application interfaces and transmission methods used between medical/healthcare devices and telecommunication networks, wireless devices, and fixed devices, and of security, which is essential when exchanging PHR data.

(4) eHealth in the event of disasters

The lessons learned after the Great East Japan Earthquake with regard to the use of eHealth in disaster situations were also introduced. A presentation was made by a representative of A&D Co., Ltd. on a system for monitoring health information such as blood pressure for use in health management of people affected by disasters. This system was actually put to use after the Great East Japan Earthquake. Professor Isao Nakajima of Tokai University—who is also the ITU-D vice rapporteur for eHealth and co-chairman of this workshop—described eHealth items that need to be studied in the event of radioactivity disasters in relation to the nuclear power plant incident. These presentations demonstrated the usefulness of eHealth in the event of a disaster and made a case for the importance of preserving two-way communications.

(5) Future direction of work with the ITU

One of the authors (Kawamori), who also acted as co-chairman of this workshop, drew up the following summary of the results of this workshop and the future direction of eHealth standardization at the ITU.

- To promote the spread of eHealth, it is important to provide education in order to eliminate misconceptions about the circumstances of developing countries.
- From the viewpoint of standardization, it is necessary to establish cooperation between ITU and related organizations with regard to requirements, terminology definitions, and data sets/applications.
- In particular, a terminology database is necessary since the technical terminology relating to eHealth covers many fields including medicine, healthcare, and ICT.
- For eHealth related regions, it is necessary to study how this technology can be best applied to elderly patients, disaster victims, and disabled people.
- In the future, information should be supplied to the ITU website including the content of speeches given at this workshop, and an enlightenment event should be held in cooperation with the WHO.

2.3 Other related events

In addition to the workshop, there were demonstrations related to mHealth by NTT Secure Platform Laboratories (**Photo 2**). A simple health management system was introduced where healthcare equipment including blood pressure gauges and SMS (short message service) is used to implement mHealth with low initial investment. These demonstrations drew a great deal of interest from many countries, including African nations.

3. The fourth meeting of ITU-T FG-DR&NRR

3.1 Background and purpose of the fourth meeting of FG-DR&NRR

In the wake of the Great East Japan Earthquake and Tsunami of March 2011, the ITU-T established a focus group (FG) in June 2012 to clarify the role of ICT in disaster situations and to investigate the need

for international standardization at ITU-T [3]. One of the authors (Araki) was appointed as the chairman of this FG. This meeting provided a forum to introduce Japan's disaster resistance research to the world. In addition to the usual FG meeting, the event also included an introduction to eHealth activities needed during a disaster, demonstrations of disaster-resistant ICT, and even a technical visit to the region affected by the Great East Japan Earthquake.

3.2 Overview of the meeting

(1) Speeches at special sessions

The Internet Engineering Task Force (IETF) gave a presentation on the provision of information relating to technical specifications (RFC: Request for Comments) for emergency situations, and demonstrated technology for transmitting high-priority traffic without delays, which has been proposed as an effective way of avoiding congestion in a disaster. A representative of the University of Tokyo's Earthquake Research Institute proposed an earthquake/tsunami monitoring system using submarine optical fiber cables and reported on the installation and planned operation of a new system off the Sanriku coast (total length: 120 km, node interval: 25–40 km). NTT DOCOMO introduced an early warning system called Area Mail that uses CBS (Cell Broadcast Service) to allow alerts and email warning messages to be transmitted to all mobile terminals in a specified region. It was agreed that the FG should hold further discussions on these technologies, and that the research items should reflect the requirements documents and other deliverables.

(2) Introduction to the state of disaster response research in Japan

In Japan, many technologies for strengthening disaster resistance have been designated for research and development (R&D) by the MIC, Japan. After the Great East Japan Earthquake, organizations including NTT, Tohoku University, SKY Perfect JSAT, NEC, NTT DOCOMO, and KDDI R&D Laboratories proposed technology for the rapid recovery and restoration of telecommunications, which can provide a lifeline during a disaster. An emergency communication system for people with disabilities was proposed by the TTC (Telecommunication Technology Committee). In order to share information about this technology and gather information on similar systems in other countries, it was agreed that a liaison statement would be sent to ITU-D, ITU-R (ITU Radiocommunication Sector), and ITU-T SG16 and JCA-AHF (Joint Coordination Activity on Accessibility and Human Factors). NTT proposed a way of configuring networks by assembling and reconfiguring resource units, and it was confirmed that ongoing discussions will continue in order to further clarify the requirements for providing people with the means of communication in disaster situations. It was agreed that this information would be partly reflected in the deliverables, including the overview and requirements documents.

Photo 2. Demonstrations related to mHealth by NTT Secure Platform Laboratories.

(3) Updates of the deliverables

The meeting participants discussed the updated draft overview document based on the results of this meeting and the previous meeting and added a list of technical specifications of IETF emergency/disaster communications, requirements for disaster message board and voice messaging services for mobile devices, and requirements relating to technology for the construction and reconfiguration of resource units. The first draft of the requirements document was also discussed, and the draft table of contents was approved. It was also agreed that requirements would be added for disaster message board services for mobile devices and evacuation guidance systems.

3.3 Technical visit to Sendai

This FG included a technical visit to Sendai, including stopovers at NTT offices that had been affected by the tsunami, and at the NICT's Resilient ICT Research Center. It was felt that a visit to the affected area during a period of cold snowy weather would help to highlight people's fears of disasters and the need for countermeasures, and would show the

Photo 3. Visiting the affected area (Nobiru area).

Photo 4. Visiting NICT's Resilient ICT Research Center (at Tohoku Univ.).

importance of working towards a rapid recovery after a disaster occurs. At the NICT center, the visitors were introduced to the R&D efforts being made by the MIC, Japan, and by NICT in order to deal with large-scale disasters, and they were given the chance to see the state of research in areas including communication devices and satellite communication equipment for ensuring regional communications after a disaster (**Photos 3** and **4**).

3.4 Future plans

The fifth meeting of the FG-DR&NRR was held in Thailand, May 20–24, 2013. In the future, we aim to continue holding meetings in countries that have experienced major disasters such as floods, hurricanes/typhoons, earthquakes, or tsunamis. Since the lifetime of this FG has been set to one year, it was confirmed that the extension of this period would be discussed at the next meeting.

4. Conclusion

eHealth is a medical care and health management solution that has been globally recognized as important by developing and developed countries alike. It is expected that this field will continue to grow in the future. For its efficient global development, international standards, with appropriate consideration of the regional characteristics and environmental conditions of each country, are essential. It is hoped that this workshop will contribute to the expansion of developing countries, which is the scope of ITU-D, as well as the further development of ICT standardization, which is the scope of ITU-T.

Disasters such as earthquakes, hurricanes, floods, tsunamis, and landslides occur all over the world. The responses to the unprecedented earthquake and tsunami that Japan experienced will be helpful for all the disaster-affected countries of the world. The establishment of international standards for dealing with disasters is essential for the construction of a safe society, so there are great hopes pinned on this FG. We are sure that the FG meeting in Japan has raised awareness of standardization efforts relating to disaster response.

References

[1] ITUWHO m-Health. http://www.itu.int/net/pressoffice/press_releases/2012/77.aspx#.URNifh0j6So
[2] ITU workshop Tokyo. http://www.itu.int/en/ITU-T/Workshops-and-Seminars/e-Health/201302/Pages/default.aspx
[3] ITU-T Focus Group on Disaster Relief system, Network Resiliency and Recover. http://www.itu.int/en/ITU-T/focusgroups/drnrr/Pages/default.aspx

Hideo Imanaka
Senior Manager, R&D Planning Department, NTT.

He received the B.E., M.E., and Ph.D. degrees in electrical engineering from Mie University in 1985, 1987, and 2001, respectively. After joining NTT Telecommunication Network Laboratories in 1987, he engaged in research on fiber optic access network architecture and network operation process reengineering methods. From 1996 to 2003, he worked on enterprise resource planning (ERP) systems integration as a consultant in the Solutions Business Division of NTT Communications. Since 2004, he has been involved in NGN standardization work at ITU-T. He was the Rapporteur of Question 1 of Study Group 13 during 2007–2010. He has also played an active role in IPTV standardization work at ITU-T. He is currently in charge of standardization strategy in the NTT Group. He received the ITU-AJ Award from the ITU Association of Japan in 2009. He is a member of the Institute of Electronics, Information and Communication Engineers (IEICE) and the Society of Instrument and Control Engineers.

Masahito Kawamori
Senior Research Engineer, NTT Service Evolution Laboratories.

He joined the Information Science Laboratory, NTT Basic Research Laboratories in 1989, where he first engaged in R&D of artificial intelligence. He then focused on researching multimedia services in the converged environment of broadcasting telecommunication and fixed/mobile systems. Since 2009, he has been the Rapporteur of Question 28 (Multimedia Framework for eHealth Applications) in SG 16 of ITU-T. He has spoken at several conferences on eHealth, including IEEE-ICC, WSIS, and Telecom World, all in 2011. He participated in the collaboration between ITU-T, ITU-D, and WHO, and in the Joint ITU-WHO Workshop on e-Health Standards and Interoperability, Geneva, 2012.

Noriyuki Araki
Senior Research Engineer, Access Media Project, NTT Access Network Service Systems Laboratories.

He received the B.E. and M.E. degrees in electrical and electronic engineering from Sophia University, Tokyo, in 1993 and 1995, respectively. He joined NTT Access Network Service Systems Laboratories in 1995. He then worked on the R&D of operation and maintenance systems for optical fiber cable networks. Since 2006, he has been engaged in standardization work for outside plants in ITU-T SG 6. He has been the Rapporteur of Question 17 of ITU-T SG 15 since 2008. He has also been contributing to the activities of IEC TC86, Fibre Optics, since 2007. He is currently serving as the chairman of ITU-T FG-DR&NRR. He is a member of IEICE.

Failure Cases in Access Facilities (Aerial Metallic Communication Facilities) and Countermeasures

Abstract

In this article, we introduce failure cases in access facilities (aerial metallic communication facilities) and countermeasures to them. This is the eighteenth in a bimonthly series on the theme of practical field information on telecommunication technologies. This month's contribution is from the Access Engineering Group, Technical Assistance and Support Center, Maintenance and Service Operations Department, Network Business Headquarters, NTT EAST.

1. Introduction

Metallic communication facilities can be said to be characterized by the following key features: 1) a huge number of facilities are currently installed in the field; 2) many years have passed since their construction; and 3) they are easily affected by weather conditions and the peripheral environment. Even today, in an era in which optical broadband facilities have become the shining star of the information-communications infrastructure, metallic communication facilities continue to play an important role as an information-communications infrastructure connecting customers. They must therefore operate effectively and achieve and maintain a certain level of service quality.

With an eye to constructing and maintaining facilities that are robust against extreme weather conditions and the peripheral environment, we present here failure cases characteristic of aerial metallic communication facilities that have been brought to the attention of the Technical Assistance and Support Center, and we explain their causes and countermeasures (**Fig. 1**).

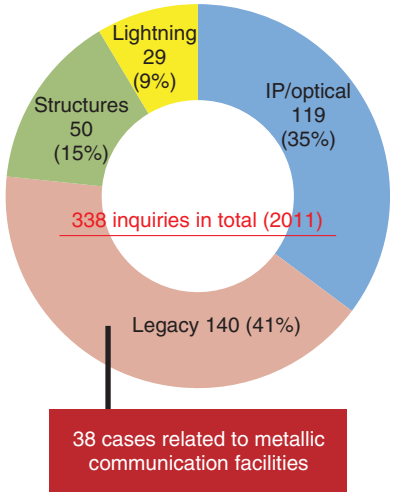

IP: Internet protocol

Fig. 1. Number of inquiries made to the Technical Assistance and Support Center regarding characteristic failures (FY2011).

2. Features of aerial metallic communication facilities and characteristic failures

Metallic communication facilities extend from the exchange (NTT building) all the way to the customer's terminal via aerial and underground metallic communication facilities.

The aerial metallic communication facilities targeted here for introducing failure cases are broadly divided into (1) cable intervals and (2) connection sections. The features and typical failures of both are presented in the following (**Fig. 2**).

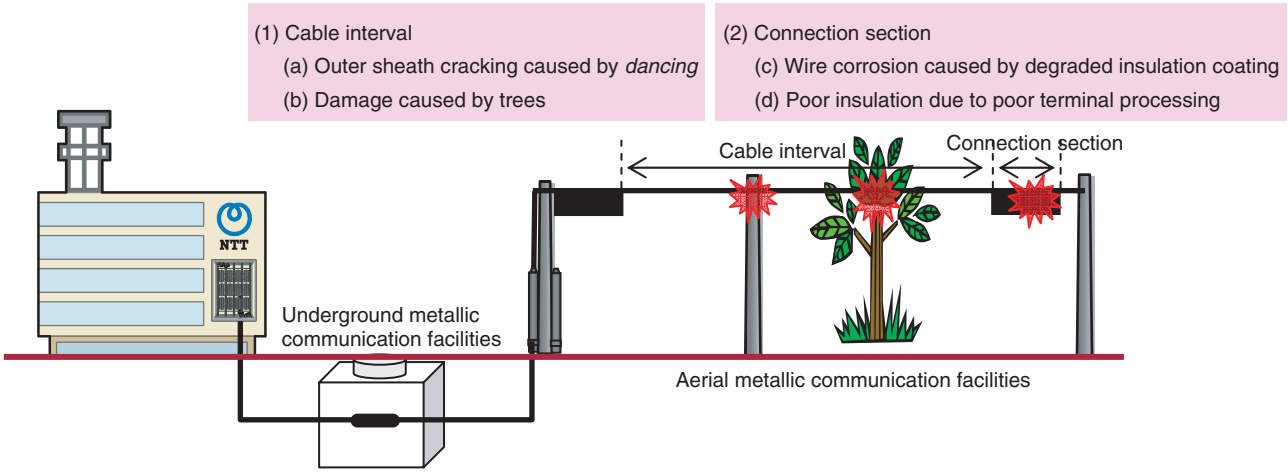

Fig. 2. Examples of failures in aerial metallic communication facilities.

2.1 Cable interval

Since the cable interval occupies most of the aerial metallic interval in terms of length of cable laid, the cable itself incorporates a certain degree of weather resistance. However, since it is naturally exposed to the peripheral environment, failures can occur such as those caused by strong winds or other types of inclement weather or by contact with trees in the immediate area.

At the initial stage of a cable-interval failure, there is often no effect on the quality of communications. This, combined with the fact that the location of such a failure is difficult to isolate, means that damage may have already spread once degraded communication service becomes noticeable. Although periodic patrols or surveys to check on facility conditions need to be performed, they require considerable work—preventive maintenance in itself is beset with problems.

2.2 Connection section

The connection section is an interval limited to the cable terminal box, but it includes coated wires in which the cable's outer sheath is removed as well as bare conductors (copper wires) in hand-soldered connectors. It is consequently easy for the connection section to be affected by temperature, humidity, sea-salt particles, and other environmental conditions. Characteristic failures include humidity-related corrosion in wires and faulty insulation caused by deterioration of the insulator.

Similar to the cable interval, a failure in the connection section will often have no effect on communications quality in its initial stage. However, as this section is also easily affected by weather conditions, deterioration across the entire area in question may have progressed by the time that facility degradation becomes noticeable. Furthermore, in contrast to the cable interval, failures may also be caused by maintenance work.

3. Failure cases in the cable interval and countermeasures

Here, we present examples of failures in aerial metallic communication facilities reported from various regions around Japan, and the countermeasures taken.

3.1 Outer sheath cracking (ring-shaped cut)

In regions affected by strong winds, dancing* (**Fig. 3**) in a self-supporting (SS) cable, especially a small-diameter one, may cause the outer sheath to crack (forming a ring-shaped cut) at the position where the cable is separated from its support line.

Outer sheath cracking in a color coded polyethylene (CCP) cable due to a ring-shaped cut is shown in **Photo 1**, and the mechanism generating this cracking is shown in **Fig. 4**. Along seashores or other places where there are no structures (intermediate pillars) to shield the cable from wind, the cable's outer sheath can be damaged in a circumferential direction at the

* dancing: A phenomenon in which an SS cable vibrates intensely from the horizontal plane due to continuous natural oscillation generated by strong wind.

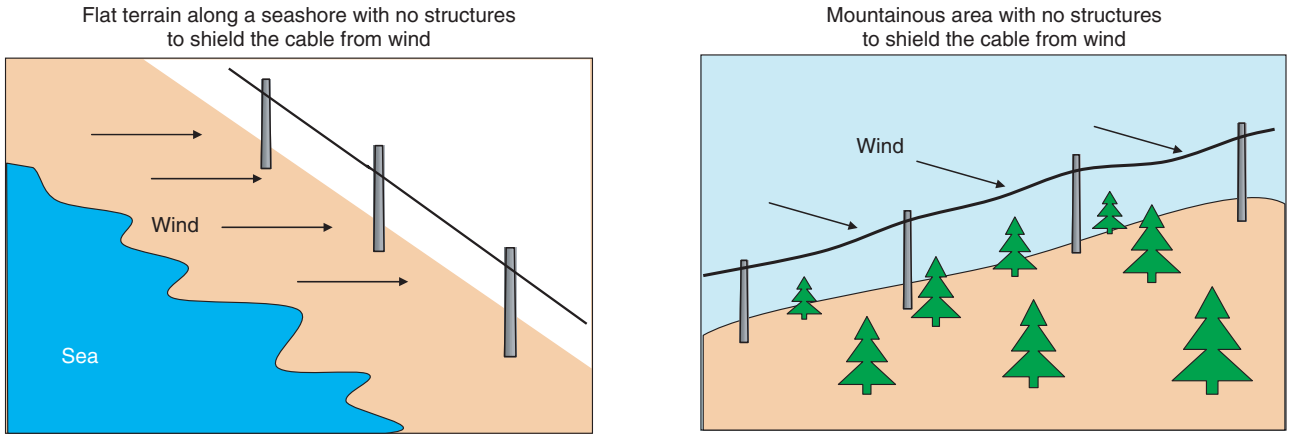

Fig. 3. Types of terrain conducive to dancing phenomenon in cables.

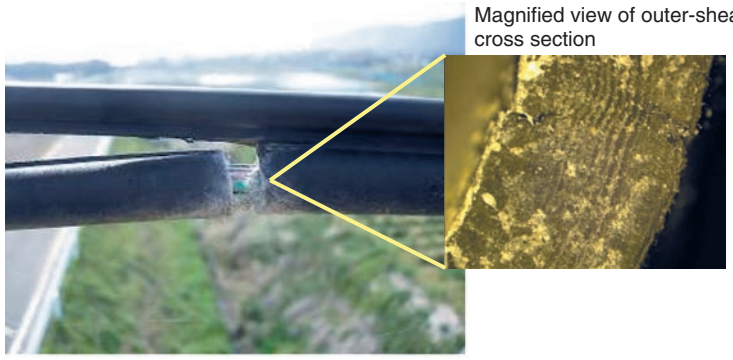

Photo 1. Outer sheath cracking by ring-shaped cut.

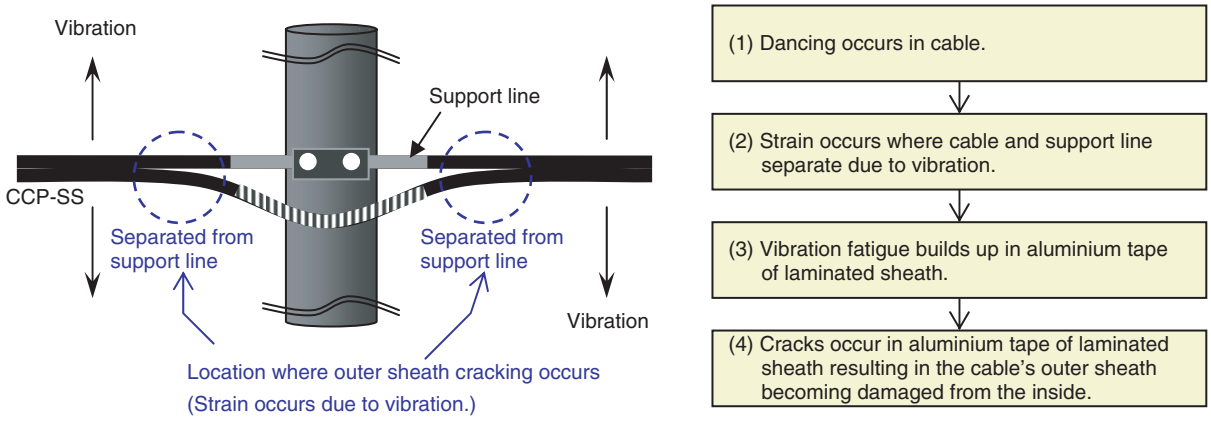

Fig. 4. Generation of outer sheath cracking in CCP-SS cable.

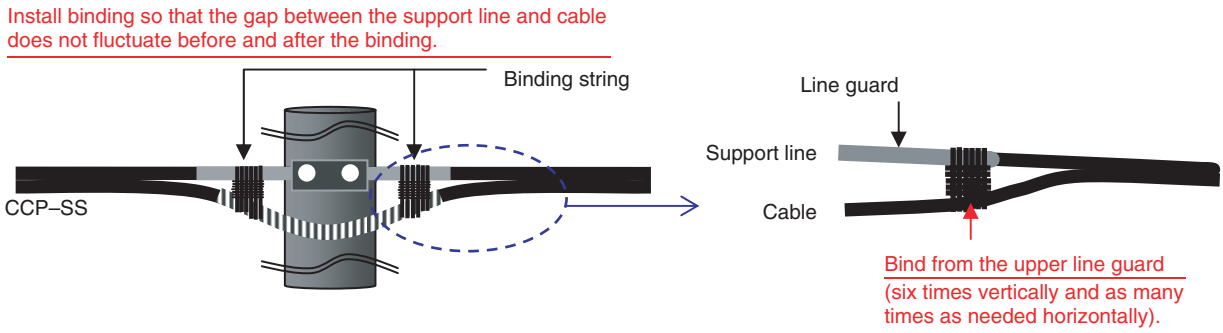

(1) Use cable binding string to bind the cable to the end of the upper line guard.
(2) Wrap binding string six times vertically and as many times as needed horizontally so that the gap between the support line and cable does not fluctuate before and after the binding.

Fig. 5. Ring-shaped cut countermeasure using cable binding string.

position where the cable is separated from the support line. This damage features circular fracture marks that are similar in appearance to annual growth rings in trees.

Countermeasures

Apply cable binding string to existing cable

This countermeasure can be applied to cable routes on which outer sheath cracking has previously occurred in CCP-SS cables because of strong winds or other factors or on routes where such damage is likely to occur. The application of cable binding string disperses the maximum strain occurring at the position where the cable separates from the support line and therefore controls the cable's degree of freedom at the section where it is suspended at the utility pole. This produces a strain-easing effect, which is why binding using cable binding string is important (**Fig. 5**).

Use high strength (HS) cable when installing new cable (or upgrading existing cable)

The use of high-strength CCP-HS-SS cable reinforced with a stainless-steel layer is an effective countermeasure against outer sheath cracking when installing new cable or upgrading existing cable when conditions (A) or (B) below apply (**Photo 2**).

Conditions for applying HS cable:

(A) The route is one on which cable outer sheath damage has occurred in the past because of dancing.
(B) The route is one that satisfies all three of the following conditions, indicating that outer sheath cracking may occur in the future:

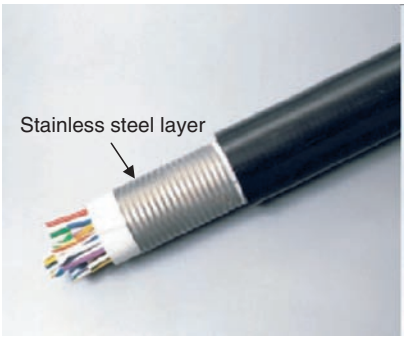

Photo 2. Appearance of HS cable

(1) The area along the route has an annual average wind speed of 2 m/s or greater (according to data from the local meteorological weather station).
(2) In that area, an average wind speed of 7 m/s or greater blows in the same direction for at least half a day from fall to spring over the long term.
(3) Dancing is likely to occur at locations on the route where wind with the speed described in (2) blows with no shielding structures.

String cable through ring fixtures

In addition to the aforementioned methods, suspending the cable through ring fixtures can suppress cable dancing and prevent ring-shaped cuts.

3.2 Cable outer sheath damage

A cable can come into contact with a tree branch

Photo 3. Example of cable damage from a tree.

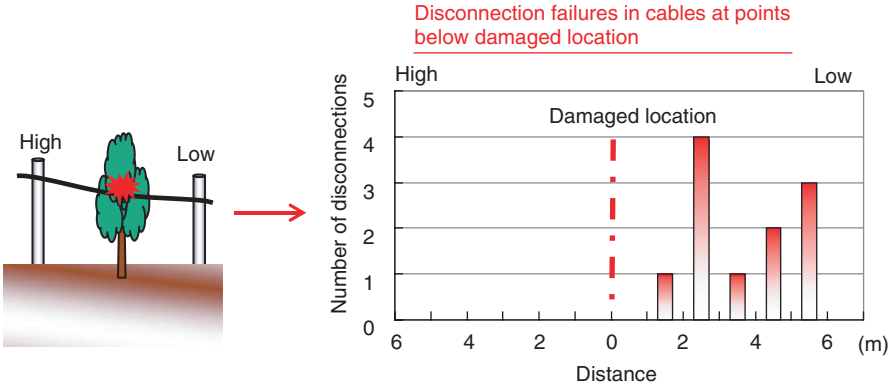

Fig. 6. Disconnection failure in cables on inclined routes.

that rubs up against the cable's outer sheath in such a way that even core wires can be negatively affected. An example of cable damage caused by a tree is shown in **Photo 3**. Although the search for faulty core wires along the span of a suspended cable can be narrowed down through a standard conduction check, isolating the exact failure location often requires a visual inspection and a great deal of labor. Some phenomena have been reported in which the damage is such that the problem can only be resolved by replacing the cable and not by simply repairing the damaged location. For example, a cable installed on an inclined route will naturally have a height difference along its span, and it has been found that core wires on the side below the damaged location can become corroded and generate disconnection failures (**Fig. 6**).

Countermeasures

Some form of protection may be applied in locations where cables and trees come into contact with each other, or trees in the immediate area may be cut down as a preventive measure against outer sheath damage.

4. Failure cases in the connection section and countermeasures

4.1 Core wire corrosion (insulation fractures)

Core wire insulation (polyethylene) in CCP cables can deteriorate for various reasons including high temperatures, humidity, and sea-salt particles that get inside a terminal box. Furthermore, infiltration of ultraviolet light into a terminal box through gaps caused by deformation in the terminal-box cover or side panels resulting in poor sealing—which was rarely seen in older types of terminal boxes—can accelerate such insulation degradation. Moreover, fractures have become quite noticeable in core wires in non-black colors that absorb a large portion of

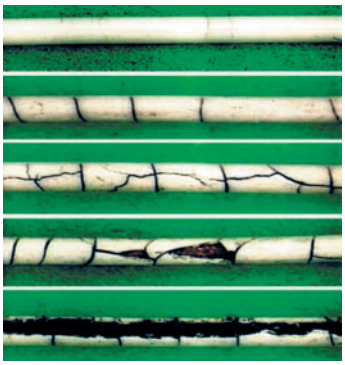

Photo 4. Classification of core wire degradation.

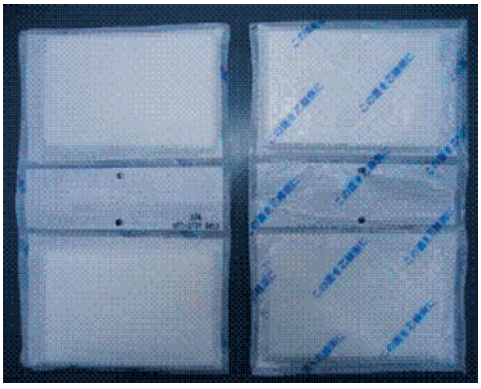

Photo 5. Humidity controlling materials.

Photo 6. Countermeasure to core-wire insulation faults using humidity controlling materials.

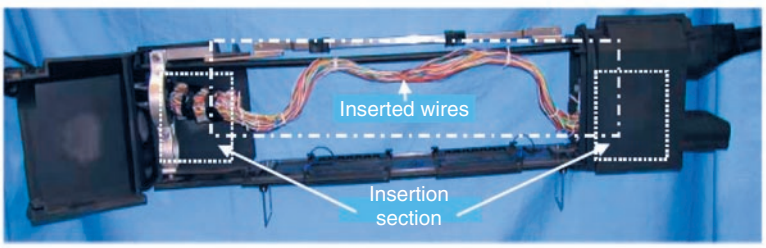

Photo 7. Repair technique using a life-extending terminal box.

ultraviolet light (**Photo 4**).

Countermeasures

The use of humidity controlling materials and life-extending terminal boxes can be used as countermeasures to core wire corrosion. Humidity controlling materials adjust the peripheral humidity and prevent condensation on core wires, which makes them effective in suppressing insulation degradation and failures. They are applicable to insulation that has a degree of degradation of 1 or 2. In the event of core-wire insulation having a degree of degradation of 3, 4, or 5, the existing terminal box can be replaced with a life-extending terminal box and wires inserted accordingly to ensure long-term reliability. Humidity controlling materials are shown in **Photo 5**, the implementation of a countermeasure to core-wire insulation faults using humidity controlling materials is shown in **Photo 6**, and a repair method using a life-extending terminal box is shown in **Photo 7**.

4.2 Faults in terminal processing section (sleeve section)

Faults in core-wire insulation in the terminal sleeve include:

(1) Hardening faults due to insufficient stirring of the liquid A/B epoxy resin, which is used to protect the edges of core wires (naked copper wire) against humidity or other materials that can cause corrosion or unwanted contact between wires
(2) End of core wires coming into contact with the bottom of the sleeve
(3) Water penetration due to direction errors at the top and bottom of the sleeve

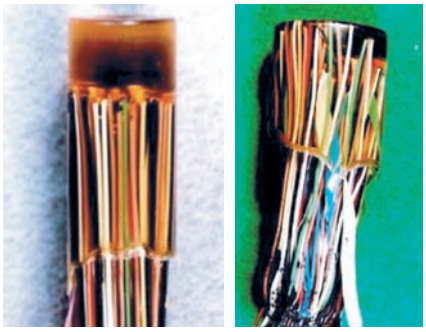

Correct processing

Incorrect processing
→Wires touch the bottom of the sleeve, causing mutual conduction.

Photo 8. Examples of terminal sleeve processing.

Examples of processing the terminal sleeve are shown in **Photo. 8**.

Countermeasures

A schematic of terminal sleeve processing is shown in **Fig. 7**. The following points should be kept in mind when processing the terminal sleeve:

(1) Stir liquid A/B epoxy resin well so that no unreacted hardening agents remain.
(2) Let the end of core wires float about 1 cm from the bottom of the terminal sleeve.
(3) Turn the terminal sleeve upside down immediately after processing so that its bottom is oriented upward.

5. Concluding remarks

This article introduced failure cases in aerial metallic communication facilities and countermeasures to these failures. These types of facilities are affected by weather conditions and the peripheral environment, and failures can occur for a variety of reasons. It is consequently very difficult to prevent such failures before they occur or to efficiently implement countermeasures to failures that have occurred. The Access Engineering Group of the Technical Assistance and Support Center hopes that the information provided here on failures and their countermeasures is useful in a small way to frontline personnel in facility management and in improving the maintenance of service quality.

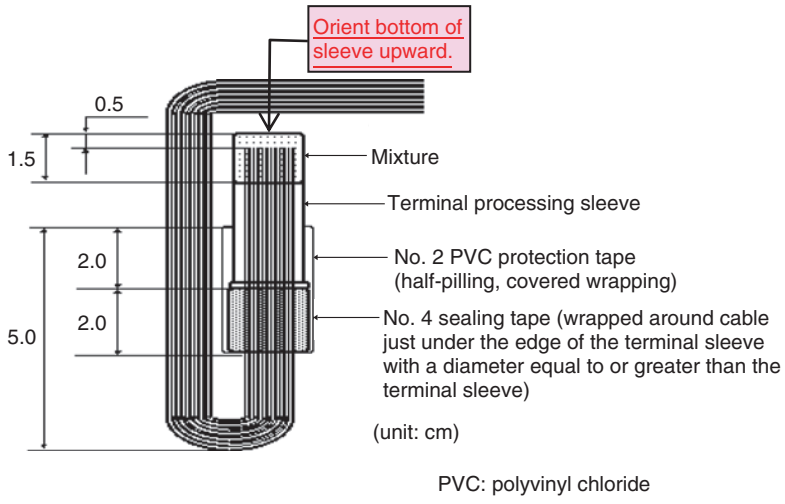

Fig. 7. Schematic of terminal sleeve processing.

External Awards

The IFIP/IEEE International Symposium on Integrated Network Management (IM 2013) Best Paper Award

Winners: Noriaki Kamiyama and Ryoichi Kawahara, NTT Network Technology Laboratories
Date: May 30, 2013
Organization: IEEE Communications Society, IFIP

For "Analysis of Content Charge by ISPs".

When rich content is delivered, a huge amount of traffic is transmitted over the network. For ISPs, the increased investment cost required to maintain stable quality is a problem. An effective way to address this problem is content charge, in which ISPs charge content providers for each delivery of content. This work models the business relationship between ISPs and content providers, and we investigate the conditions for introducing content charge by ISPs.

Published as: N. Kamiyama and R. Kawahara, "Analysis of Content Charge by ISPs," Proc. of the IFIP/IEEE International Symposium on Integrated Network Management, IM 2013, Ghent, Belgium, May 2013.